DISTRIBUTION OF LEVEL SPACING RATIOS IN RANDOM MATRIX THEORY AND CHAOTIC QUANTUM SYSTEMS: VARIANTS AND APPLICATIONS

A THESIS

submitted for the award of Ph.D. degree of

Indian Institute of Science Education and Research Pune

by

Sai Harshini Tekur

(20123215)

Under the Supervision of

Dr. M. S. Santhanam

Associate Professor

IISER Pune, India

Department of Physics

Indian Institute of Science Education and Research Pune

2019

To

Avva and Ajji,

my grandmothers

CERTIFICATE

I feel great pleasure in certifying that the thesis entitled, **"Distribution of level spacing ratios in random matrix theory and chaotic quantum systems: variants and applications"** embodies a record of the results of investigations carried out by Sai Harshini Tekur under my guidance.

She has completed the following requirements as per Ph.D. regulations of IISER Pune.

(a) Course work as per the Institute rules.

(b) Residential requirements of the Institute.

(c) Presented her work in the departmental committee.

(d) Published/accepted minimum of two research papers in a referred research journal.

I am satisfied with the analysis of data, interpretation of results and conclusions drawn.

I recommend the submission of thesis.

Date :

Dr. M. S. Santhanam

(Thesis Advisor)

Countersigned by

Chair, Physics Program

DECLARATION

I, **Sai Harshini Tekur**, *hereby declare that the work incorporated in the present thesis entitled,* **"Distribution of level spacing ratios in random matrix theory and chaotic quantum systems: variants and applications"** *is my own and original. This work (in part or in full) has not been submitted to any University for the award of a Degree or a Diploma.*

Date :

(Sai Harshini Tekur)

Acknowledgments

An African proverb goes, "It takes a village to raise a child." This holds true in academia as well, where the village consists of all the people who mentored, pushed, supported and cheered the academic child taking her first unsteady steps in research. This is the part where everyone is thanked for all that they have done to set me on this path, and kept me going till the end of my PhD (or depending on how you look at it, this is the list of people who are to be blamed for it).

First and foremost, I am deeply thankful to my supervisor, Dr. M. S. Santhanam for his guidance, support, amiableness and general ability to remain unfazed in most situations. He has always given me the freedom to explore new ideas and opportunities (even if they went nowhere most of the time), and molded my abilities as well as my world-view as a researcher.

Next, I am thankful to my Research Advisory Committee members, Dr. Sudhir Jain (BARC Mumbai) and Dr. Umakant Rapol (IISER Pune) for their advice and encouragement. Discussing my findings with them has given me perspective as well as confidence regarding my research, and their insights and feedback and have shaped my PhD in a big way.

I thank my lab members (current and former), Sanku Paul, Vimal Kishore and Udaysinh Bhosale their support, openness to discussion and learning, and for the camaraderie that comes with being a part of the same research group.

I would like to acknowledge collaborators Dr. Santosh Kumar (Assistant Professor, Shiv Nadar University) and Dr. Udaysinh Bhosale (Postdoctoral Fellow, IISER Pune) for complementing my findings with their expertise and helping me learn how to formulate and address research problems.

I am very grateful to Dr Giacomo Livan for providing S&P 500 correlation matrix data for S&P 500 stocks, whose eigenvalues are analyzed in Chapter 3 of this thesis. I would also like to thank Sanku Paul and Uday Bhosale for providing eigenvalues for the intermediate map and kicked top respectively, which were again used in Chapter 3. I am also grateful to Danveer Singh and Adarsh Vasista for helping me start off with COMSOL.

ABSTRACT

Quantum systems with classically chaotic counterparts are studied in the realm of quantum chaos. A popular indicator of quantum chaos are the level spacing statistics, whose mathematical formulation is given by Random Matrix Theory (RMT). In this thesis, we study the distribution of ratios of spacings between eigenvalues of a random matrix or a Hamiltonian matrix corresponding to a quantum chaotic system. We also briefly consider other complex systems whose spectral fluctuations are described by random matrix theory. The main object of interest in this thesis, the spacing ratio, has recently been introduced, and has gained popularity in RMT as well as quantum chaos due to its ease of computation.

We study variants of the spacing ratio, and show that its distribution takes different forms depending on the particular scenario considered. In order to study the effect of localized states on the spectral statistics of a quantum chaotic system, we propose a basic random matrix model for this interaction, and analytically derive a form for the distribution of spacing ratios for this model. We show that this model may be used to understand the strength of interaction between localized states and their generic neighbors, for various model systems. Next, we show numerically the form taken by the spacing ratio distribution over longer energy scales, which is an indicator of long-range correlations in the spectra of random matrices and complex systems that are modeled by them. Finally we how numerical evidence of scaling relationships in random matrices, for higher order ratio distributions, as well as for superpositions of random matrices. These results provide a straightforward but powerful application of the higher order ratios in determining the number of symmetries present in the Hamiltonian of a given quantum chaotic system.

List of Publications

1. *Exact distribution of spacing ratios for random and localized states in quantum chaotic systems*

   S. Harshini Tekur, Santosh Kumar and M. S. Santhanam,

   Phys. Rev. E **97**, 062212 (2018)

2. *Higher order spacing ratios in random matrix theory and complex quantum systems*

   S. Harshini Tekur, Udaysinh T. Bhosale and M. S. Santhanam,

   Phys. Rev. B **98**, 104305 (2018)

3. *Scaling in the eigenvalue fluctuations of the empirical correlation matrices*

   Udaysinh T. Bhosale, S. Harshini Tekur and M. S. Santhanam,

   Phys. Rev. E **98**, 052133 (2018)

4. *Symmetry deduction from spectral fluctuations in complex quantum systems*

   S. Harshini Tekur and M. S. Santhanam,

   arXiv:1808.08541 (2018)

Contents

List of Figures

Introduction

Trying to understand the way nature works involves a most terrible test of human reasoning ability. It involves subtle trickery, beautiful tightropes of logic on which one has to walk in order not to make a mistake in predicting what will happen.

-Richard P. Feynman

1.1 Introduction

The basis of the scientific method is the idea that given a hypothesis based on previous observations, predictions may be made regarding the behavior of the system in question. And these predictions may be tested via experiments, which should yield identical results when replicated. The development of two physical theories, however, brought into question the nature of observation and prediction itself; one being quantum mechanics, and the other, chaos theory.

The study of chaos in the classical regime, starting from the three-body problem studied by Kepler, established that sensitivity to initial conditions in a dynamical

system makes it behave apparently 'randomly', and makes long-time prediction of the system's evolution impossible, though it remains deterministic. The reason being that an infinitesimal perturbation in the initial conditions of the system leads to an exponential divergence of trajectories, a statement that is the crux of the often-used but thoroughly misunderstood term, ``the butterfly effect´´. It thus became increasingly evident that all predictions would be limited by accuracy in measurements and more powerful numerical techniques would be required to understand the proliferation of chaos in physical systems. Even with the analytical groundwork for the field laid through the works of Henri Poincaré, Andreï Nicolaïevitch Kolmogorov and others, it was only sufficient advances in computational techniques that made the study of chaos in dynamical systems feasible, as increasingly accurate numerical solutions could be provided for the (nonlinear) equations governing the system in question. This lends a sense of universality to the theory, as the evolution equations for most dynamical systems fall into the same mathematical framework.

Thus, chaotic behavior is observed in a wide variety of physical [1], chemical [2] and biological systems [3], apart from other areas like economics [4], social sciences [5], engineering [6, 7] etc., and may all be treated within the same mathematical framework. There is, however, one notable area where the ideas and formalism of classical chaos cannot be directly implemented. The game-changer, so to speak, is quantum theory.

The idea of trajectories loses meaning in the quantum regime, restricted as it is by Heisenberg's Uncertainty Principle. It is not straightforward then, to define chaos in the manner in which it is talked about classically. This was pointed out by Albert Einstein in 1917, in the context of Bohr's Correspondence Principle, which was an attempt towards bridging the gap between the classical and quantum regimes. Einstein argued that since there is a breakdown of invariant tori in the phase space of classically chaotic systems, the idea of quantization of periodic orbits (whose areas should be integral multiples of the Planck's constant, according to Bohr's theory) is not applicable. It was only later in the 1970s, through the efforts of M.

Gutzwiller and M. V. Berry [8, 9] towards developing the semiclassical theory of periodic orbits, that this problem could be addressed.

Thus, what is now studied as quantum chaos [10,11], is really the study of quantum systems which are chaotic in the classical limit [12]. There were some hiccups along the way regarding the name itself, with Berry preferring the term 'quantum chaology' [13], as there does not exist a direct correspondence with respect to sensitivity to initial conditions between the classical and quantum regimes. Instead, the object of investigation is the presence of universal signatures in quantum systems [14] with classically chaotic counterparts, that are not seen in regular quantum systems. Several of these systems are discussed in Section 1.2. A second class of systems that have no classical analogues, like compound nuclei are also included in the discussion as they exhibit all the same signatures of quantum chaos as the former class of systems.

These signatures are seen in the eigenspectra of the Hamiltonians of the quantum systems, obtained by solving the corresponding Schrodinger equation, and they are studied in the mathematical framework of Random Matrix Theory (RMT), which will be discussed in greater detail in Section 1.3. Random Matrix Theory itself originated in the study of complex quantum systems, namely the spectra of compound nuclei (although strictly speaking, the first random matrix was introduced by John Wishart in Ref. [15], in the context of multivariate statistics), but has now expanded in scope to include a multitude of fields, as will be discussed below. Again, the ubiquity of the quantum signatures of chaos implies that it may be found to be encompassing various fields of physics including atomic and nuclear physics [16], quantum optics [17], condensed matter physics [18] and so on [10].

Several of the systems discussed in this thesis are popular theoretical and experimental models in the fields mentioned above, and the motivation for studying quantum chaotic systems like these, and the mathematics that describes them, may be understood in terms of its applicability in problems of quantum transport, entanglement and quantum computation, optical resonators and laser microcavities, acoustics in systems ranging from crystals to oceans, nuclear resonances, and even

the Riemann zeta function and generalized L-functions (See references cited above). The first step in understanding these systems is by building or studying simpler variations, like some of the models described in the next section. Most of these will be studied throughout the thesis in the limits in which they are chaotic and in which they are integrable (a Hamiltonian system with n degrees of freedom is said to be classically integrable if it possesses n constants of motion, making the corresponding equations of motion completely integrable. Its quantum counterparts are also referred to as integrable, and analytical solutions exist for their corresponding Schrodinger equations.)

1.2   Model Quantum Chaotic Systems

1.2.1   Coupled Quartic Oscillator

The two-dimensional coupled quartic oscillator is a classically chaotic system whose Hamiltonian is given by

$$H = \frac{p_x^2}{2} + \frac{p_y^2}{2} + x^4 + y^4 + \alpha x^2 y^2. \tag{1.1}$$

In the absence of the coupling parameter α, the system would decouple into two one-dimensional quartic oscillators, which are integrable. The system is also integrable for $\alpha = 2$ and 6, and becomes chaotic for all other values of α. The classical phase space has both regular and chaotic regions even as $\alpha \to \infty$, making this a mixed system, and several features including its stability, Poincare sections [19], scaling in energy [20], existence and occurrence of periodic orbits as well as bifurcation sequences [21, 22] have been extensively studied for the classical and quantum versions, as applicable.

Solving the Schrodinger equation corresponding to Eq. 1.1 leads to the study of the quantum counterpart [23] of this system. It is an interesting model for studying the quantum signatures of chaos for the following reasons:

- The classical periodic orbits induce localization of quantum eigenfunctions,

a feature which will be further explored in Chapter 2.

- The scaling in the classical Hamiltonian leads to a scaling in the quantum energy levels for different values of the Planck's constant.

- It can be mapped to problems of atoms in strong magnetic fields as the corresponding potentials yield qualitatively similar dynamical features.

- Entanglement dynamics in the system may be studied by considering the coupled quartic oscillator as a bipartite system.

The eigenvalues and eigenvectors of the quantum system may be obtained by diagonalizing the Hamiltonian in the basis of a linear combination of the corresponding unperturbed system. This is because of the existence of symmetries in the potential, leading to a block diagonal representation of the Hamiltonian matrix. Thus it is sufficient to diagonalize only one of the symmetry sectors. The system has C_{4v} point group symmetry, in the group theory representation, and a desymmetrized basis set may be constructed as follows [24]:

$$\psi_{n_1,n_2}(x,y) = N(n_1, n_2)[\phi_{n_1}(x)\phi_{n_2}(y) + \phi_{n_2}(x)\phi_{n_1}(y)]. \tag{1.2}$$

Here, $N(n_1, n_2)$ is the normalization constant and $\phi(x), \phi(y)$ are the eigenfunctions of the unperturbed system (that is, Eq. 1.1 with $\alpha = 0$). Depending on whether the indices n_1 and n_2 are odd or even integers, the four irreducible representations for this system are obtained, and it is sufficient to consider one of them for diagonalizing the Hamiltonian.

The level spacing distribution for this system, which will be discussed in Section 1.3.5, distinguishes it as a quantum chaotic system, with deviations attributed to the presence of localized states, which will be dealt with in greater detail in Chapter 2.

1.2.2 Quantum Billiards

The problem of a particle (or ray) confined in a region of space undergoing reflections from a specified boundary [25] occupies an important position in the study of

dynamical systems owing to its being analytically tractability [26–28], experimental feasibility [29–32], and the fact that it exhibits a variety of interesting physical phenomena [33–38].

The Hamiltonian for a particle moving in two-dimensions in a region Ω defined by the boundary of the billiard is given by

$$H = \frac{p_x^2}{2} + \frac{p_y^2}{2} + V(x, y), \tag{1.3}$$

with $V(x, y) = 0$ for $x, y \in \Omega$ and $V(x, y) = \infty$ for $x, y \notin \Omega$.

The classical system shows both integrable and chaotic behavior, depending on the shape of the boundary, which is the chaos parameter. Integrability is seen for some basic geometries like circles, ellipses, square and rectangles, and a smooth transition from integrability to chaos may be studied by treating the shape parameter as a perturbation of the integrable geometries. The classical phase space shows a mixture of regular and chaotic regions, and the areas of these regions depend on the strength of the perturbations (that is, the deformed geometry of the boundary), which also influences the nature of the periodic orbits.

The quantum version of this system is studied by solving the corresponding time-independent Schrodinger equation,

$$(\nabla^2 + V)\psi = E\psi. \tag{1.4}$$

Written in this form, the equation is reminiscent of the Helmholtz equation, $(\nabla^2 + \mu^2)\psi = E\psi$, where μ is the wave vector, and ψ may be interpreted as the solution of the electromagnetic wave equation, as well as a quantum wavefunction. The corresponding analogy between ray and wave chaos is thus extended to the realm of quantum mechanics, when the wavelength of the incident wavefunction is comparable in dimension to the size of the billiard.

This leads to several interesting effects, the most important of which is localization along classical periodic orbits and dynamical localization due to interference effects. These aspects will be discussed further in Chapter 2. But the very idea

of deformations inducing chaos in billiards, and the consequent effects has made it a very popular system for experimental realization, and it has found several applications as microwave resonators, laser cavities, acoustic resonators, optical fibres etc.

Numerically, there exist several methods to analyze this system. In this thesis, the various kinds of billiards discussed have all been simulated using finite element method (FEM), via a commercial software, COMSOL Multiphysics [39]. This is especially useful in the studying billiards with broken time-reversal symmetry, as it is possible to simulate the experimental set-up exactly, and use the same parameters and even materials as the experiment.

Analysis of the eigenspectrum of the billiards may be done by specifying the geometry and the boundary conditions in the software. For billiards possessing discrete symmetries like rotation and reflection (the number of these depends on the geometry), the whole boundary need not be considered, and a part of the full geometry corresponding to an irreducible representation may be studied. For example, for the popular Bunimovich stadium billiard (whose boundary is defined as the deformation of a circle, with two straight parallel walls and two curved walls opposite to each other) that has been studied in Chapters 2 and 4, one quarter of the whole stadium corresponds to the irreducible representation. Dirichlet boundary conditions ($\psi = 0$) are used at all the boundaries, which preserves time-reversal symmetry. Other symmetry aspects of billiards are discussed in greater detail in Chapter 4.

One of the methods of breaking time-reversal symmetry is by application of a static magnetic field, and attaching a magnetized ferrite strip on one of the walls of the billiards as described in Ref. [40]. The electromagnetic interaction between the magnetized ferrite and the applied magnetic field leads to the breaking of time-reversal symmetry, and in this case the boundary conditions are not as straightforward. However, COMSOL takes into account these interactions and it is not necessary to specify the boundary conditions explicitly, making it convenient to calculate the eigenvalues and eigenvectors of this system.

1.2.3 One-dimensional Spin chains

Spin chains, like the previously discussed systems are also very popular models to study a variety of phenomena, chaos being just one of them [41,42]. This popularity, in large part, is due to their conceptual simplicity, especially considering that they are many-body systems. Nevertheless, they can be used to model disparate phenomena in statistical mechanics [43–45], condensed matter physics [46–48], quantum field theory [49, 50], quantum computation [51, 52] etc. Further, spin chains have mathematically elegant structures and solutions [53], and they lend themselves very easily to numerical simulations as well [54,55]. Finally, they are experimentally realizable in studies involving magnetization [56,57], critical behavior [58,59], quantum chaos [60,61] etc.

The starting point in the study of spin chains, is the one-dimensional spin 1/2 Heisenberg model [62], whose Hamiltonian is given by

$$H = \sum_{i=1}^{L-1} [J_x S_i^x S_{i+1}^x + J_y S_i^y S_{i+1}^y + J_z S_i^z S_{i+1}^z]. \tag{1.5}$$

Here, L denotes the number of sites, or the length of the spin chain. At each of the sites, a spin 1/2 object is placed, which can have its spin pointing either 'up' (+1/2) or 'down' (-1/2). The spin operators in all three directions, x, y and z at a given site are $S^{x,y,z} = \sigma^{x,y,z}/2$, where $\sigma^{x,y,z}/2$ are the 2×2 Pauli spin matrices. There are nearest-neighbor couplings between the spin, with the spin at site i interacting only with its nearest neighbors. If the spin chain is along a line, the spins at the ends of the chain (that is, those at sites 1 and L) couple to only one neighbor (open boundary conditions), but if the spins are arranged on a ring, the spin at site L couples to the spins at sites $L - 1$ and 1 (periodic boundary conditions). $J_{x,y,x}$ is the coupling strength along all three directions. If $J_x = J_y = J_z$, the system is called the isotropic Heisenberg spin chain or XXX spin chain, whereas if $J_x = J_y \neq J_z$, it is the popular XXZ spin chain.

While the above system is integrable even if $J^x \neq J^y \neq J^z$, there are several ways of inducing chaos in the system, including the addition of a random magnetic

field at each site in one of the directions, by the placement of a disorder (or defect) at one of the sites (as will be seen in Chapter 3), or by introducing higher order interactions, which may also lead to broken time-reversal symmetry (see Chapters 3 and 4). Other (discrete) symmetries in the spin chain have been further discussed in Chapter 4, but one that deserves mention at this stage, is invariance under rotation about the z-axis, leading to conservation of total spin in the z-direction (S^z). This is an important factor especially when the total Hamiltonian commutes with the S^z operator, as diagonalization of the Hamiltonian in the basis of S^z (often called the site basis), leads to a block diagonal structure for the Hamiltonian matrix, with each block corresponding to a fixed value of S^z. Thus, solving for the eigenspectrum becomes easier, as it is sufficient to diagonalize one of the blocks. The eigenvalues and eigenvectors are thus obtained and statistical features of the system may be studied.

1.2.4 Complex atoms and nuclei

The complexity in the spectra of atoms and molecules arises due to the interactions between the many particles that constitute the given system. For an atom like Samarium (discussed in Chapter 2), with a high atomic number (Z=62), the atomic spectrum exhibits complex behavior due to the presence of a large number of valence electrons, existing in various configurations, as well as the effects of spin-orbit interactions. Though the exact Hamiltonian for such systems has not yet been given, these high-Z atomic systems may be simulated using the Dirac-Coulomb (relativistic) Hamiltonian, which, for an N-electron atom, has the form

$$H = \sum_{i=1}^{N}(c\boldsymbol{\alpha}_i \cdot \boldsymbol{p}_i + c^2(\beta_i - 1) - \frac{Z(r_i)}{r_i}) + \sum_{i>j}^{N} \frac{1}{|\boldsymbol{r}_i - \boldsymbol{r}_j|}. \tag{1.6}$$

Most nuclei are considered complex, as the presence of many nucleons leads to complicated interactions involving the strong, weak and electromagnetic forces. There are several models to explain nuclear spectra and excitations, including the nuclear shell model and the collective model [63, 64], but no exact Hamiltonian

exists to understand experimental observations like neutron resonances or scattering cross-section data. And it was realized in the 1950s, that models that could exactly model these features may be next to impossible to construct, given the complex many-body dynamics of large nuclei.

1.3   Random Matrix Theory

Eugene Wigner, in the 1950s, was studying quantities like the distribution of spacings of nuclear resonance and widths, which prompted him to put forth the idea that fluctuations in these spectra may be captured in a statistical sense, by comparison with eigenvalues of large symmetric matrices with random entries. That is, as a simplification at the grossest level, the eigenspectrum of the Hamiltonian corresponding to the complex nucleus must share some statistical features with the spectrum coming from a matrix whose elements are chosen at random. The Hamiltonian then, may be considered a black box of sorts, whose output (the energy eigenspectrum) is compared with the corresponding output of a purely mathematical object (a random matrix), subject to some symmetry considerations. Not only is this a remarkable insight, but the fact that this was, and continues to be a highly successful approach is, in itself, astonishing and non-trivial.

This idea, that some features of a system arising due to its inherent complexity, can be captured by a mathematical object which is random by design, has a certain universality. Indeed, Wigner's proposition gave rise to a field of mathematics studied as Random Matrix Theory(RMT) [65], and finds widespread application in various branches of physics, including, but not limited to atomic and nuclear physics [66, 67], statistical and condensed matter physics [68, 69], quantum field theories [70, 71], and of course, quantum chaos and mesoscopic physics [11]. It also has applications in finance, mathematics, biology, climate science, as well as the social sciences, and is used in multivariate statistics, image processing, control theory, and basically any field of study that would require modeling of stochastic features contained within it. [72, 73]

A more detailed review of Random Matrix Theory, its history and its applications in physics may be found in Refs. [74, 75] and the references therein.

1.3.1 RMT: Some Mathematical Preliminaries

The mathematical formulation of RMT was put forth in a series of papers by Wigner and Dyson and several others (collected in Ref. [76]) in the nineteen fifties and sixties, and Dyson devised a rather elegant classification of random matrices using symmetry arguments, especially invariance of systems under time reversal, where the action of the time-reversal operator T on a function $\phi(t)$ may be expressed as

$$T\phi(t) = \phi(-t).$$

A given system may not possess time-reversal symmetry at all, and if it does, then the eigenvalues of the time-reversal operator must be ± 1. These are the only possibilities, and the Hamiltonian matrix for these three cases must have the following properties:

- If time-reversal symmetry does not exist, the Hamiltonian must be invariant under a unitary transformation, and its matrix elements are complex.

- If time-reversal symmetry exists, with the eigenvalue of T being $+1$, the Hamiltonian must be invariant under an orthogonal transformation, and a basis may be found where the matrix elements of the Hamiltonian are real.

- If time-reversal symmetry exists, with the eigenvalue of T being -1, the Hamiltonian must be invariant under a symplectic transformation, and its matrix elements are quaternions.

This leads to the classification of random matrices as Orthogonal, Unitary and Symplectic ensembles. If the elements of the random matrix are Gaussian-distributed random numbers, the most popular class of random matrices, called the Gaussian Ensemble is obtained.

1.3.2 Gaussian Ensembles

For random matrices with Gaussian-distributed random numbers, depending on the symmetry class, they may be classified as Gaussian Orthogonal Ensemble (GOE), Gaussian Unitary Ensemble (GUE) or Gaussian Symplectic Ensemble (GSE).

The eigenvalues $E_1, E_2, \cdots E_N$ of the Gaussian ensembles have a joint probability distribution function(JPDF) given by

$$\varrho(E_1, \cdots E_N) = \frac{1}{Z_{N,\beta}} \prod_{k=1}^{N} e^{-\beta N E_k^2/4} \prod_{i<j} |E_j - E_i|^{\beta}. \qquad (1.7)$$

Here, $Z_{N,\beta}$ is a normalization constant, and the index β is called the Dyson index. For $\beta = 1, 2$ and 4, the above equation gives the JPDF for the Orthogonal, Unitary and Symplectic ensembles. The Dyson index could also be thought of as counting the number of real components in the matrix elements corresponding to each of the ensembles. A GOE matrix is real, symmetric, and has $\beta = 1$, a GUE matrix is Hermitian with complex elements, with $\beta = 2$, and a GSE matrix is self-dual, with quaternion elements and has $\beta = 4$. Other values of β do not have a matrix representation (yet). Hamiltonians of most physical systems belong to one of these classes, as will be seen in the subsequent chapters.

The Gaussian ensembles may be modified to obtain other classes of random matrices, and these again correspond to different kinds of physical systems.

1.3.3 Circular Ensembles

If, instead of Hermitian matrices, the statistical properties of Unitary matrices are investigated, this becomes a useful tool to study the spectra of Floquet systems or time-periodic systems, as the evolution of these systems are dictated by a unitary operator. This led to the development of the Circular random matrix ensembles, in the framework of which, the eigenphases (ϕ_i) of the unitary operator (or matrix) U are studied.

Symmetry considerations appear here as well, and depending on the symme-

try class (or Dyson index), they can be classified as Circular Orthogonal, Unitary or Symplectic Ensembles (COE, CUE and CSE). They are called circular, as the unitary matrices have eigenvalues of the form $e^{i\phi}$, and can be considered to be uniformly distributed on a unit circle in the complex plane.

The JPDF of the eigenphases $\phi_1, \phi_2, \cdots \phi_N$ is given by

$$\varrho(\phi_1, \cdots \phi_N) = \frac{1}{Z'_{N,\beta}} \prod_{1 < j < k < N} |e^{i\phi_j} - e^{i\phi_k}|^\beta, \qquad (1.8)$$

where $Z'_{N,\beta}$ is the normalization constant and $\beta = 1, 2, 4$ is the Dyson index.

As mentioned earlier, the circular ensembles are used to study Floquet systems like the kicked rotor and kicked top, and are discussed in greater detail in Chapter 3.

1.3.4 Wishart Ensembles

Wishart matrices may be considered the first example of random matrices, formulated by John Wishart in 1928. In general, given a random $N \times M$ random matrix X, Wishart matrices may be constructed as $W = XX^S$. Depending on whether X has real, complex or quaternion elements, the operation X^S may be considered as transposition, complex conjugation, or self-dual operation respectively.

Wishart matrices are generally encountered in the study of multivariate statistics and used to estimate empirical correlation matrices of order $N \times T$ whose elements represent the pair-wise Pearson correlation among the N variables, each one being a time series of length T.

The JPDF for eigenvalues $E_1, E_2, ...E_T$ for Wishart (also known as Wishart-Laguerre) ensembles is given by

$$f(E_1, E_2, ..E_T) = \frac{1}{W_{a\beta T}} \prod_{i=1}^{T} E_i^{\beta a/2} e^{-\beta E_i/2} \prod_{1 \le j < p \le T} |E_p - E_j|^\beta,$$

where $a = N - T + 1 - 2/\beta$, $W_{a\beta T}$ is a normalization constant and $\beta = 1, 2, 4$ is the Dyson index.

1.3.5 Level fluctuations in quantum chaos and RMT

Initially only used in the study of the spectra of complex nuclei, RMT received a boost with regard to applicability in 1984, due to a conjecture put forth by O. Bohigas, M. J. Giannoni, and C. Schmit [77] (known as the BGS Conjecture), according to which RMT should be applicable to *all* chaotic quantum systems, and not just complex systems as previously thought, making a fine distinction between complexity and chaos in the context of quantum mechanics.

To understand the gist of the BGS Conjecture, it is necessary to take a few steps back to examine Wigner's original idea, as applied to the spectra of complex nuclei. Beyond the hydrogen atom, there does not exist an analytical solution for the Schrodinger equation, that would predict the energy of any given state in the spectrum. In the atomic nucleus the nuclear shell model is successful to a certain extent, in that it provides a good first approximation for many calculations. Beyond the low-lying levels, and for increasing number of nucleons however, the observed spectrum is considered chaotic and analytical predictions cannot be made. However, fluctuations in the energy levels follow a characteristic distribution, as observed by Wigner. For an ordered set of energy levels $E_1 \leq E_2 \leq E_3 \cdots$, the spacings between the energy levels are given by $s_i = E_{i+1} - E_i$, for $i = 1, 2, 3 \cdots$. Sequences of spacings coming from different nuclei were all observed to have the same distribution, characterized by what has now come to be known as 'level repulsion'. That is, there is zero probability of having degeneracies in the spectrum, as consecutive levels 'repel' each other. The notion of level repulsion has come to characterize the spectra of different kinds of quantum chaotic systems, and this is where the connection to RMT become more tangible.

In 1956, Wigner derived a form for the distribution of spacings between consecutive levels [78] by considering a 2×2 Gaussian random matrix with real elements, resulting in what is now popularly known as the Wigner surmise, which has the form

$$P(s) = \frac{\pi}{2} s e^{-\frac{\pi s^2}{4}},$$

where $s = E_2 - E_1$ is the spacing between the eigenvalues of the 2×2 matrix. The surmise is an excellent approximation for the distribution of spacings for the eigenvalues of an $N \times N$ matrix, even for large N.

In general, for a given ordered level sequence $E_1, E_2, \cdots, E_N$, the spacings between consecutive eigenvalues is defined as $s_i = E_{i+1} - E_i, i = 1, 2, ..N - 1$, and the Wigner surmise takes the form

$$P(s) = A_\beta s^\beta e^{-B_\beta s^2}. \tag{1.9}$$

Here β can take the values $1, 2$ and 4, indicating the class of random matrices to be considered. The values of $A(\beta)$ and $B(\beta)$ are given by $A(\beta) = 2\frac{\Gamma^{\beta+1}(\beta+2)/2)}{\Gamma^{\beta+2}(\beta+1)/2)}$ and $B(\beta) = \frac{\Gamma^2(\beta+2)/2)}{\Gamma^2(\beta+1)/2)}$. The factor s^β in the above equation denotes the nature of the level repulsion, and it is observed to be linear, quadratic or quartic depending on the value of β.

With this information, the essence of the BGS Conjecture can be put forth as follows: The spectra of time reversal invariant quantum systems having classically chaotic counterparts show the same spectral fluctuations as GOE matrices. This correspondence was later extended to GUE and GSE matrices as well. Though not rigorously proved, this conjecture has been found to be valid in a host of physical systems, with semiclassical methods emerging from the works of M. Gutzwiller and M. V. Berry, that work towards justifying this conjecture, and producing formulae for calculating eigenvalues of a given system.

In the integrable limit, the distribution of spacings has the form

$$P_P(s) = e^{-s}, \tag{1.10}$$

and hence the spacing distribution for integrable systems is referred to as Poissonian. This is the essence of the Berry-Tabor Conjecture [79], and this feature, where the probability of occurrence of degeneracies is the highest, is called level clustering. However, the effect of symmetries on the spectra of quantum chaotic systems will be discussed in Chapter 4, where Poisson statistics are seemingly obtained even

when the system exhibits chaos.

The level spacing distribution continues to be the most popular estimator of spectral fluctuations. However, the local density of states is a factor that has to be figured into the calculations, in order to treat spacings from disparate systems on an equal footing, as it is usually energy-dependent. Thus, the mean level spacing is renormalized to 1 via a process called *unfolding*. The idea behind unfolding is that energy levels should be rescaled such that it maps the spectrum to a constant local density of states. However, unfolding is often cumbersome, ambiguous and system-specific.

To overcome this drawback, a new quantity, the ratio of spacings has recently been proposed as an alternative. The local density of states becomes immaterial when considering ratios, and hence does not require unfolding. Spacing ratios are calculated as $r_i = s_{i+1}/s_i, i = 1, 2, \ldots$ where s_i is the spacing between eigenvalues as defined above.

The RMT averages for the spacing ratios, drawn from three standard random matrix ensembles with $\beta = 1, 2$ and 4 corresponding to GOE, GUE and GSE respectively, have been obtained as [80, 81],

$$P(r, \beta) = C_\beta \frac{(r + r^2)^\beta}{(1 + r + r^2)^{1 + \frac{3}{2}\beta}}, \tag{1.11}$$

where $C_\beta = \frac{3^{3(1+\beta)/2}\Gamma(1 + \frac{\beta}{2})^2}{2\pi\Gamma(1+\beta)}$ is a constant that depends on β.

The integrable limit for this quantity can be trivially obtained by determining the distribution of the quotient of two Poisson-distributed random variables (level spacings of integrable systems are uncorrelated), and has the form

$$P_P(r) = \frac{1}{(1 + r)^2}. \tag{1.12}$$

This quantity, the ratio of spacings is the primary object of study in this thesis, and several variants have been discussed in the context of RMT as well as quantum chaos. But first, it must be noted that the above results for distribution of spacings

and spacing ratios have been derived for the Gaussian ensembles, but hold good for Circular and Wishart ensembles as well, in the limit of large matrix dimensions, though this has not been proved. This correspondence will be carried over in some of the results presented.

1.4   Thesis Outline

The plan of the thesis is as follows:

- In Chapter 2, localization in quantum chaotic systems is discussed, and the effect of localized states on the corresponding spectra is studied by considering the ratio of spacings, where one of the spacings involves a localized state. A basic RMT model is proposed to simulate the interaction between a localized state and its nearest neighbors, and analytical expressions for the distribution of these special kinds of ratios are derived for systems with and without time reversal symmetry. The analytical and numerical (RMT) results are tested on some of the systems described earlier in this chapter, and the importance of the estimation of these ratios is discussed. These results have been published in Ref [82].

- In Chapter 3, the concept of spacing ratios is generalized to higher orders, and a functional form is proposed for the higher order spacings, with compelling numerical evidence provided for this formula, in terms of random matrices as well as physical systems, with even experimentally observed spectra following the proposed form for ratios. Here, Gaussian, Circular as well as Wishart random matrices are studied, and physical systems from each of these classes are discussed as well. Also, the proposed formula involves a scaling relation with respect to the Dyson index β, and it is conjectured that the index may be generalized to any positive integer. The higher order ratios could also prove to be a useful probe of spectral correlations at larger energy scales. The results have been published in Refs. [83] and [84].

- In Chapter 4, another scaling relation involving higher order spacing ratios is proposed, this time for superpositions of independent spectra. This relation is shown to be useful in determining the number of discrete symmetries or irreducible representations present in the Hamiltonian of a given level sequence. This idea has been justified by considering superpositions of random matrices, and has been tested on quantum chaotic systems that have not undergone symmetry reduction. The relation proposed here is interesting not only in the framework of RMT, but has direct consequences in the measurement of correlations in observed spectra. These results are under review and the corresponding manuscript may be found in Ref. [85].

- Chapter 5 summarizes and concludes the work in the thesis, and provides some future perspectives for the results presented.

CHAPTER 2

Exact distribution of spacing ratios for random and localized states in quantum chaotic systems

The existence of regular and chaotic regions in the classical phase space of a chaotic system affects the spectral statistics of the corresponding quantum version. The generic eigenstates of the quantum system display uniform probability density, except for feature-less fluctuations, and consecutive eigenvalues of these generic states states tend to repel one another in accordance with the Bohigas-Giannoni-Schmidt conjecture. The spectral statistics for such levels is given by the Wigner surmise for nearest neighbor level spacings and level spacing ratios. Physically, this reflects the underlying irregular dynamics of a typical classical trajectory in agreement with the correspondence principle.

However, a subset of eigenstates selectively display pronounced enhancements of probability density, effectively localizing in configuration or momentum space. Such sub-sequences of levels are commonly encountered in quantum chaotic systems with mixed classical phase space as well as in atomic and nuclear spectra [66, 86, 87]. Some classes of localized states can be identified with the regular regions in classical phase space, although in general they could occur even in the

19

absence of stable classical structures. Their corresponding eigenvalues are uncorrelated and the level spacing statistics are of the Poisson type.

These represent two limiting kinds of behavior, and in a mixed quantum system (one which has both regular and chaotic regions in the classical phase space), the existence of eigenvalues of both types leads to the level statistics having a form intermediate to the Poisson and Wigner distributions. The question now arises about whether or not there exists some kind of level repulsion between these two types of eigenvalues. If the localized states do interact with their neighboring chaotic states, how can this be modeled? The answers to these questions form the basis of this chapter, where we have proposed a single-parameter 3×3 random matrix model for this interaction, and derived an analytical form of the corresponding distribution. We have then tested it on various physical systems that display localized eigenmodes, considering both time-reversal-invariant and non-invariant scenarios.

2.1 Localization in quantum chaos

Localized states in quantum chaotic systems could have several physical origins. They could be induced by classical dynamical structures like periodic orbits, or by dynamical effects like wavefunction interference. The most prominent examples of the latter are the localization of a single-particle wavefunction in the presence of a disordered potential, called Anderson localization, and its many-body analogue, called many-body localization. The theoretical paradigm here is the standard kicked rotor, and its localization properties have been well-investigated. In many-body systems like nuclei, localization is a consequence of several complex interactions occurring in the system. Localization of this type has been studied in condensed matter systems, cold atom, billiards, optical systems and several other physical systems.

The presence of classical structures could also cause localization and can be explained based on semiclassical approaches. For a quantum eigenfunction having an enhanced intensity in the vicinity of stable periodic orbits, like the bouncing ball

modes in billiards, localization is accounted for, by considering the semiclassical theory of integrable systems. However, this probability density enhancement is considered anomalous if it occurs due to unstable periodic orbits, as these orbits cover all of the classical phase space eventually, retaining no memory of their short-time behavior. This phenomenon is called 'scarring' [88], and was first discovered experimentally in billiards [31], and a semiclassical explanation for its occurrence was found in due course [89, 90].

Since then, localized states have been experimentally observed in a variety of chaotic systems including deformed microcavity lasers [17, 91–93], quantum well with chaotic electron dynamics [94] and hydrogen atom in strong external fields [95–98]. Recently, scarring localization was also reported in Dirac Fermions [99], strongly doped quantum wells [100], driven spin-orbit coupled cold atomic gases [101], a chaotic open quantum system [102] and in an isomerizing chemical reaction [103–105]. Further, localized modes appear in spectral graph theory in relation to random graphs [106, 107].

In a semiclassical sense, localized states are associated with short time periodic orbits with time scales much shorter than the Heisenberg time $t_H \sim \hbar/\Delta$, where Δ is the mean level spacing. This is reflected in their spectral properties, with localized states not interacting with each other and essentially behaving like eigenstates of integrable systems. Their presence in a chaotic spectrum, however, causes deviation from the standard Wigner surmise, and there have been several attempts to quantify this deviation. The most popular approach in this direction, is the Brody distribution [108], which is a straightforward attempt to interpolate between the two extremes of the Poisson and Wigner distributions. The Brody distribution has the form

$$P(s) = (q+1)a_q s^q \exp\left(-a_q s^{q+1}\right), \qquad (2.1)$$

where

$$a_q = \left[\Gamma\left(\frac{q+2}{q+1}\right)\right]^{q+1}.$$

Here, $\Gamma(q)$ is the Euler's gamma function, and the parameter $0 \leq q \leq 1$, called the

Brody parameter, and was later shown to be related to the fraction of irregular component of classical phase space. For $q = 0$, $P(s)$ has the form of the Poisson distribution and represents integrability, and $q = 1$ takes $P(s)$ to the Wigner distribution which implies that the system is completely chaotic. Although phenomenological, this approach is popular by virtue of its success when applied to different systems. Other approaches by Izrailev [109], and Berry and Robnik [110], though having a stronger physical foundation, have not found the same level of success. However, the Brody distribution does not take into account the statistical weight of generic and localized states, the latter occurring sparsely in most mixed systems, and also less frequently in higher energy ranges. Thus, using it to quantify the correlation between generic and localized states, may lead to the desired correlation signal getting masked by the sheer statistical weight of the generic states. But it is important to note that the mere existence of several such methods indicates the presence of nontrivial correlations between the two kinds of states in the spectrum.

The most direct method of probing this correlation is by considering only the spacings between localized states and their nearest generic neighbors, and obtaining a probability distribution for these kinds of spacings. It is reasonable to assume that if the localized states are more and more strongly correlated with their neighbors, the distribution should eventually converge to the Wigner surmise. To this end, a simple random matrix model is proposed here to locally account for the interaction between localized and generic states. The ratio of spacings is the most suitable quantity to investigate this since unfolding becomes an even more ambiguous process here in this case. A 3×3 model is considered, from which three eigenvalues may be obtained to get two spacings and hence one spacing ratio. Any of of these three eigenvalues may be considered to be localized.

The main motivation behind the random matrix model can be inferred from Fig. 2.1. A short sequence of energy levels of stadium billiards is displayed in Fig. 2.1(a) with localized states indicated by dashed lines. In Fig. 2.1(b) two pairs of consecutive eigenstates $|\Psi(x, y)|^2$ are shown; (i) consecutive generic states (the k-th and $(k + 1)$-th states, and we call the corresponding level spacing s_{gg} to be of g-g
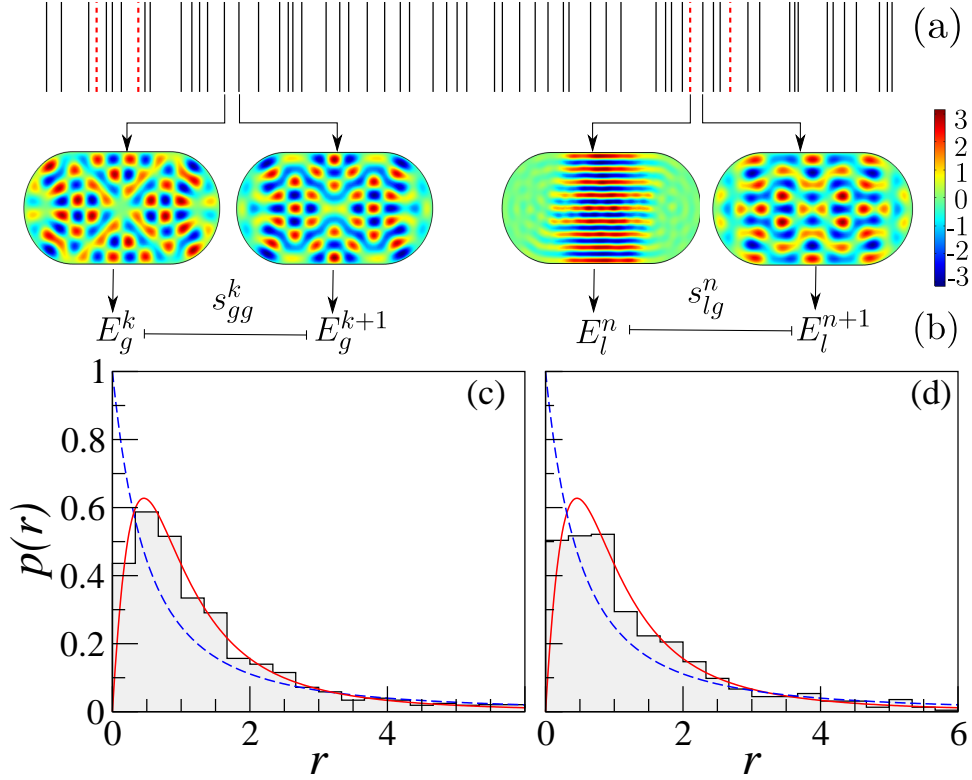
Figure 2.1: (a) Energy levels of stadium billiard. Localized levels are marked in dashed (red) lines. A g-g type and g-l type spacing is shown. (b) Two consecutive generic eigenstates (state numbers 200 and 201), and two consecutive states (245 and 246) (a generic state next to a localized state). (c) distribution of spacing ratios for g-g type spacings, (d) distribution of spacings for g-l type spacings. The red (solid) and blue (broken) lines are the standard results for $p_W(r)$ and $p_{poisson}(r)$ respectively.

type and (ii) localized and its nearest neighbor generic state (the n-th and $(n+1)$-th states) with spacing s_{gl} of g-l type.

2.2 Random Matrix Model

Consider a chaotic quantum system whose Hamiltonian operator is $\widehat{H}$ and its energy spectrum is E_i, where $i = 1, 2, ...$ denotes the state number. The usual approach is to analyze all the level spacings in the spectrum. In contrast, in this work, we focus on the spacings s_{gl} between generic and localized states (Fig. 2.1(b)) defined as follows. From a sequence of consecutive energy levels $E_{k-1} < E_k < E_{k+1}$, where

one of them corresponds to a localized state, two spacings, $s_k = E_k - E_{k-1}$ and $s_{k+1} = E_{k+1} - E_k$, and hence one spacing ratio $r_k = s_k/s_{k+1}$ may be obtained, where at least one of the spacings is of the g-l type. Figure 2.1(c) shows the distribution of spacing ratio $p(r)$ obtained using only the generic levels (g-g type spacings) and in Fig. 2.1(d) for spacings involving a localized state (g-l type). For g-g type spacings, agreement with Wigner-type surmise

$$p_W(r) = C_\beta \frac{(r + r^2)^\beta}{(1 + r + r^2)^{1+(3/2)\beta}} \tag{2.2}$$

(with $\beta = 1$ and $c_\beta = \frac{27}{8}$ for GOE, and $\beta = 2$ and $c_\beta = \frac{81\sqrt{3}}{4\pi}$) is clearly evident whereas the g-l type spacings show marked, though weak, deviation from $p_W(r)$. Hence, the Hilbert space around a localized eigenstate can be locally modeled as a 3×3 Hamiltonian matrix.

Thus, we are led to consider an ensemble of 3×3 real-symmetric (for $\beta = 1$) or complex-Hermitian (for $\beta = 2$) random matrices H from the probability measure

$$\mathcal{P}(H) \, d[H] \propto \exp\left(-\frac{\beta}{2} \operatorname{tr} \Sigma^{-2} H^2\right) \, d[H]. \tag{2.3}$$

where 'tr' represents trace, and $d[H]$ represents the product of differentials of all the independent parameters in the matrix elements, and $\Sigma = \operatorname{diag}\left(1, 1, \sqrt{\frac{k^2}{2-k^2}}\right)$. Within the framework of Eq. 2.3, the random matrix is of the form

$$\mathbf{R_3} = \begin{bmatrix} H_{11} & H_{12} & H_{13} \\ H_{12} & H_{22} & H_{23} \\ H_{13} & H_{23} & H_{33} \end{bmatrix} \tag{2.4}$$

where, $0 \le k^2 < 2$, and k is a parameter that represents the strength of coupling between a 2×2 (Gaussian Orthogonal Ensemble(GOE) or Gaussian Unitary Ensemble(GUE)) block and a 1×1 block representing a localized state. For systems with time-reversal symmetry (TRS), i.e., $\beta = 1$, the matrix elements are drawn from

independent Gaussian distributions with mean zero and variances given as

$$\langle H_{11}^2 \rangle = \langle H_{22}^2 \rangle = 1, \quad \langle H_{33}^2 \rangle = \left(\frac{k^2}{2 - k^2} \right),$$

$$\langle H_{12}^2 \rangle = \frac{1}{2}, \quad \langle H_{13}^2 \rangle = \langle H_{23}^2 \rangle = \frac{k^2}{2}. \tag{2.5}$$

For $\beta = 2$, corresponding to the broken time-reversal symmetry (TRSB) case, the matrix elements are Gaussian distributed with mean zero (real and complex for diagonal and off-diagonal), and variances given as

$$\langle H_{11}^2 \rangle = \langle H_{22}^2 \rangle = \frac{1}{2}, \quad \langle \mathrm{Re}(H_{12})^2 \rangle = \langle \mathrm{Im}(H_{12})^2 \rangle = \frac{1}{4},$$

$$\langle \mathrm{Re}(H_{13})^2 \rangle = \langle \mathrm{Im}(H_{13})^2 \rangle = \frac{k^2}{4},$$

$$\langle \mathrm{Re}(H_{23})^2 \rangle = \langle \mathrm{Im}(H_{23})^2 \rangle = \frac{k^2}{4},$$

$$\langle H_{33}^2 \rangle = \frac{1}{2} \left(\frac{k^2}{2 - k^2} \right). \tag{2.6}$$

Physically, $0 \leq k \leq 1$ indicates the strength of correlation between localized and generic states. Thus, $k << 1$ implies strong localization effects and might require semiclassical methods to understand its physical mechanism. On the other hand, $k \approx 1$ implies negligible localization and RMT framework would be a suitable model. As $k \to 1$, the 3×3 matrix tends to that of standard Gaussian ensembles. In physical systems the localized and generic states are generally weakly coupled and we anticipate the coupling strength to be weak, i.e., $k \ll 1$. Hence, this weak coupling limit is the main regime of interest in this work. In this limit, H becomes the direct sum of a 2×2 GOE or GUE matrix (for $\beta = 1, 2$, respectively) and 0, the latter being also one of the eigenvalues and it notionally corresponds to the localized state.

It may be noted that similar matrix models have been used to model effects like chaos-assisted tunneling (see Ref. [111]), wherein locally, the system considered may be modeled using a three-level mechanism with the energy levels corresponding to two chaotic and one localised state. These states are identified with regions

of classical phase space that contain regular and chaotic regions. In this case, however, we show that the matrix model may be used even in the absence of a classical analogue, as in the case of the Sm atom which will be discussed in 2.4.3.

2.3 Distribution of spacing ratios: Analytical results

The main result of the chapter, namely, the distribution $p(r)$ of spacing ratios r for the random matrix model defined in Eqs. (2.3-2.6), is obtained analytically in this section for the cases of $\beta = 1$ and $\beta = 2$.

2.3.1 $\beta = 1$ case

To derive an expression for $p(r)$, firstly the joint probability density of the eigenvalues $\{\lambda\}(\equiv \lambda_1, \lambda_2, \lambda_3)$ of the matrix model in Eq. (2.3) is obtained as

$$P(k; \{\lambda\}) \propto |\Delta(\{\lambda\})| \int_{O_3} d\mu(O) \, e^{-\mathrm{tr}\Sigma^{-2} O^T \Lambda^2 O}, \qquad (2.7)$$

where $\Lambda = \mathrm{diag}(\lambda_1, \lambda_2, \lambda_3)$, $\Delta(\{\lambda\}) = |(\lambda_2 - \lambda_1)(\lambda_3 - \lambda_1)(\lambda_3 - \lambda_2)|$ is the Vandermonde determinant and $d\mu(O)$ represents the Haar-measure over group O_3 of 3×3 orthogonal matrices with T being the transpose.

To calculate the ratio of consecutive spacings r we order them as $-\infty < \lambda_1 \leq \lambda_3$, $-\infty < \lambda_3 < \infty$, and $\lambda_3 \leq \lambda_2 < \infty$. Then, $r = (\lambda_2 - \lambda_3)/(\lambda_3 - \lambda_1)$. Moreover, the joint probability density for the ordered eigenvalues is given by $\widetilde{P}(k; \lambda_1, \lambda_2, \lambda) = 3! P(k; \lambda_1, \lambda_2, \lambda)$, where the intermediate eigenvalue $\lambda_3 = \lambda$.

Introducing $x = \lambda - \lambda_1$ and after some calculations whose details are in Appendix A, the distribution of r can be obtained as,

$$p(k; r) = \frac{\sqrt{2 - k^2}}{\pi k^3} r(r+1) \int_{-\infty}^{\infty} d\lambda \int_0^{\infty} dx \int_0^{\frac{\pi}{4}} d\phi x^4 \cos \phi$$

$$e^{-\frac{(2+k^2)}{2k^2}\lambda^2 + \frac{1}{2}\left[\left(\frac{1}{k^2}-1\right)\cos 2\phi + 1\right]\left[2\lambda^2 - (\lambda - x)^2 - (\lambda + rx)^2\right]}$$

$$\times I_0\left(\frac{x}{2}\left(\frac{1}{k^2} - 1\right)(r+1)[2\lambda + (r-1)x]\cos 2\phi\right). \qquad (2.8)$$

As $k \to 1$, the correct GOE result $p(1; r) = \frac{27}{8} \frac{r^2+r}{(r^2+r+1)^{5/2}}$ is recovered as originally obtained in Ref. [80]. The limiting case $k \to 0$, relevant for the localized states of chaotic systems, is difficult to obtain using Eq. (2.8). However, starting from the joint probability density for $k = 0$ case, it is directly obtained as

$$p(0; r) \;\; = \;\; \frac{1}{2\sqrt{2}} \left[\frac{(r+1)}{(r^2+1)^{3/2}} + \frac{1}{(2r(r+1)+1)^{3/2}} + \frac{r}{(r(r+2)+2)^{3/2}} \right] \tag{2.9}$$

In particular, note that $p(0; r)$ is different from $p_{poisson}(r) = \frac{1}{(1+r)^2}$ obtained for the case of uncorrelated levels with Poisson spacing distribution [112].

2.3.2 $\beta = 2$ case

For $\beta = 2$, the joint probability density of (unordered) eigenvalues turns out to be

$$P(k; \lambda_1, \lambda_2, \lambda_3) \propto \Delta^2(\{\lambda\}) \int_{\mathcal{U}_3} dU \exp\left(-\Sigma^{-2} U \Lambda^2 U^\dagger\right). \tag{2.10}$$

In this case, the unitary group integral can be performed using the Harish-Chandra-Itzykson-Zuber formula [113, 114],

$$\int_{\mathcal{U}_N} dU \exp\left(-s\, \mathrm{tr}\, X U Y U^\dagger\right) = \prod_{m=1}^{N-1} m! \cdot \left(-s\right)^{-N(N-1)/2}$$

$$\times \frac{\det\left[\exp(-s\, x_j y_k)\right]_{j,k=1,\dots,N}}{\Delta(\{x\})\Delta(\{y\})}. \tag{2.11}$$

Here, dU is the Haar measure on unitary group $\mathcal{U}_N$, and $X = \mathrm{diag}(x_1, ..., x_N)$, $Y = \mathrm{diag}(y_1, ..., y_N)$.

After some calculations whose details may be found in Appendix A, the distri-

bution of the ratio of spacings can be obtained as

$$p(k; r) = \frac{\sqrt{2 - k^2}}{4\pi k(1 - k^2)^2} r(r + 1) \sum_{j=1}^{3} \left[\frac{b_j(5a_j^2 + 2b_j^2)}{a_j^4(a_j^2 + b_j^2)^2} + \right.$$
$$\frac{3}{(a_j^2 + b_j^2)^{5/2}} \sinh^{-1}\left(\frac{b_j}{a_j}\right) - \frac{c_j(5a_j^2 + 2c_j^2)}{a_j^4(a_j^2 + c_j^2)^2} -$$
$$\left. \frac{3}{(a_j^2 + c_j^2)^{5/2}} \sinh^{-1}\left(\frac{c_j}{a_j}\right) \right]. \tag{2.12}$$

The forms of a_j, b_j and c_j for $j = 1, 2, 3$ (which are functions of k and r) are rather unwieldy and is shown in Appendix A. In the limit $k \to 0$, the exact result is obtained as

$$p(0; r) = \frac{1}{\pi} \left[\frac{r^2}{(r(r + 2) + 2)^2} + \frac{r(r + 2) + 1}{(r^2 + 1)^2} + \frac{1}{(2r(r + 1) + 1)^2} \right]. \tag{2.13}$$

As anticipated, when $k \to 1$, the distribution in Eq. (2.12) coincides with the GUE result, obtained in Ref. [80], namely, $p(1; r) = \frac{81\sqrt{3}}{4\pi} \frac{(r^2 + r)^2}{(r^2 + r + 1)^4}$.

2.4 Numerical results

2.4.1 Identification of localized states

Localization is determined by examining the individual eigenstates which are expanded in a given basis, as, by definition, it implies a preferential occupation of a few basis states. For example, in the 3×3 model, if $k = 0$, $\mathbf{R}_3$ is block diagonal; one 2×2 block with eigenvalues λ_1, λ_2 and a 1×1 block with eigenvalue λ_3. The eigenvector corresponding to $\lambda_i, (i = 1, 2, 3)$, is $(a_{i,1}, a_{i,2}, a_{i,3})$. The eigenvalue whose eigenvector is $(0, 0, 1)$ is far from a generic state and hence can be called 'localized' eigenvalue for our purposes.

Of the methods used to determine whether a given state is localized or not, the participation ratio (or its inverse), and entropy measures [115, 116] are the most popular. Of these, in this chapter, information entropy [117, 118] is used to determine

localized states both for the RMT simulations as well as for the physical systems discussed.

For an eigenstate $|\psi_i\rangle$, which can be expanded in terms a given finite basis set $|\phi_j\rangle$, such that $|\psi_i\rangle = \sum_{j=1}^{N} a_{i,j} |\phi_j\rangle$, the corresponding information entropy is given by

$$S_i = -\sum_j |a_{i,j}|^2 \ln |a_{i,j}|^2. \tag{2.14}$$

As an illustration, the calculated information entropy for 2000 states of the coupled quartic oscillator (which were determined in the basis of the uncoupled quartic oscillator), is shown in Fig. 2.2(a) as a function of the energy level of the corresponding state. Fig. 2.2(b) shows an enlarged portion of (a),consisting of 175 states, out of which 4 may be identified as localized.

It may be noted that for stadium billiards, the most strongly localized states correspond to the bouncing ball modes, although other kinds of localized states like the bow-tie modes also exist in the spectrum. In the calculation presented here, there is no differentiation made between the classes of localized states.

In practice, for most physical systems which display localized states, adiabatic methods can estimate the energies of localized states without computing the eigenvectors and information entropy. Such results exist for quartic oscillator [119, 120] and stadium billiards [121].
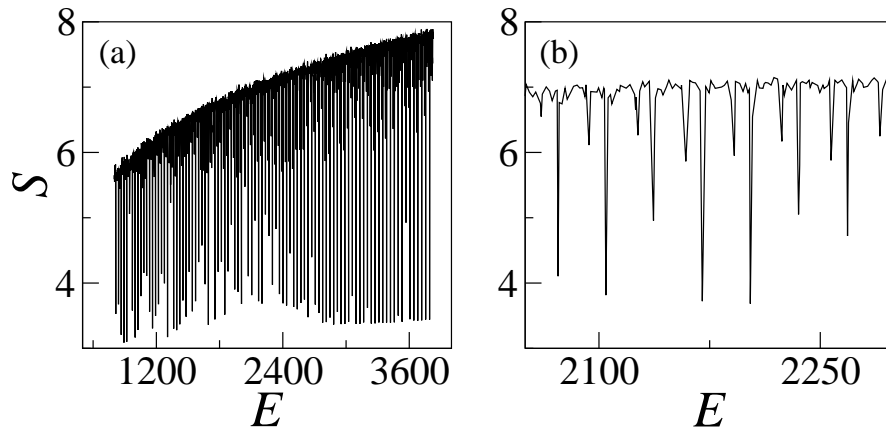
Figure 2.2: (a) Information entropy(S) as a function of energy(E) for the coupled quartic oscillator system at α=90. The eigenstates having magnitude of information entropy $\lesssim 5.5$ can be identified as localized states. For the bulk of chaotic states that form the envelope, value of S is consistent with the random matrix average for the information entropy (not shown here). (b) Enlarged view of a portion of (a), consisting of 175 states, out of which 4 may be considered to be localized.

2.4.2 Random Matrix Model: Numerical results
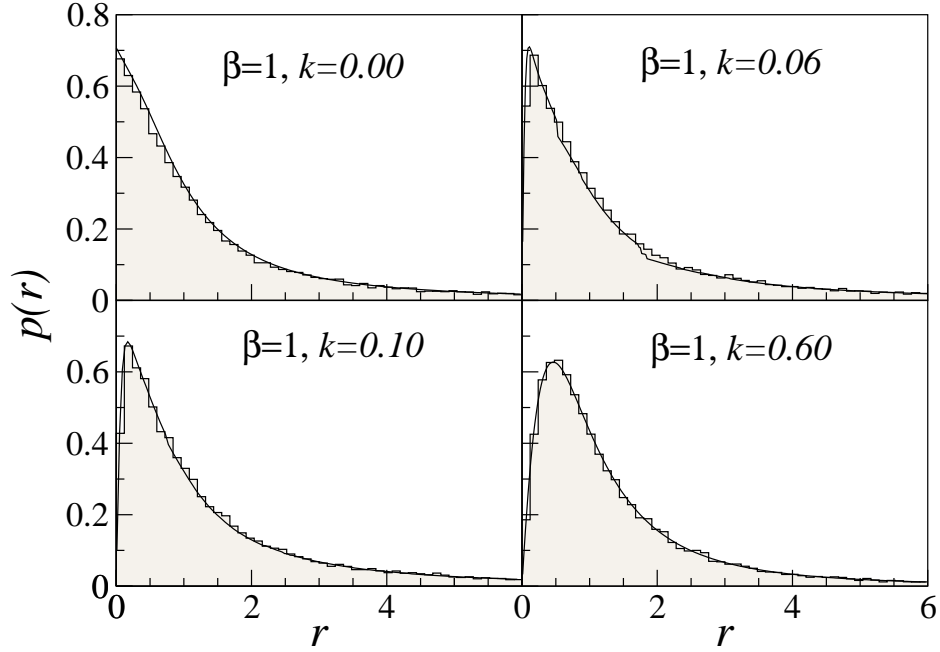
Figure 2.3: Spacing ratio distribution, for g-l type spacings for $\beta = 1$, obtained from random matrix simulations of 3×3 random matrices (histogram) compared with analytical $p(r)$ (black line).

In Figs.2.3-2.4, the analytically obtained $p(r)$ in Eqs. (2.8) and (2.12) is compared with the results obtained by simulating an ensemble of 3×3 random matrices $\mathbf{R}_3$ following the prescription in Eqs. (2.3) and (2.5). The numerical simulations are performed by generating matrix elements with prescribed mean and variances. The eigenvalue corresponding to a localized state is identified using the information entropy of the eigenstate. If λ is the eigenvalue of the localized state, then the spacing ratio is calculated as either $r = (\lambda - \lambda_2)/(\lambda_2 - \lambda_1), r = (\lambda_3 - \lambda)/(\lambda - \lambda_1)$, or $r = (\lambda_3 - \lambda_2)/(\lambda_2 - \lambda)$, depending on whether the localized state corresponds to λ_3, λ_2 or λ_1 respectively.

It may be observed that as $k \to 1$, the analytically obtained $p(r)$ tends towards the Wigner surmise corresponding to $\beta = 1$ and 2, as given by Eq. 2.2.
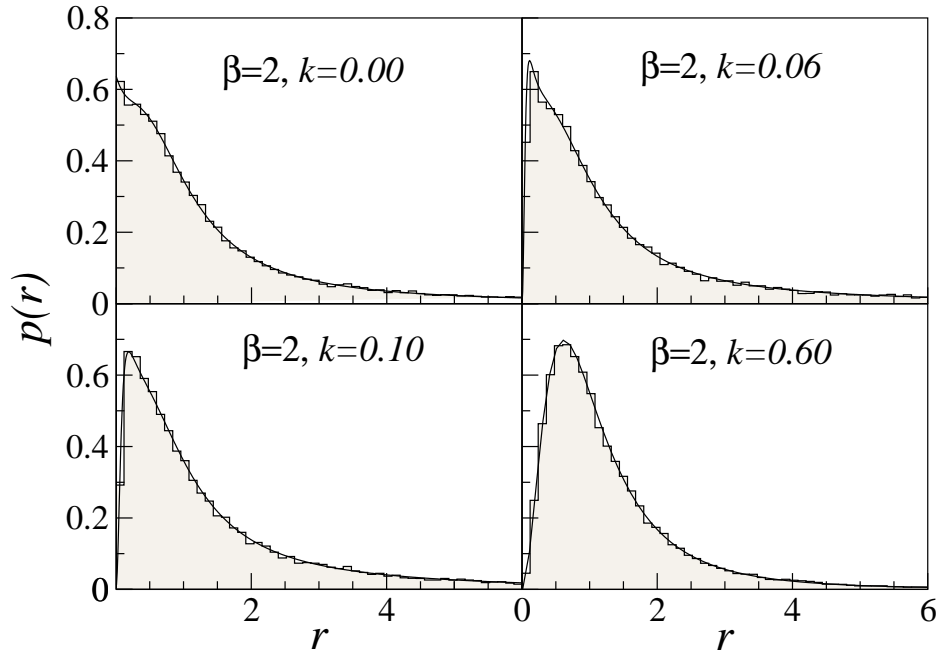
Figure 2.4: Spacing ratio distribution, for g-l type spacings for $\beta = 2$, obtained from random matrix simulations of 3×3 random matrices (histogram) compared with analytical $p(r)$ (black line).

2.4.3 Applications to Physical Systems

The spacing ratio distribution for g-l type spacings is obtained for Hamiltonian systems whose classical limit is chaotic and hence their spacings are Wigner distributed, $P_W(s)$. The systems chosen for illustration are (i) the coupled quartic oscillator, (ii) computed levels of Sm atom, and (iii) stadium billiards ($\beta = 1$ and $\beta = 2$ variants). All of them contain localized eigenstates in their spectrum. The computed distribution for g-l type spacing ratios agrees with the analytical results and in this k is treated as a fitting parameter.

Coupled Quartic Oscillator

In Fig. 2.5(a), the results are displayed for the coupled quartic oscillator, with $\alpha = 90$, such that the classical phase space is largely chaotic, with small regular regions due to the presence of a series of periodic orbits studied in detail in Ref [119]. This is manifested in the corresponding quantum system as localized eigenstates, which are identified using information entropy. In Fig. 2.5(a), the computed distribution

of g-l type spacings for coupled quartic oscillator displays a good agreement with the analytical result shown in Eq. 2.8 with $k \approx 0.2$.

As an independent verification, the variance of the off-diagonal elements of the Hamiltonian operator locally around every localized state was calculated. By comparing with the form of the variance obtained from the 3×3 model, these estimates were used to extract the value of k, and they were found to be in agreement with each other to within 30% error.

Sm atom (Atomic number 62)

Lanthanide atoms, like Samarium (Sm) have been studied in the context of chaos and localization, using the multi-configuration Dirac-Fock method to compute their spectra and identify localized states. Localization in this context, is known to occur due to strong Coulomb mixing between configuration state functions having similar occupancy numbers of their subshells [122, 123]. The energy levels of Sm exhibit complex configuration and mixing and were computed in Ref. [122] using General-purpose Relativistic Atomic Atomic Structure Package or GRASP code [124]. Figure 2.5(b) shows $p(r)$ for g-l type spacings in the computed levels of the Sm atom. The computed histogram of g-l type spacing ratios agree with $p(r)$ for $k \approx 0.3$.
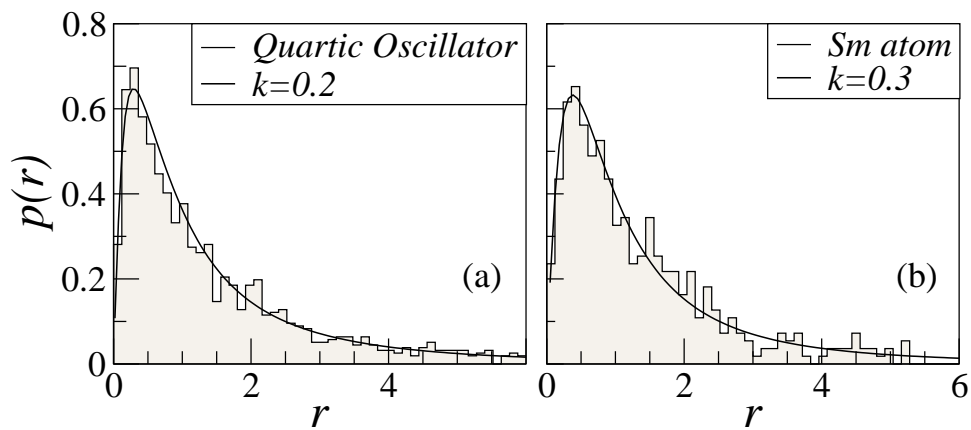
Figure 2.5: Spacing ratio distribution, for g-l type spacings, obtained from systems whose classical limit is chaotic. Histograms are obtained from spectrum computed for (a) quartic oscillator and (b) levels of Sm from ab-initio calculations. The solid (black) line is the fit obtained using the analytical relation in Eq. (2.8).

Quantum Billiards with and without time-reversal symmetry

The ratio distribution $P(r)$ for quarter stadium billiards is shown in Fig. 2.6(a,b), respectively, for TRS and TRSB cases. Since the class of localized states the can occur depends on the shape of the billiard, same kinds of localized modes are observed in both the TRS and TRSB cases. The bouncing ball modes, which correspond classically to a particle undergoing successive reflections between the two parallel walls of the stadium, form a prominent class of localized modes, although other kinds of localized states occur in the spectrum as well.

In general, depending on the shape, a variety of localized states may exist, including bow-tie modes (whose name indicates the form of the underlying periodic orbit), whispering gallery modes (which are confined to the walls of the billiard) as well as general polygonal modes.

In Fig. 2.6(a), the simulated histogram of g-l type spacing for billiards agrees with the analytical result in Eq. (2.8) for $k \approx 0.4$.

In order to compute the g-l type spacings, firstly the eigenspectrum of this system was computed. Then, using the computed eigenvalues and normalized eigenvectors, i.e. the magnitude of the electric field E, the information entropy for each state is calculated using the relation $S_i = -\sum_j |E_{i,j}|^2 \ln |E_{i,j}|^2$, where j is the index for discretized position space. The localized states may be differentiated from the bulk of the chaotic states since the former have a significantly smaller magnitude of information entropy compared to the latter. Using the information entropy, the localized states are picked from the spectrum (as illustrated in Fig 2.2(b)), and the required ratio distribution is determined. The result for $p(r)$ is shown as histogram in Fig. 2.6(b) and it agrees with the analytical result (Eq. (2.12)) with $k \approx 0.2$.

2.5 Conclusion

A typical spectrum of a chaotic quantum system has generic and localized eigenstates occurring as neighbors. Physically, they represent two distinct limiting behaviors. The former is modeled by random matrix assumptions and the latter deviates
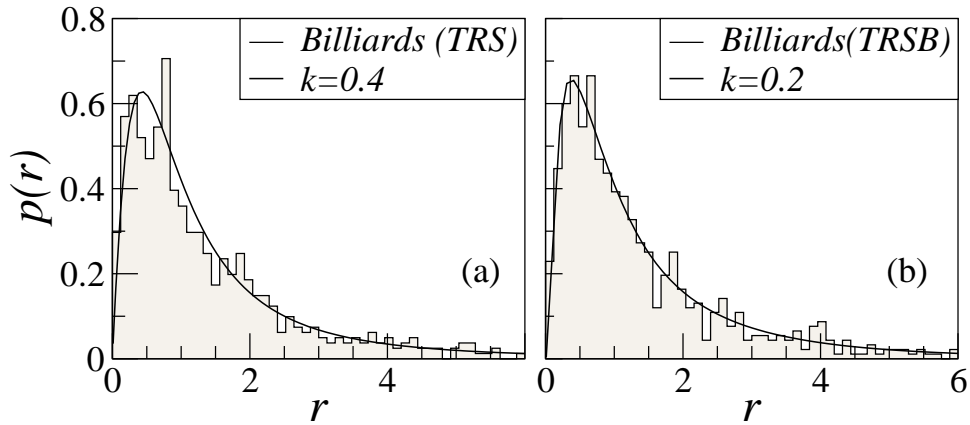
Figure 2.6: Spacing ratio distribution, for g-l type spacings, obtained from systems whose classical limit is chaotic. Histograms are obtained from spectrum computed for stadium billiards, with time-reversal symmetry (a) preserved ($\beta = 1$) and (b) broken ($\beta = 2$). The solid (red) line is the fit obtained using the analytical relation in Eqs. (2.8) and (2.12) for (a) and (b) respectively.

strongly from RMT based models. In this work, it is demonstrated that they display non-trivial correlations, quantified by the parameter k, the average strength of the Hamiltonian matrix element coupling these states. Physically, k is a measure of the strength of correlation between localized and generic states.

This is a robust characterization that remains unaffected by the semiclassical limit ($\hbar \to 0$) in contrast to the phenomenological approach such as Brody distribution which is often used to model the spectral transition from Poisson to GOE type statistics. In such an analysis, all the levels (localized and generic) are taken into account. Then, in the semiclassical limit of $\hbar \to 0$ or energy $E \to \infty$, localized modes ultimately would become a set of measure zero and the Brody distribution would nearly coincide with random matrix distributions. Hence, signatures of the localized states are masked by the large number of chaotic states. Thus, the Brody parameter being a single number representing this transition would become insensitive to presence of localized modes in the semiclassical limit. In the approach presented in this paper, since the spacings (by construction) always involve at least one localized mode, the estimated value of k remains unaffected by the semiclassical limit.

In summary, by considering a 3×3 random matrix model depending on a single

parameter k (representing the strength of the coupling between a generic and a localized eigenstate), we have obtained an exact result for the distribution of the spacing ratio between a generic and a localized state. The analytical results are in good agreement with numerically computed spectra that we have obtained from chaotic quantum systems such as billiards, coupled oscillator and atomic spectra. Quantum stadium billiard had been experimentally realized and hence the results presented here can be experimentally verified as well.

Higher-order spacing ratios in random matrix theory and complex systems

The nearest neighbor spacings and the spacing ratios are spacing measures that probe fluctuations in the spectral scales of the order of unit mean spacing. Long-range correlations in RMT are usually via quantities like the n-point correlation function, number variance and spectral rigidity, but their computation is usually not a trivial exercise. In many physical situations, knowledge of spectral fluctuations at larger spectral intervals is useful. For quantum chaotic systems with a classical limit, semiclassical theories [125] dictate that the higher-order spectral fluctuations would be related to short time periodic orbits, effectively acting as a probe of short time dynamics [11], at shorter than Heisenberg time-scale. The rare-region effects or Griffith effects [126] in the vicinity of many-body localization transition influences the transport and entanglement properties, whose time-scales can be probed by the higher-order spectral scales. In the study of empirical correlation matrices, RMT-based tools such as the nearest neighbor eigenvalue spacing and eigenvector distributions have been employed to extract the significant modes of variability present in such empirical correlations.

Thus we are led to consider the distribution of higher-order spacings and spacing ratios, as a potential probe for higher order fluctuations, owing to their popularity in the literature as well as their relative ease of computation, as opposed to the other probes for higher-order correlations mentioned above. In this chapter, we show that the higher-order spacing ratios exhibit a scaling relation with respect to the Dyson index β and the order of the spacing k considered. We provide ample numerical evidence from RMT simulations as well as examples from disparate physical systems and show that this scaling relation holds good for the Gaussian, Circular and Wishart random matrix ensembles as well as for physical systems corresponding to each of these.

While computing higher-order spacings or the spacing ratios, it must be noted that there is no unique way of defining the quantity in question. If higher-order spacings are to be computed for a sequence of ordered eigenvalues $E_1, E_2, E_3, \cdots$, the form is straightforward, given by

$$s_i^{(k)} = E_{i+k} - E_i \qquad i, k = 1, 2, \ldots \tag{3.1}$$

for the k-th order spacing, where $k = 1$ gives the NNSD. After unfolding, it is seen that the mean spacing $\langle s \rangle = k$. The higher-order spacings may also be rescaled such that $\langle s \rangle = 1$, in which case the unfolded spectrum is divided by $\langle s \rangle$.

The definition of higher spacing order ratios is more open to interpretation. By extension of the definition of higher-order spacings as given in Eq. 3.1, for a sequence of ordered eigenvalues $E_1, E_2, E_3, \cdots$, higher-order ratios may be defined as

$$r_i^{(k)} = \frac{s_{i+k}^{(k)}}{s_i^{(k)}} = \frac{E_{i+2k} - E_{i+k}}{E_{i+k} - E_i}, \qquad i, k = 1, 2, 3, \ldots . \tag{3.2}$$

In Eq. 3.2, going from r_i to r_{i+1} involves moving down the spectrum by one eigenvalue. It is also possible to define ratios where the r_{i+1} varies from r_i by k eigenvalues. For example, in the former case, we would have $r_1^{(2)} = (E_5 - E_3)/(E_3 - E_1)$ and $r_2^{(2)} = (E_6 - E_4)/(E_4 - E_2)$, whereas in the latter it would be defined as

$r_1^{(2)} = (E_5 - E_3)/(E_3 - E_1)$ and $r_2^{(2)} = (E_7 - E_5)/(E_5 - E_3)$. The difference between the two is of course that in the second case, a subset of all spacings are not included in the statistics, and should show the same behavior for large matrix dimensions.

An alternative definition of k-th order ratios has been given in Ref. [81] for *overlapping* ratios, where overlapping implies the existence of shared eigenvalues between the numerator and denominator of the ratio. Thus for the k-th overlapping ratio, there are k shared eigenvalues between the numerator and denominator. That is,

$$r_i^{(k)} = \frac{E_{i+k+1} - E_i}{E_{i+k} - E_{i-1}} \tag{3.3}$$

Throughout this thesis, we will use Eq. 3.2 to define higher-order ratios, and this will be used in all RMT numerics as well as for data obtained from quantum chaotic and other complex systems.

3.1 Scaling relation for the distribution of higher-order ratios

A Wigner-like surmise for the nearest neighbor spacing ratios gives

$$P(r, \beta) = C_\beta \frac{(r + r^2)^\beta}{(1 + r + r^2)^{1 + \frac{3}{2}\beta}}, \tag{3.4}$$

where $\beta = 1, 2, 4$ is the Dyson index for the matrix representation corresponding to the orthogonal, unitary and symplectic ensembles of random matrix theory. The form of this distribution has been proved for the Gaussian ensembles, but can be extended to the Circular and Wishart ensembles in the limit of large matrix dimensions. It is shown below that even for the higher-order spacing ratios, the form of the distribution is the same for these three classes of random matrices. In each case, compelling numerical evidence is provided, which demonstrate an elegant relation between the $k-$th order spacing ratio distribution $P^k(r, \beta)$ and the nearest neighbor

spacing ratio distribution $P(r, \beta')$:

$$P^k(r, \beta) = P(r, \beta'), \quad \beta = 1, 2, 4, \tag{3.5}$$

$$\beta' = \frac{k(k+1)}{2}\beta + (k-1), \quad k \geq 1. \tag{3.6}$$

Note that $4 \leq \beta' < \infty$ can take large integer values and, unlike $\beta = 1, 2, 4$, does not have corresponding random matrix model as yet. Thus, Eq. 3.5 may be considered as a generalization of the Wigner surmise, that holds good for integer values of $\beta > 0$. A special case of Eq. 3.5 has been proved by Forrester for $0 \leq \beta \leq 1$ at the level of the joint distribution of eigenvalues. However, only spectral fluctuations like spacings and spacing ratios will be discussed in this chapter.

It is also pertinent to point out that similar relation between the higher-order and nearest neighbor *spacing distributions* had been proposed earlier without rigorous proof [127, 128], though their validity had never been tested on spectra from random matrices or physical systems. One exception is the well-known relation that the next-nearest neighbor ($k = 2$) level spacings of levels from circular orthogonal ensemble are distributed as the nearest neighbor ($k = 1$) spacings of levels from circular symplectic ensemble [129]. As pointed out earlier, in the limit of large matrix dimensions, this is known to be valid for the corresponding Gaussian ensemble as well. Some numerical results are shown below for the higher-order spacings for Gaussian ensembles but whether or not the scaling relation holds, is inconclusive from the results obtained. For the Wishart case, the leading behavior for higher-order spacings may be extracted from the form of the full distribution and related analytical results have been shown below in 3.6.

Remarkably, the functional form of $P^k(r, \beta)$ is identical to $P(r, \beta')$ with order of the spacing ratio k and Dyson index β dependence entering through the modified parameter β'.

3.2 Gaussian Ensembles

First, Eqs. 3.5-3.6 are verified for the spectra computed from Gaussian random matrix ensembles. The eigenvalues of random matrices (drawn from Gaussian ensembles) of order $N = 10^5$ are computed for $\beta = 1, 2$ and 4. The resulting histograms of higher-order spacing ratios shown in Fig. 3.1 are averaged over 1000 realizations. The solid curves in this figure represent $P(r, \beta')$ and its excellent agreement with the histograms points to the validity of Eq. 3.5. Corresponding averages $\langle r \rangle_{theory}$, as calculated from Eq. 3.5, and determined from numerics $\langle r \rangle_{num}$ are tabulated in Table 3.1.

Further, to quantitatively check that the value of β' predicted by Eq. 3.6 is precisely the one that best fits the histogram $P^k(r, \beta)$ obtained from random matrix simulations, we compute the difference between the cumulative distributions defined as,

$$D(\beta') = \sum_i \left| I^k(r, \beta) - I(r_i, \beta') \right|, \tag{3.7}$$

where $I(r, \beta')$ and $I^k(r, \beta)$ are the cumulative distributions corresponding, respectively, to $P(r, \beta')$ and $P^k(r, \beta)$. Then, the value of β' for which $D(\beta')$ is minimum is the one that best fits the observed histogram. The insets in Fig. 3.1 display the quantitative verification of scaling in Eqs. 3.5-3.6. As seen in the insets, the minima of $D(\beta')$ remarkably coincides with the value of β' predicted by Eq. 3.6. As an additional verification, the Kolmogorov-Smirnov test has also been performed for this data, and the p-values obtained indicate that the histograms correspond to the predicted distribution in Eq. 3.5 with a very high probability.
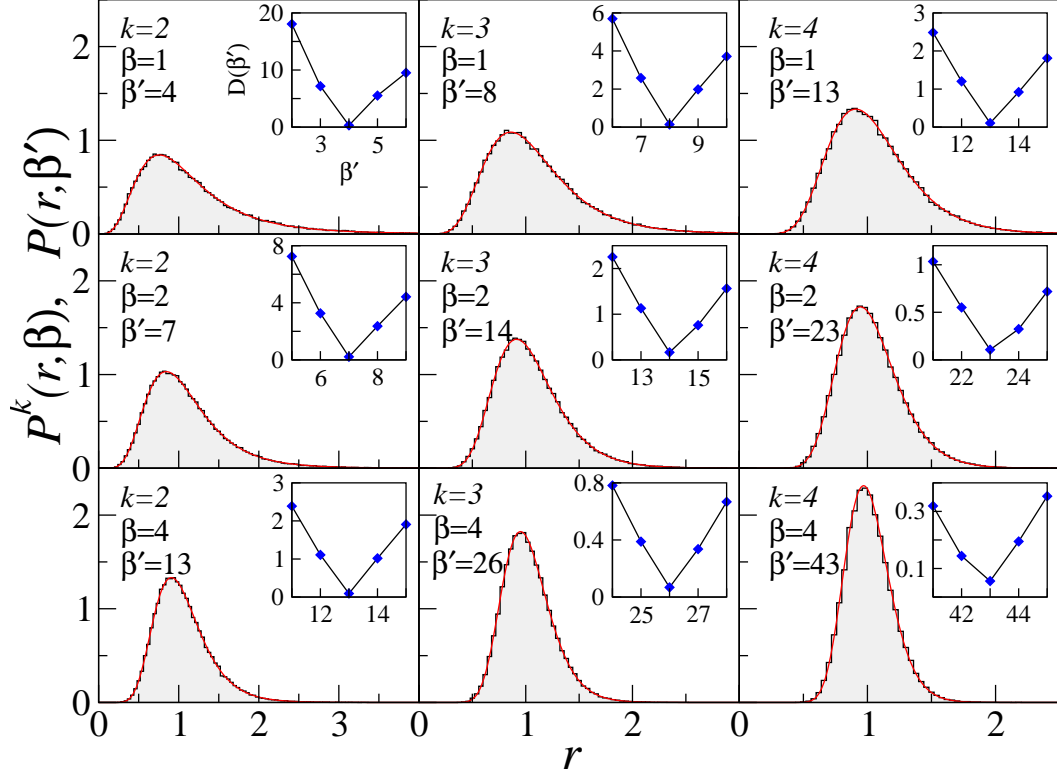
Figure 3.1: Distribution of k-th order spacing ratios (histograms) for the spectra of random matrices drawn from GOE, GUE and GSE and the distribution $P(r, \beta')$ (solid line) with β' given by Eq. 3.6. (Inset) shows D as a function of β'.

3.2.1 Gaussian Orthogonal Ensemble ($\beta = 1$)

The validity of this scaling relation is now shown for two examples of many-body systems whose nearest-neighbor spectral statistics had been well-established as coinciding with that of GOE.

One-dimensional disordered spin-1/2 chain

The Hamiltonian for the spin chain, studied in [41] with a defect placed at one of the sites, is given by

$$H = \sum_{i=1}^{L} \omega S_i^z + \epsilon_d S_d^z + \sum_{i=1}^{L-1}[J_{xy}(S_i^x S_{i+1}^x + S_i^y S_{i+1}^y) + J_z S_i^z S_{i+1}^z]. \qquad (3.8)$$

Here, L is the length of the chain and $S_i^{x,y,z}$ are the spin operators in three directions, acting on site i. The first term of the Hamiltonian represents a static magnetic field in the z-direction, accounting for a Zeeman splitting of strength ω at all sites, except the defect site d where it is $\epsilon_d + \omega$. The second term, by itself is the well-known XXZ Hamiltonian, and couples nearest-neighbor spins in all directions, with J_{xy} (taken here to be 1) being coupling strength along x and y directions, and J_z (taken as 0.5) that along the z direction.

For the spectra from the Hamiltonian in Eq. 4.9, the upper panel of Fig. 3.2 displays a good agreement between the computed k-th spacing ratio distribution and $P(r, \beta')$ given by Eqs. 3.5-3.6. Finite size effects have been discussed for this system in Fig. 3.9(c), by varying L, which changes the Hilbert space dimension. For the distributions shown in Figs. 3.2(a-d), the length of the spin chain was considered to be $L = 14$, the site of the disorder was taken to be at $L/2$, and the magnitude of the disorder was $\epsilon_d = 0.5$.

Measured resonances of Erbium atom

A similar excellent agreement can be inferred from the lower panel of Fig. 3.2 for the experimentally measured data for neutron resonances of the Erbium atom [130]. Even with only about 200 measured resonances, a good agreement with the theoretical form of $P^k(r, \beta')$ is observed for $k = 1$ to 4.
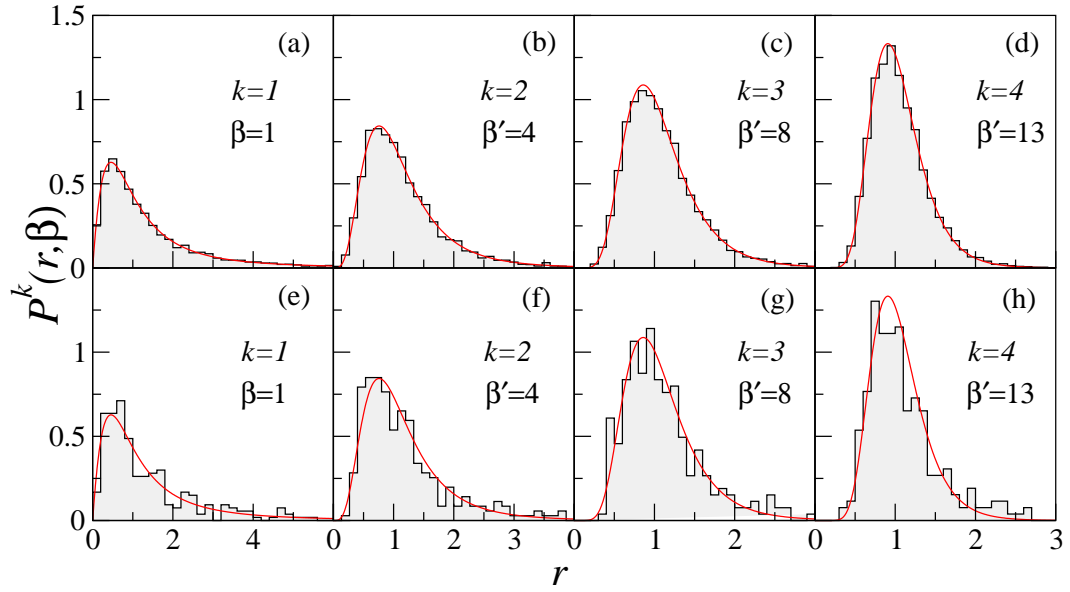
Figure 3.2: Distribution of k-th spacing ratio for many-body systems of the GOE class ($\beta = 1$). The histograms are for the computed spectra from a disordered spin chain (upper panel) and nuclear resonance of ^{167}Er atom (lower panel). The solid line corresponds to $P(r, \beta')$ predicted by Eqs. 3.5-3.6, with β'=1, 4, 8 and 13 for k=1 to 4.

3.2.2 Gaussian Unitary Ensemble ($\beta = 2$)

The validity of Eqs. 3.5-3.6 for two physical systems belonging to GUE symmetry class is discussed.

One-dimensional disordered spin-1/2 system

The Hamiltonian for the disordered spin chain, discussed in Ref. [131] is

$$H = \sum_{i=1}^{L}[J_1(\mathbf{S}_i \cdot \mathbf{S}_{i+1}) + h_i S_i^z + J_2\mathbf{S}_i \cdot (\mathbf{S}_{i+1} \times \mathbf{S}_{i+2})],$$

in which J_1 and J_2 represent strength of coupling between sites. The first term (by itself, the Heisenberg spin chain) corresponds to nearest neighbor couplings in all directions, with J_1 giving the strength of the coupling. The second term introduces

a Gaussian distributed, random magnetic field of mean 0 and strength h_i in the z-direction. The third term breaks time reversal symmetry by introducing a three-spin interaction with the nearest as well as the next-nearest neighbor couplings with strength J_2. The parameters used to obtain data for Figs. 3.3(a-d) are $L = 12$, $h/J_1 = 1$ and $J_2/J_1 = 1$, with open boundary conditions. The computed spacing ratio distribution $P^k(r_i, \beta = 2)$ shown in the upper panel of Fig. 3.3 for $k = 2, 3, 4$ is consistent with $P(r, \beta')$.

Quantum billiards without time reversal symmetry

This system has been discussed previously in Chapter 2. However, in this case, even the shape of the billiard is exactly as that described in Ref. [40], to ensure that the system is completely chaotic. As seen in lower panel of Fig. 3.3, the distribution of k-th spacing ratios provides another instance of the validity of the scaling relation in Eqs. 3.5-3.6 for GUE systems with β=2.
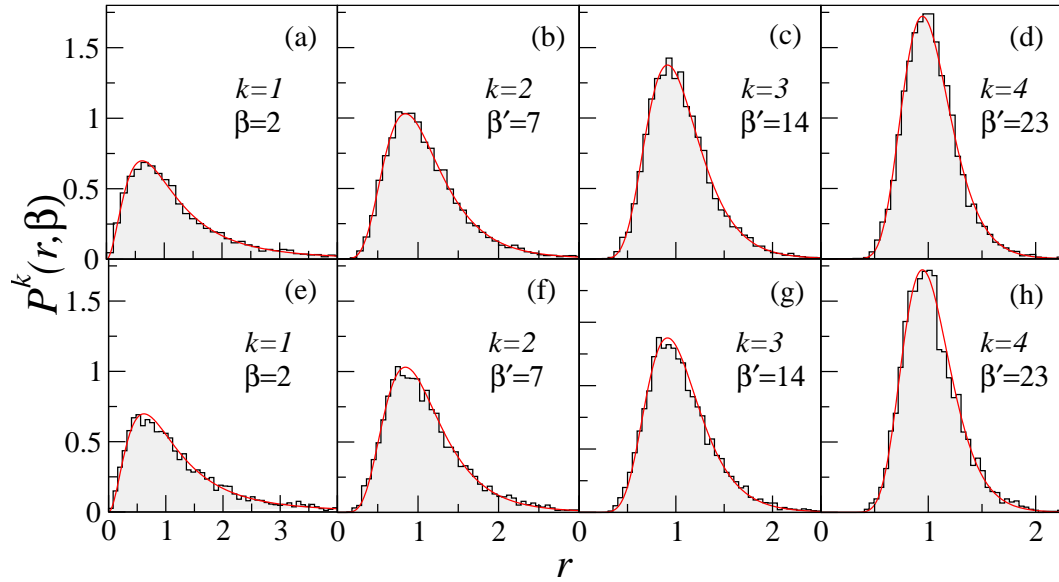
Figure 3.3: Distribution of k-th spacing ratio for physical systems of the GUE class ($\beta = 2$). Histogram is for a spin chain with a three-spin interaction (upper panel), and chaotic billiards with a magnetized ferrite strip (lower panel). The solid line represents the predicted $P(r, \beta')$, with $\beta' =$2, 7, 14 and 23 for k=1 to 4.

3.3   Circular Ensembles
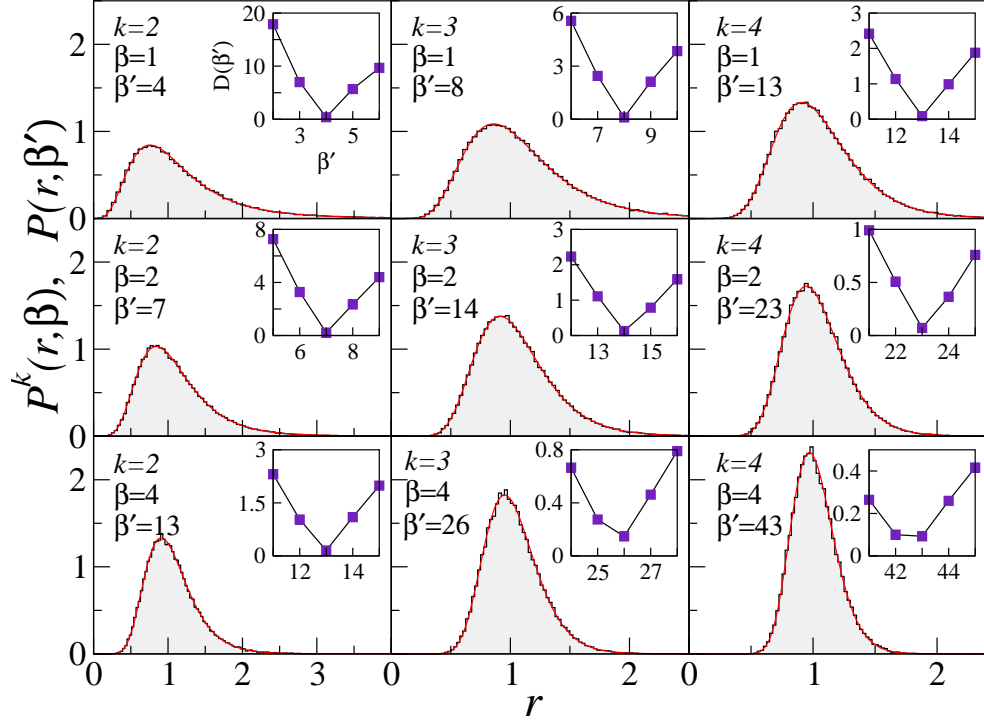
Figure 3.4: Distribution of k-th order spacing ratios (histograms) for the spectra of random matrices of dimension ~ 7000 drawn from COE, CUE and CSE and the distribution $P(r, \beta')$ (solid line) with β' given by Eq. 4. (Inset) shows D as a function of β'.

3.3.1   Circular Orthogonal Ensemble ($\beta = 1$)

The quantum kicked top is a popular model of quantum chaos whose classical limit is chaotic [132]. Its level statistics is well-modeled by that of COE matrices. As this system is periodically kicked, the quantum version can be studied in terms of the unitary time evolution operator

$$\widehat{U} = \exp\!\left(-iqJ_z^2/2\right)\,\exp(-ipJ_y), \qquad (3.9)$$

where the parameter q=10 is the kick strength that acts as chaos parameter and $p = 1.7$. The action of this operator on a particle of angular momentum **J**, taken

to be 200 here, is a precession about the y-axis, followed by state-dependent rotation about the z-axis as a consequence of periodic kicking. The eigenvalues of $\widehat{U}$ are computed by diagonalizing this operator and its fluctuations are known to be consistent with COE statistics [132]. Figure 3.5 (upper panel) shows the k-th spacing ratio distribution for this system which, as anticipated by Eqs. 3.5-3.6, follows $P(r, \beta')$ with β=1.

3.3.2   Circular Unitary Ensemble ($\beta = 2$)

As another instance of CUE class ($\beta = 2$), a unitary operator corresponding to the so-called intermediate map is considered. The quantum version of this map has been investigated previously in the context of multifractal eigenstates, and in a specified range, has spectral fluctuations similar to CUE matrices [133]. The unitary operator can be written in terms of an $N \times N$ matrix as

$$U_{ab} = \frac{\exp(-i\phi_a)}{N} \frac{1 - \exp[i2\pi\gamma N]}{1 - \exp[i2\pi(a - b + \gamma N)/N]}, \qquad (3.10)$$

with Hilbert space dimension $N = 12000$. Here, ϕ_a is a random variable uniformly distributed between $[0, 2\pi]$, and for any irrational γ the spectral statistics is of the CUE type. The computed distribution of k-th spacing ratios for this system, shown in Fig. 3.5 (lower panel), agrees well with Eqs. 3.5-3.6.
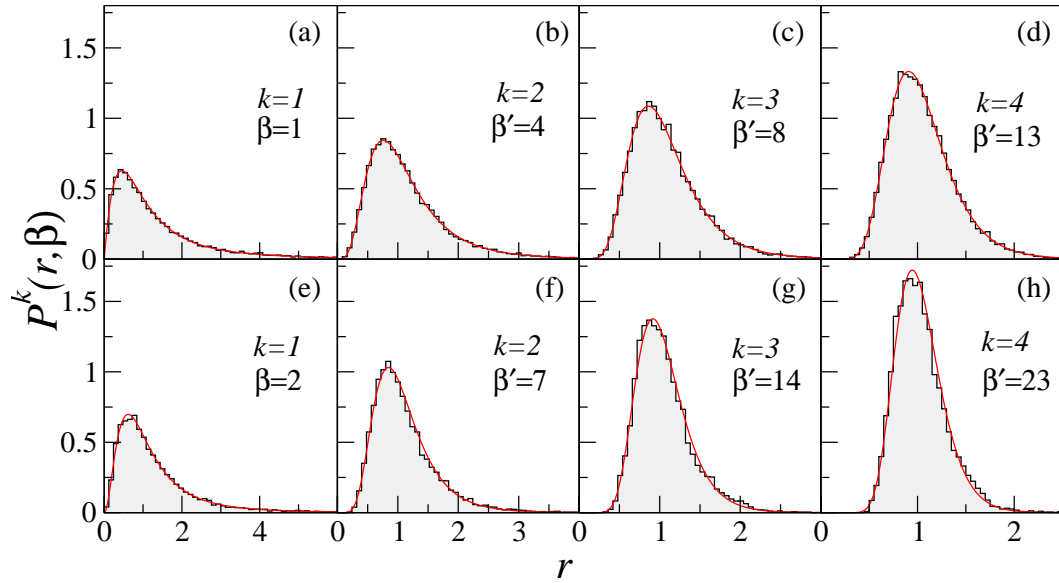
Figure 3.5: The distribution of the k-th spacing ratios, for k=1, 2, 3, 4 is shown for Floquet systems; (upper panel) the kicked top, belonging to the COE class, and (lower panel) the intermediate map, belonging to the CUE class. The histograms are obtained from computed eigenvalues of these systems, and the solid line represents $P(r, \beta')$, with $\beta' =1, 4, 8, 13$ for COE and $\beta' =2, 7, 14, 23$ for CUE.

3.4   Wishart-Laguerre ensemble

The eigenvalues $E_i, i = 1, 2..N$ of the empirical correlation matrix of order N are positive definite, i.e., $E_i \geq 0$. Typically, the corresponding eigenmodes fall in two broad groups: (*i*) eigenmodes of the top and bottom few eigenvalues (in magnitude) that carry most of the information embedded in the original dataset (*ii*) the bulk of rest represents random correlations. It is the latter group that displays a broad agreement with random matrix based results. The nearest neighbor spacing distribution continues to be a popular test for RMT-like behavior, especially for the claim that spectral fluctuations of empirical correlation matrices display universal characteristics irrespective of the dataset or system considered for analysis.

     The elements of the empirical correlation matrix represent the pair-wise Pear-

son correlation among the N variables, each one being a time series of length T. From the point of view of random matrix theory, correlation matrices fall within the class of Laguerre-Wishart ensemble of random matrix theory represented by $W = D_R D_R^S$, where D_R represents the standardized data matrix of order N by T with real, complex or quaternion elements depending on the Dyson index $\beta = 1, 2, 4$ of the ensemble and X^S represents self-dual operation on matrix X. For the Laguerre-Wishart ensemble indexed by β the random matrix average for the spacing ratios is not yet known, though in the limit of matrix size $N \to \infty$, it is well-approximated by that for the Gaussian ensembles.

3.4.1   RMT Results

First, we consider the spectra obtained from an ensemble of Wishart matrices with $\beta = 1$ and compute higher-order spacing ratio. In Fig. 3.6, the k-th order spacing ratio distributions are shown as histograms for two cases, namely, $N = T$ and $N \neq T$. It must be noted that the form of the distribution remains the same for both these cases. The validity of the scaling in Eq. 3.5 can be clearly inferred from the excellent agreement of the histogram with a solid curve representing $P(r, \beta')$, where β' given by Eq. 3.6.
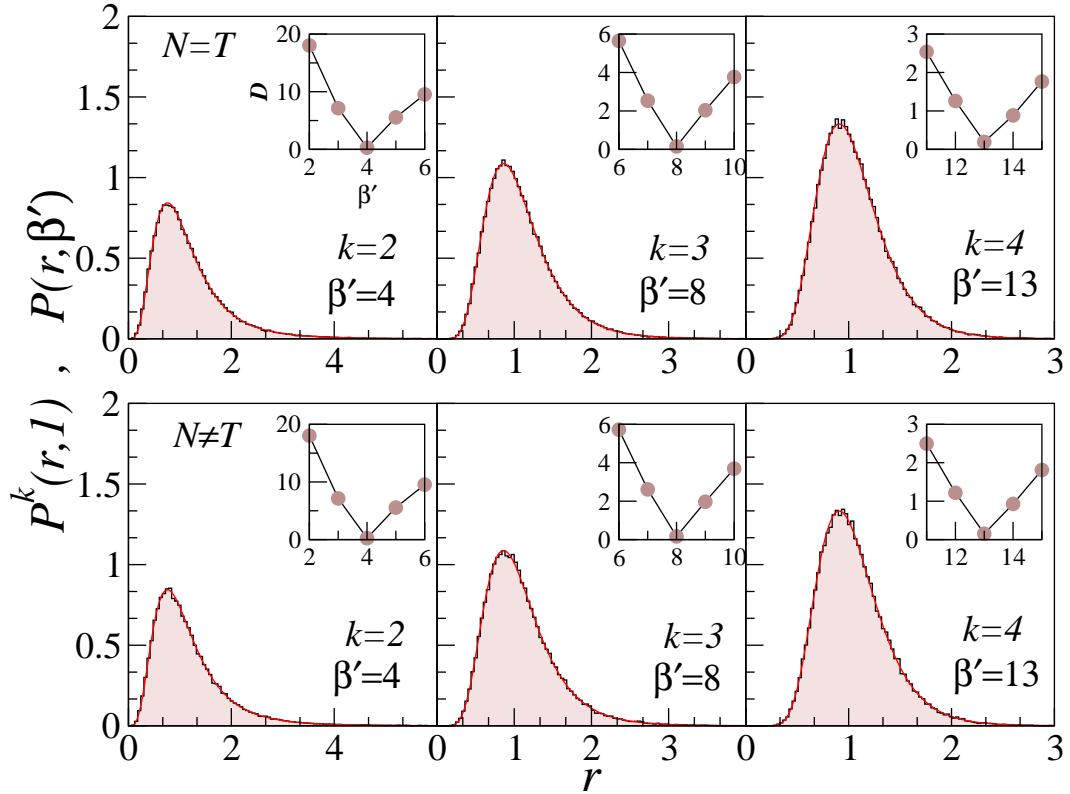
Figure 3.6: The histograms are the k-th spacing ratio distribution for the spectra of random Wishart matrix for $\beta = 1$ with (top panel) $N = T = 40000$, and (bottom panel) $N = 20000, T = 30000$. The computed histograms display a good agreement with $P(r, \beta')$ shown as solid line. In this, β' is given by Eq. 3.6. Inset shows that the minima in $D(\beta')$ corresponds to the value of β' predicted by Eq. 3.6.

The results displayed in Fig. 3.7 show that the higher-order spacing ratio distributions computed from the spectra from Wishart matrices with $\beta = 2$ and 4 are consistent with the scaling relation postulated in Eq. 3.5-3.6. The elements of Wishart matrices with $\beta = 2$ and 4 are, respectively, complex numbers and quaternions and empirical correlations with such elements are rarely encountered in practice. The symbols in this figure represent the histograms and solid curves represent $P(r, \beta')$. The results are shown for both $N = T$ and $N \neq T$ and, as anticipated, the agreement with Eqs. 3.5-3.6 is good irrespective of the relative values of N and T.

Another form of evidence in Table 3.1 for the mean ratio $\langle r \rangle$ shows a good agreement between the theoretically expected value based on Eqs. 3.5-3.6 and that
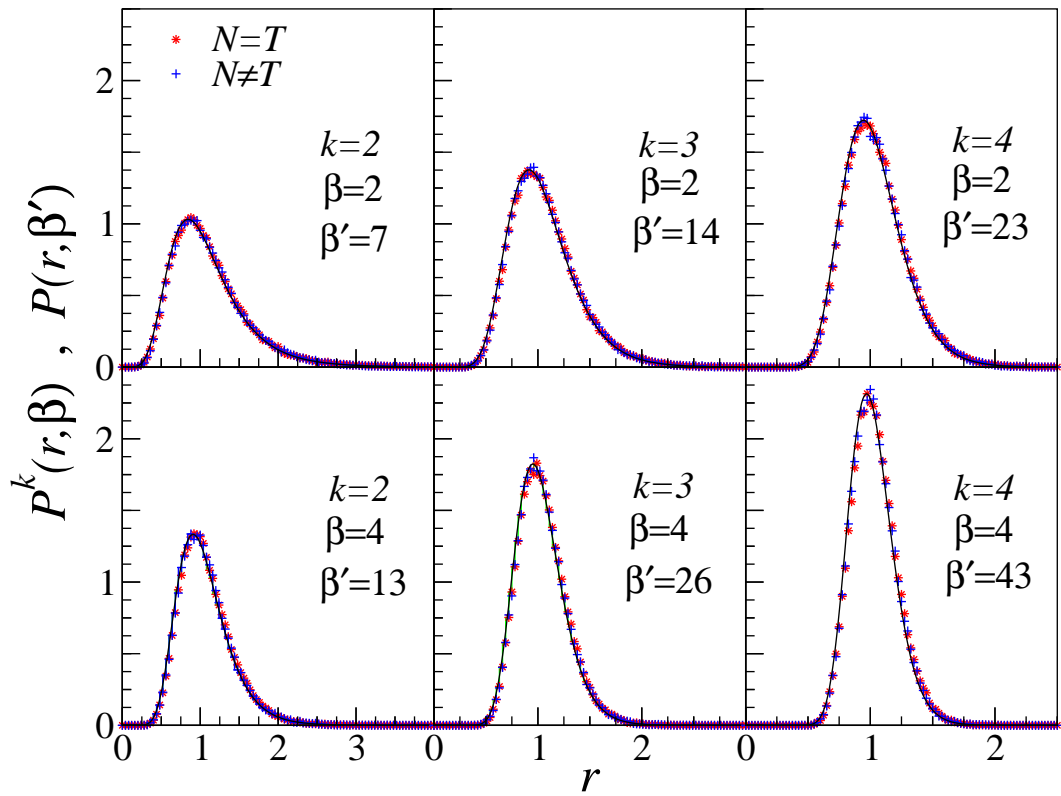
Figure 3.7: The histograms are the k-th spacing ratio distribution for the spectra of random Wishart matrix with (a-c) $\beta = 2$ and (d-f) $\beta = 4$. For the $N = T$ case, $N = T = 20000$; and for $N \neq T$ case, $N = 10000$ and $T = 20000$. The computed histograms display a good agreement with $P(r, \beta')$ shown as solid line (β' given by Eq. 3.6).

obtained from computed Wishart spectra.

3.4.2   Results for empirical correlation matrices

Next, we demonstrate the validity of the scaling relation Eq. 3.5-3.6 for the spectra of empirical correlation matrices drawn from two different domains, namely, the stock market and atmospheric data set.

Stock market data

the data of the time series of stocks that are part of the S&P500 index for the years 1996-2009 is considered [134]. This dataset continues to be extensively used to understand the ramifications of how an RMT-based approach might work in the context of empirical correlation matrices. The data consists of daily (log) returns for $T = 3400$ days for $N = 396$ assets. The elements of the correlation matrix denote the Pearson correlation between pairs of stocks averaged over time. Note that $T \geq N$ implying that the correlations can be assumed to have converged. The statistical properties of its spectra have been reported in [135–138].

In Fig. 3.8(a-c), we display the spacing ratio distribution for various orders. Fig. 3.8(a) shows the nearest neighbor spacing ratio distribution and it agrees with the analytical result in Eq. 3.4 obtained for the case of Gaussian Orthogonal Ensemble [81]. The higher-order spacing ratio distributions are displayed in Fig. 3.8(b,c) and we notice a good agreement with the postulated theoretical distribution $P(r, \beta')$, with β' as given by Eq. 3.6.

Atmospheric data

The time series of monthly mean sea level pressure over the north Atlantic ocean is considered. The monthly data is drawn from NCEP reanalysis archives and is available over equally spaced latitude/longitude grids for the North Atlantic region bounded by $(0 - 90^o$ N, 120° W $- 30^o$ E) for the years 1948 to 2017. Thus, in this case, $N = 434$ grid points and $T = 840$ months, satisfying the condition

$T/N > 1$. An analysis of the climate phenomenon of north Atlantic oscillation was performed by constructing an empirical correlation matrix from this data and using RMT statistics such as the spacing and eigenvector distributions [139]. In Fig. 3.8(d), the spacing ratio distributions for the nearest neighbor spacings obtained from the spectra of this correlation matrix is shown. The computed histogram is seen to be well-described by the theoretical distribution in Eq. 3.4 obtained for Gaussian ensembles. The higher-order spacing ratio distributions shown in Fig. 3.8(e-f) display a good agreement with $P(r, \beta')$, as anticipated by Eq. 3.6.

Both these empirical correlation matrix spectra are computed from a relatively short sequence of time series compared to the length of time series used in computing Wishart spectra for Fig. 3.6. Hence, the noise level for the correlations are higher than for the Wishart case, and it is evident in the higher-order spectral statistics shown in Fig. 3.8.
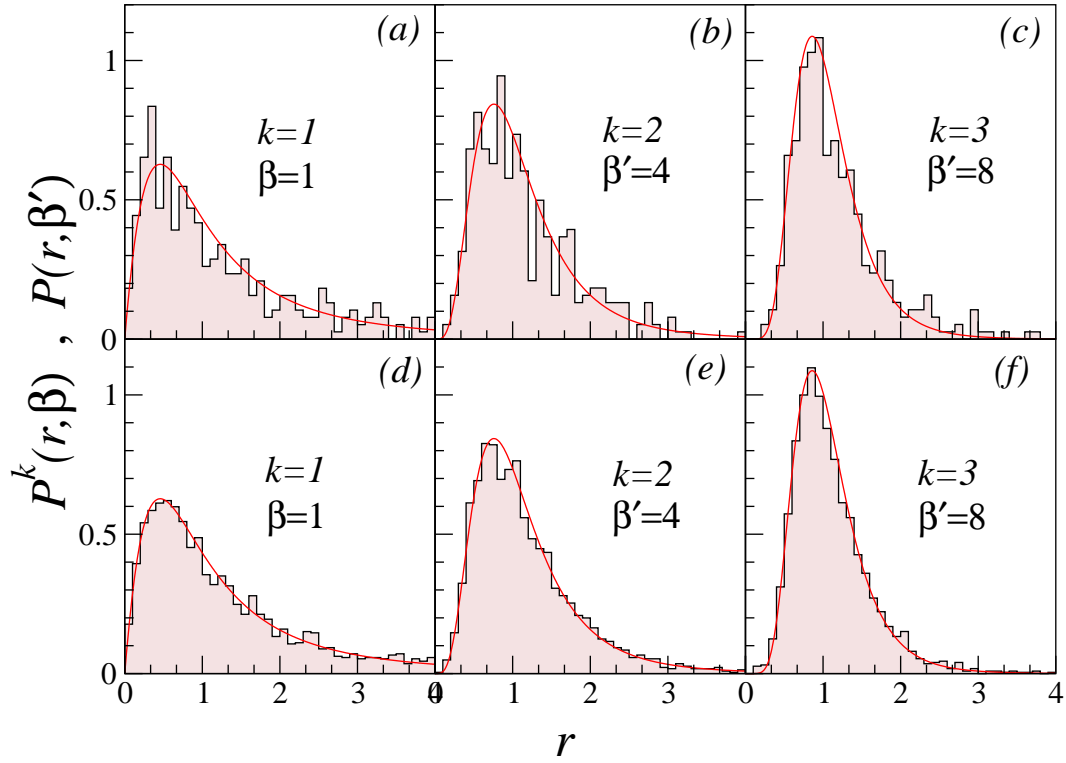
Figure 3.8: The histograms are the k-th order spacing ratio distribution for the spectra of correlation matrix (a-c) from S&P500 stock market data and (d-f) from mean sea level pressure data. The computed histograms display a good agreement with $P(r, \beta')$ shown as solid line. In this, β' is given by Eq. 3.6.

3.5   Convergence or finite size effects

The scaling relation in Eqs. 3.5-3.6 suffers from finite size effects with different systems converging to the scaling relation at different rates, especially if $k >> 1$. In the spectra of physical systems as well as in the random matrices of the Gaussian and circular ensembles, it was observed in practice that for higher order spacing ratios, say $k > 5$, the value of β' obtained by fitting $P(r, \beta')$ to the empirical distribution did not quite agree with that predicted by Eq. 3.6. It is seen that the convergence to the predicted β' is strongly pronounced as the order N of the random matrix increases. This is illustrated in Fig 3.9 for two distinct values of k. In one

β	k	β'	$\langle r \rangle_{theory}$	$\langle r \rangle_G$	$\langle r \rangle_C$	$\langle r \rangle_{W_{(N=T)}}$	$\langle r \rangle_{W_{(N \neq T)}}$
	2	4	1.1747	1.1757	1.1767	1.1777	1.1761
1	3	8	1.0855	1.0847	1.0860	1.0868	1.0856
	4	13	1.0521	1.0518	1.0524	1.0533	1.0525
	2	7	1.0980	1.0976	1.0969	1.0995	1.0975
2	3	14	1.0483	1.0478	1.0478	1.0502	1.0489
	4	23	1.0293	1.0289	1.0291	1.0319	1.0303
	2	13	1.0521	1.0522	1.0525	1.0542	1.0524
4	3	26	1.0259	1.0258	1.0262	1.0294	1.0266
	4	43	1.0156	1.0156	1.0158	1.0203	1.0167

Table 3.1: The average value of r, as calculated from Eq. 3.5 ($\langle r \rangle_{theory}$) and as determined numerically from data for Gaussian ($\langle r \rangle_G$), Circular ($\langle r \rangle_C$) and two cases of Wishart ensembles ($\langle r \rangle_{W_{(N=T)}}$ and $\langle r \rangle_{W_{(N \neq T)}}$) is shown for different values of k and β'.

case, for $k = 9$ and based on Eq. 3.6, the expected value of $\beta' = 53$. Fig. 3.9(a) shows a clear convergence to this predicted value as the order N of the random matrix increases. For $k = 20$, Eq. 3.6 predicts β' to be 229. However, as seen in Fig. 3.9(b), the convergence to the predicted value of β' is rather slow, and up to N=40000 for which spectra was computed it had not converged at all. Fig. 3.9(c) shows the same effect for the GOE spin chain (Eq. 4.9) for $k = 4$ as a function of the size of Hilbert space for the system. In this case, the dimension N of the Hamiltonian matrix increases upon increasing the length L of the spin chain. As Fig. 3.9(c) reveals convergence is achieved for $N \approx 40000$.

A similar effect is observed (not shown here) in the RMT simulations for Circular and Wishart ensembles, where for higher-order ratios, or for larger values of k, convergence to the predicted values is better for larger matrix dimensions. A possible explanation for this is that as k increases, i.e. the order of level spacing increases, the variation in the local density of states may lead to deviations from the predicted value of β'. However, this can be overcome by increasing the dimensions
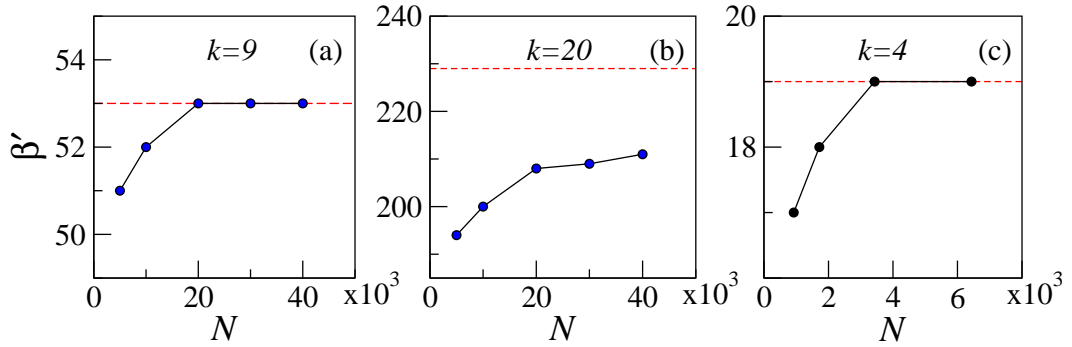
Figure 3.9: Variation of β' as a function of matrix dimension N, for random matrices of the GOE class, for (a) $k = 9$ and (b) $k = 20$. For $k = 9$, β' converges to the predicted value ($\beta' = 53$) as N increases, while for $k = 20$, a steady increase of β' towards the predicted value of $\beta' = 229$ is observed. (c) Variation of β' as a function of matrix dimension N for the GOE spin chain (Eq. 4.9). In this case, as N increases, β' converges to 19, the predicted value.

of the random matrix, as illustrated in Fig. 3.9(a), where convergence is restored to the appropriate value of β' as matrix dimension is increased. For a given value of k then, there exists a suitable N, such that convergence to the scaling relation is achieved.

The finite-size effect are a manifestation of the fact that since the energy levels are not unfolded, as longer energy ranges are considered for ratios, the local density of states comes into the picture, causing deviations from the predicted formula. The deviations begin to occur once the local density of states does not remain a constant in a given energy range. Thus, increasing the dimensionality of the random matrix considered, amounts to finding a region within which the local density of states remains approximately constant.

3.6 Spacing distributions

The level spacing distribution, owing to its long history of usage since the inception of RMT, continues to be a popular measure of spectral fluctuations. The first indications of the scaling relation, Eq. 3.6 were in terms of level spacings, although no numerical verification of the same was given. Here, the validity of this scaling

relation is examined for the spacings between k-th nearest neighbors, defined as

$$s^{(k)} = \frac{s_{i+k} - s_i}{\langle s \rangle}, i = 1, 2, \ldots. \tag{3.11}$$

where $\langle s \rangle$ is the mean spacing. The eigenspectrum is first unfolded and the k-th order spacings are calculated, giving $\langle s \rangle \approx k$. Division by the mean spacing is necessary for comparing the obtained distribution of spacings, $F^k(s, \beta)$ with the relation Eq. 3.5-3.6, as the following normalization conditions are implicitly required:

$$\int_0^\infty F^k(s, \beta) = 1, \qquad \int_0^\infty s F^k(s, \beta) = 1. \tag{3.12}$$

It must be noted that the second condition is not necessary for the distribution of spacing ratios.

The corresponding scaling relation for the distribution of higher-order spacings is then given by

$$F^k(s, \beta) = F(s, \beta'), \quad \beta = 1, 2, 4, \tag{3.13}$$

$$\beta' = \frac{k(k+1)}{2}\beta + (k-1), \quad k \geq 1. \tag{3.14}$$

The validity of the relation is shown for $k = 2$ and $k = 3$ for GOE, COE and real Wishart matrices (all corresponding to $\beta = 1$) in Fig. 3.10, and is observed to hold good for all the cases.

However, beyond this limit, the validity of this relation is unclear. This could again be due to the finite size effects discussed earlier, causing deviations from the scaling at a much earlier point than for the ratios. This required further exploration and constitutes a separate study, as analytical relations are not discussed here for all cases.

For the case of the Wishart ensemble, however, it is possible to analytically obtain a form for the higher-order spacing distributions for $k = 2$ and 3, as follows:

A random Wishart matrix W of order N is constructed as $W = AA^T$, where A is a random matrix of order N by T. The elements of A are Gaussian-distributed
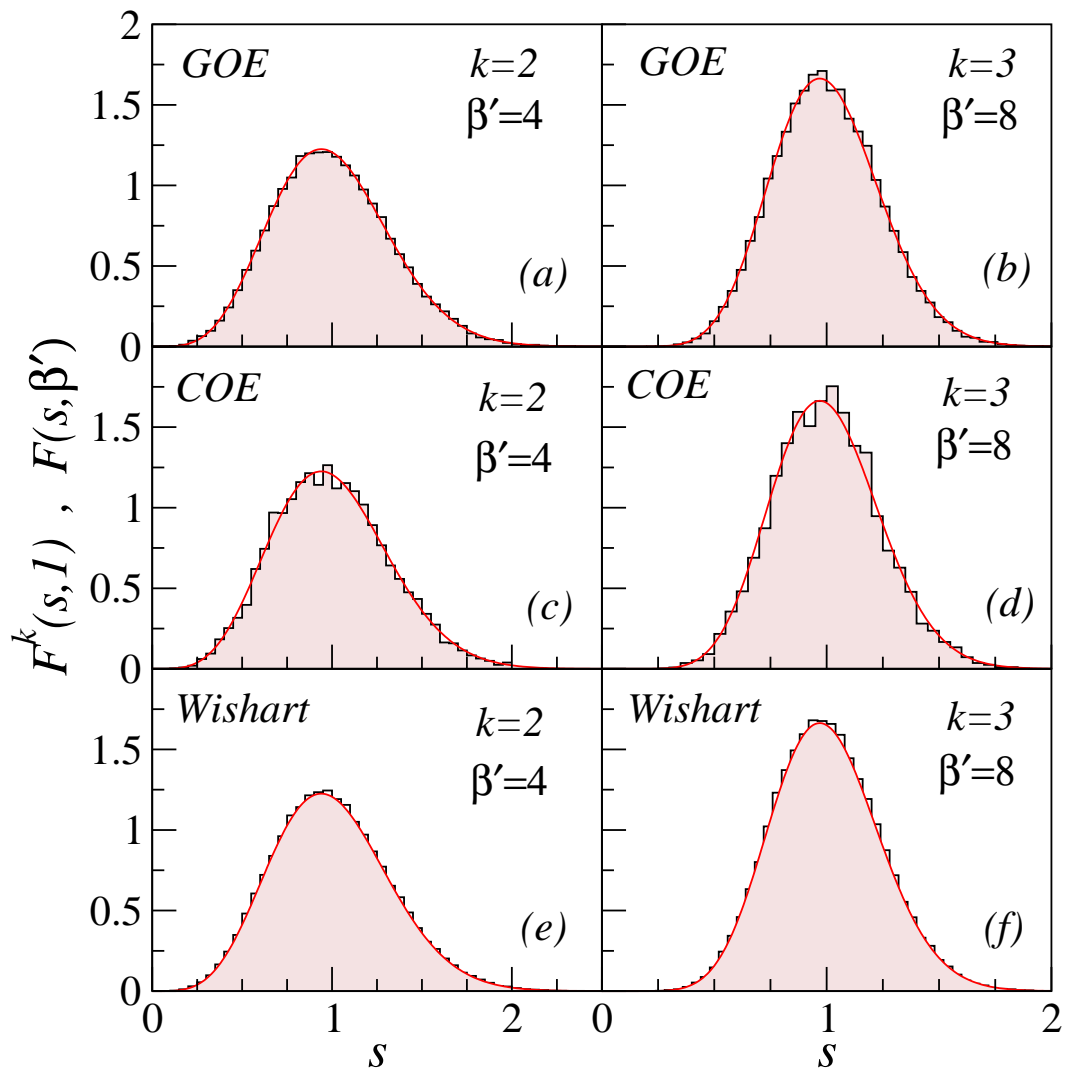
Figure 3.10: Higher-order spacing distributions for the orthogonal($\beta = 1$) ensembles of the Gaussian, Circular and Wishart random matrices for $k = 2$ and 3 (histograms), with the corresponding $P(s, \beta')$ with $\beta' = 4$ and 8, as given by Eq.3.6.

random numbers with zero mean and unit variance. It is possible to specialize to the case of the next-nearest neighbor ($k = 2$) spacing distribution by considering Wishart matrix of order $T = 3$ with three eigenvalues, $\{E_1, E_2, E_3\}$. Then, the joint probability distribution function (jpdf) of the eigenvalues $E_l \geq 0, l = 1, 2, 3$ for the Wishart ensemble is [68]

$$f(\{E_l\}) = \frac{1}{W_{a\beta T}} \prod_{i=1}^{T} E_i^{\beta a/2} e^{-\beta E_i/2} \prod_{1 \leq j < p \leq T} |E_p - E_j|^\beta,$$

where $a = N - T + 1 - 2/\beta$ and $W_{a\beta T}$ is a constant. Further, with $T = 3$, choosing N and β such that $a = 0$. Then, the jpdf can be obtained as,

$$f(E_1, E_2, E_3) = \frac{3!}{W_{0\beta 3}} \prod_{i=1}^{3} e^{-\beta E_i/2} \prod_{1 \leq j < p \leq 3} |E_p - E_j|^\beta. \tag{3.15}$$

Then, $E_2 = E_1 + x$ and $E_3 = E_1 + x + y$ is obtained using the transformation $x = E_2 - E_1, y = E_3 - E_2$, giving

$$f(E_1, x, y) = \frac{3!}{W_{0\beta 3}} x^\beta y^\beta (x + y)^\beta e^{-c\beta(3E_1 + 2x + y)/2} \tag{3.16}$$

Let $K_1 = 3!/W_{0\beta 3}$ and by integrating over E_1,

$$f(x, y) = \frac{2K_1}{3\beta c} x^\beta y^\beta (x + y)^\beta e^{-c\beta(2x+y)/2}. \tag{3.17}$$

It can be seen that $0 \leq x + y = E_3 - E_1 = s$ and $y = s - x$. After some algebra, the next-nearest-neighbor ($k = 2$) spacing distribution $\widetilde{F}^2(s)$ can be obtained as,

$$\widetilde{F}^2(s) = \frac{s^{3\beta+1} e^{-c\beta s/2}}{2^{-1} K_1^{-1} 3\beta c} \sum_{q=0}^{\beta} \sum_{n=0}^{\infty} \binom{\beta}{q} \frac{s^n (-1)^{\beta-q} (-c\beta/2)^n}{n!(2\beta - q + n + 1)} \tag{3.18}$$

In the limit of $s \to 0$, the leading behavior is proportional to $s^{\beta'}$, where $\beta' = 3\beta + 1$. The result derived above can be extended for the case of $k = 3$ as well, resulting in $\beta' = 6\beta + 2$. Thus, based on these analytical results and in the spirit of the

scaling relation Eqs. 3.5-3.6, it is postulated that the second (third) order spacing distribution is $F(s, \beta') = A_{\beta'} s^{\beta'} e^{-B_{\beta'} s^2}$, a form that is reminiscent of the Wigner surmise, where $\beta' = 3\beta + 1$ ($\beta' = 6\beta + 2$). The constants $A_{\beta'}$ and $B_{\beta'}$ (given in Chapter 1) depend on β' (Eq. 3.6).

This is also verified in Fig. 3.10, and in both these cases, a good agreement with the anticipated $F(s, \beta')$ is evident. For $k > 3$, it does not appear straightforward to extend these results due to pronounced finite size effects and the limitations of pushing the spacing distributions postulated based on $s \to 0$ results well beyond its regime of validity.

3.7   Conclusion

In summary, we have proposed a scaling relation for the higher-order spacing ratios of random matrices of different classes (Circular, Gaussian and Wishart), and provided numerical evidence for both random matrices and physical systems corresponding to each of these classes. Further, the Dyson index β has been generalized to all positive integers, though it presently lacks a matrix representation. Finally, deviations from the scaling relation were observed on varying the dimensionality of the matrices.

In physical systems, the deviations from scaling could arise due to the finite size effects discussed here, or due to purely quantum effects such as tunneling and localization that are not accounted for by RMT-type universality.By studying these deviations in physical systems from expectations based on Eqs. 3.5-3.6 and comparing it with random matrices of identical dimensions in which the deviations are purely due to finite size effects, it might be possible to distinguish whether the deviations occur due to finite size effects or system-dependent causes. The distribution of higher-order ratios may then be useful to differentiate between and understand the effects of random and system-dependent fluctuations in any physical system, and also determine the timescales over which RMT-like fluctuations hold good for empirical correlation matrices. Further, systems having β' beyond 4 may be found

in the study of log gases, and many other phenomena including fractional quantum Hall effect. Thus the ability to generate the distribution of ratios for an arbitrary β' could prove useful in such cases and could also find other uses. One such application of higher-order ratios is discussed in the next chapter.

Symmetry deduction from spectral fluctuations in complex quantum systems

The discussion on random matrices in this thesis has so far been focused on spectral fluctuations occurring in individual spectra. That is, the spectral statistics have been obtained by diagonalizing the random matrices independently, and then compared with the corresponding spectra of Hamiltonian matrices of real physical systems. However, in the presence of discrete symmetries like invariance of the potential under parity, reflection, rotations etc., the Hilbert space of the system splits into invariant subspaces, or the Hamiltonian matrix H becomes block diagonal, *i.e.*, $H = H_1 \oplus H_2 \oplus \ldots H_m$. Each block $H_i, i = 1, 2...m$ is characterized by good quantum numbers corresponding to the respective symmetries, which, in turn, label the eigenstates of the Hamiltonian. For integrable systems, each state can be identified by a unique set of quantum numbers, and hence its Hamiltonian matrix has a diagonal structure, leading to degeneracies in the eigenvalues, as they are all uncorrelated.

In complex quantum systems, if symmetries are not taken into account, and the full Hamiltonian matrix is diagonalized, mixing of uncorrelated eigenvalues
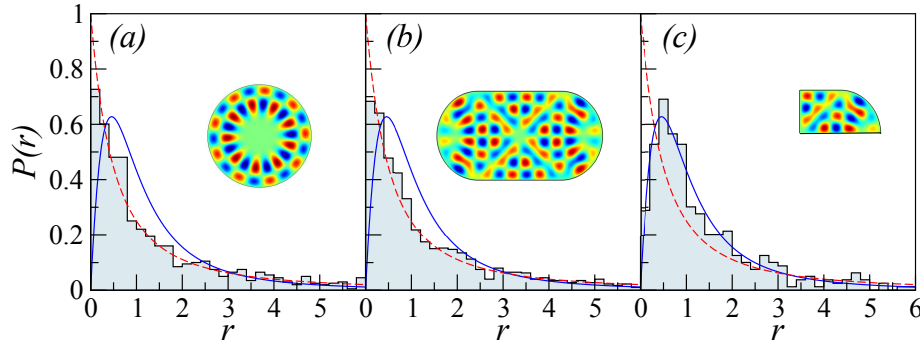
Figure 4.1: Distribution $P(r)$ of the nearest neighbor spacing ratios (histograms) for the (a)circular, (b)stadium and (c)desymmetrized stadium billiards. The broken (red) line represents $P_P(r)$ and the solid (blue) curve represents the Wigner surmise for ratios. The inset shows the shape of billiards and its typical eigenfunction superposed on it to emphasize its symmetry structure.

of different symmetry sectors takes place, and a misleading spectral signature is obtained, as the true spectral correlations in the system are masked by the erroneous mixing.

This is demonstrated in Fig. 4.1 where the numerically computed distribution of nearest neighbor spacing ratios $P(r)$ is shown for circular (integrable) [140] and stadium (chaotic) [31] billiards. The integrable billiards expectedly agrees with $P_P(r) = 1/(1+r)^2$. Note that stadium billiard has C_{2v} point group symmetry with four irreducible representations (irreps). If the spectra from each irrep is analyzed separately, by BGS conjecture, an agreement with $P(r, 1)$ of GOE is observed (Fig. 4.1(c)). However, in Fig. 4.1(b), the spectra from all the irreps are superposed, and hence the ratio distribution is closer to $P_P(r)$ with pronounced deviation from $P(r, 1)$. Thus, if symmetries are ignored and the levels from different blocks are superposed, the genuine correlation between levels (that might have produced level repulsion) is masked by the near-degeneracies resulting in level clustering.

From the random matrix perspective, mixing of m individually chaotic subspaces or superposition of m independent spectra, may be modeled by considering the direct sum of m random matrices. That is, if $G_i, i = 1, 2..m$ is a random matrix belonging to Gaussian ensemble, $G = G_1 \oplus G_2 \oplus \ldots G_m$ is a superposition of m

blocks each of which is a Gaussian random matrix. The eigenspectrum of G may be obtained by individually diagonalizing each of the blocks. As has been demonstrated in Ref. [65], for a superposition of m uncorrelated sequences, the probability of two neighboring eigenvalues coming from the same sequence is very small for large m, and the distribution of nearest neighbor spacings is close to Poissonian.

Then, given a sequence of eigenvalues whose nearest neighbor distribution tends to the Poissonian limit, is it possible to determine whether it consists of eigenvalues that are truly uncorrelated (like in integrable systems), or whether it appears so, due to the presence of symmetries? This question has been previously considered in experiments [141, 142], and even in RMT and semiclassical theory (involving cumbersome calculations of two-point correlation functions) [74, 143, 144]. In this chapter, we propose a straightforward and definitive method presented along with rigorous numerical evidence to show that higher order fluctuation measures, namely the k-th order spacing ratio not only identify the true fluctuation characteristics but also allow a quantitative inference about the block structure present in the Hamiltonian matrix H.

4.1   Distribution of higher order spacing ratios for integrable systems

For an integrable system, higher order spacing ratios must also reflect the fact that all the eigenvalues are uncorrelated with each other. To obtain a form for the distribution of higher order spacing ratios, $r^{(k)}$, the higher order spacings may be expressed in terms of nearest neighbor spacings as

$$
\begin{aligned}
s_i^{(k)} &= E_{i+k} - E_i \\
&= E_{i+k} - E_{i+k-1} + E_{i+k-1} - E_{i+k-2} + \cdots + E_i \\
&= s_k + \cdots + s_{i+1} + s_i.
\end{aligned}
\tag{4.1}
$$

Then the distribution of $s_i^{(k)}$ may be calculated as the distribution of a sum of k

random variables s_i, each of which is distributed as $P(s) = e^{-s}$. For simplicity, $s_i^{(k)}$ is denoted as z below. The distribution of z is given by

$$P(z) = \frac{e^{-z}z^{k-1}}{(k-1)!} \tag{4.2}$$

Then the distribution of higher order spacing ratios is simply the distribution of the quotient of two random variables, each of which is distributed as Eq. 4.2. This distribution may be calculated as

$$P_P^{(k)}(r) = \int |z|P(rz)P(z)dz$$

Substituting for $P(z)$ and $P(rz)$ from Eq. 4.2,

$$P_P^{(k)}(r) = \int_0^\infty |z|\frac{e^{-rz}(rz)^{k-1}}{(k-1)!}\frac{e^{-z}z^{k-1}}{(k-1)!}dz$$
$$= \frac{r^{k-1}}{(k-1)!^2}\int_0^\infty z^{2k-1}e^{-z(r+1)}dz.$$

In terms of the incomplete gamma function $\Gamma(x)$, this gives

$$P_P^{(k)}(r) = \frac{\Gamma(2k)}{(k-1)!^2}\frac{r^{k-1}}{(1+r)^{2k}}$$

Thus, the k-th order ratio distribution takes the form

$$P_P^k(r) = \frac{(2k-1)!}{[(k-1)!]^2}\frac{r^{k-1}}{(1+r)^{2k}}. \tag{4.3}$$

For $k = 1$, it reduces to the familiar form

$$\frac{1}{(1+r)^2}.$$

For $k = 2$,

$$P_P^2(r) = \frac{6r}{(1+r)^4}, \tag{4.4}$$

for $k = 3$,

$$P_P^3(r) = \frac{30r^2}{(1+r)^6},$$

(4.5)

and for $k = 4$,

$$P_P^4(r) = \frac{140r^3}{(1+r)^8}.$$

(4.6)

If a given spectrum has higher order ratio distributions of the form given by Eq. 4.3, the system can be concluded to be integrable. This is illustrated in Fig. 4.2, showing the distribution of k-th order spacing ratios for two integrable systems, the circular billiards and Heisenberg spin chain, both of which have been discussed earlier. Also shown is the form of the corresponding analytical expressions for $k = 2$ to 4 given by Eq. 4.3, and they are seen to be in good agreement.
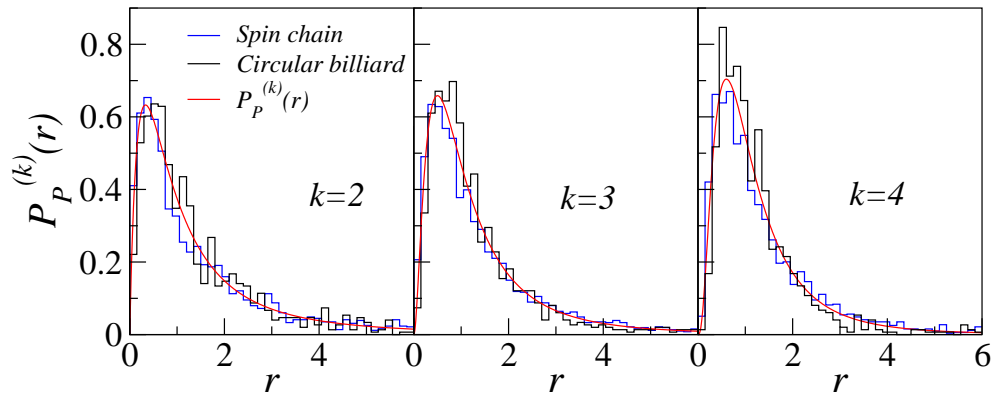
Figure 4.2: Higher order spacing ratio distributions for $k = 2$ to 4, for circular billiards (black) and integrable spin chain (blue). The corresponding analytical result (Eq. 4 in the main paper) is also shown (red curve).

4.2 Distribution of higher order spacing ratios for a superposition of GOE spectra

Next, the higher order ratios for a superposition of m spectra is considered. That is, the spectra from m independent blocks are superposed, and the distribution of

k-th order spacing ratios for the full spectrum is denoted by $P^k(r, \beta, m)$. In this chapter, only TRI systems are considered, and hence β is considered to be equal to 1 throughout. For the special case involving nearest neighbor ratios, we denote $P^1(r, \beta, 1) = P(r, \beta)$.

The motivation for considering higher order fluctuation statistics arises from a seminal result conjectured in Ref. [145] and proved by Gunson [146] for the case of circular ensembles of RMT. If two independent spectra from the circular orthogonal ensemble (COE) are superposed, and upon integrating out every alternate eigenvalue, the joint probability distribution of the remaining eigenvalues follow circular unitary ensemble (CUE) statistics. In terms of higher order measures, this result states that the second order statistics of two superposed COE spectra converges to nearest neighbor statistics of CUE. This is reflected in the distribution of spacings and spacing ratios as well. In the limit of large matrix dimensions, this result holds for Gaussian ensembles too yielding $P^2(r, 1, 2) = P(r, 2)$ for two superposed spectra.

This may be generalized for the superposition of m GOE spectra as

$$P^k(r, 1, m) = P(r, \beta'), \text{ where } \beta' = m = k, \tag{4.7}$$

implying that its k-th order spacing ratio distribution converges to nearest neighbor statistics $P(r, \beta')$ with $\beta' = k$.

It must be noted that using this method of superposing k independent spectra, and computing the distribution of the k-th order ratios, it is possible to obtain the distribution $P(r, \beta' = k)$ for any $\beta' > 0$. This can then be considered an extension (beyond the orthogonal, unitary and symplectic ensembles) of the statement in [129], that "... the statistical properties of all three types of ensemble are reducible to properties of the orthogonal ensemble alone."

For the superposition of $k = 2$ to 5 independent GOE spectra Eq. 4.7 is numerically verified in Fig. 4.3 . In this figure, an excellent agreement is seen between the histograms obtained from the computed eigenvalues of GOE matrices and the solid
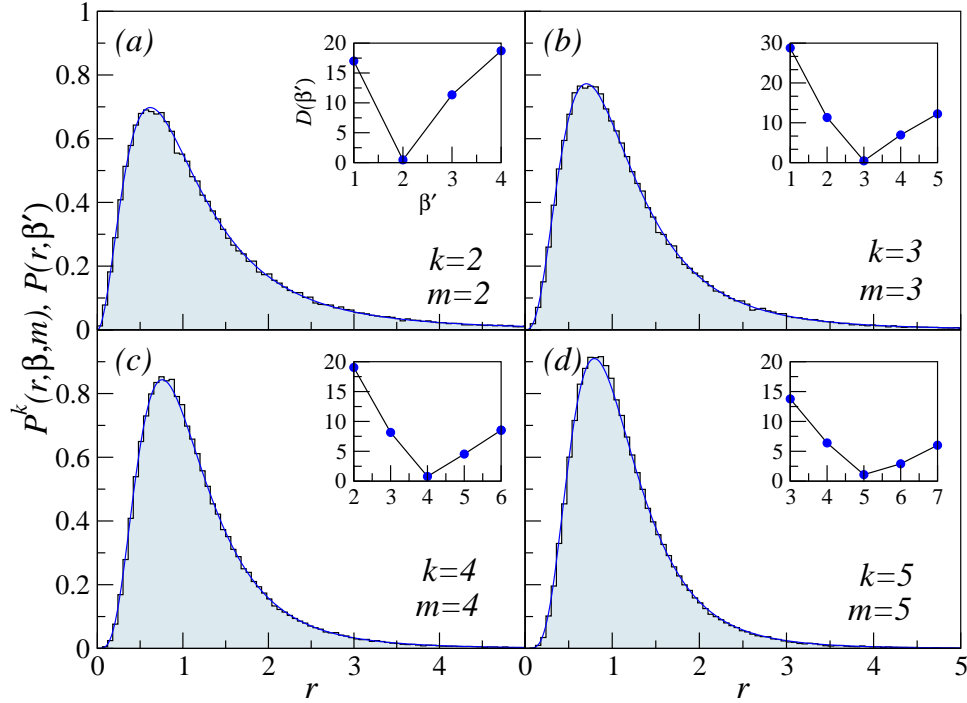
Figure 4.3: Distribution of k-th order spacing ratios (histograms) for a superposition of k GOE spectra, each obtained by diagonalizing matrices of dimension $N = 40000$, shown for $k = 2$ to 5. The solid curve corresponds to $P(r, \beta')$, with $\beta' = k$.

As seen in the insets of Fig. 4.3, the minima in $D(\beta)$ coincides with the value of m, the number of superposed spectra. A fuller picture is revealed in Fig. 4.4 for a superposition of four independent GOE spectra, where the computed histogram for the k-th order ratio is shown for $k = 2$ to 7. Based on Eq. 4.7, we expect it to be consistent with $P(r, \beta' = 4)$. For each k, $P^k(r, 1, 4)$ is matched against the corresponding $P(r, \beta')$ and the function $D(\beta')$ is calculated. Both visually and quantitatively (the minima of $D(\beta')$ in Fig. 4.4(e)), best agreement is observed for $k = 4$, verifying the main result in Eq. 4.7.
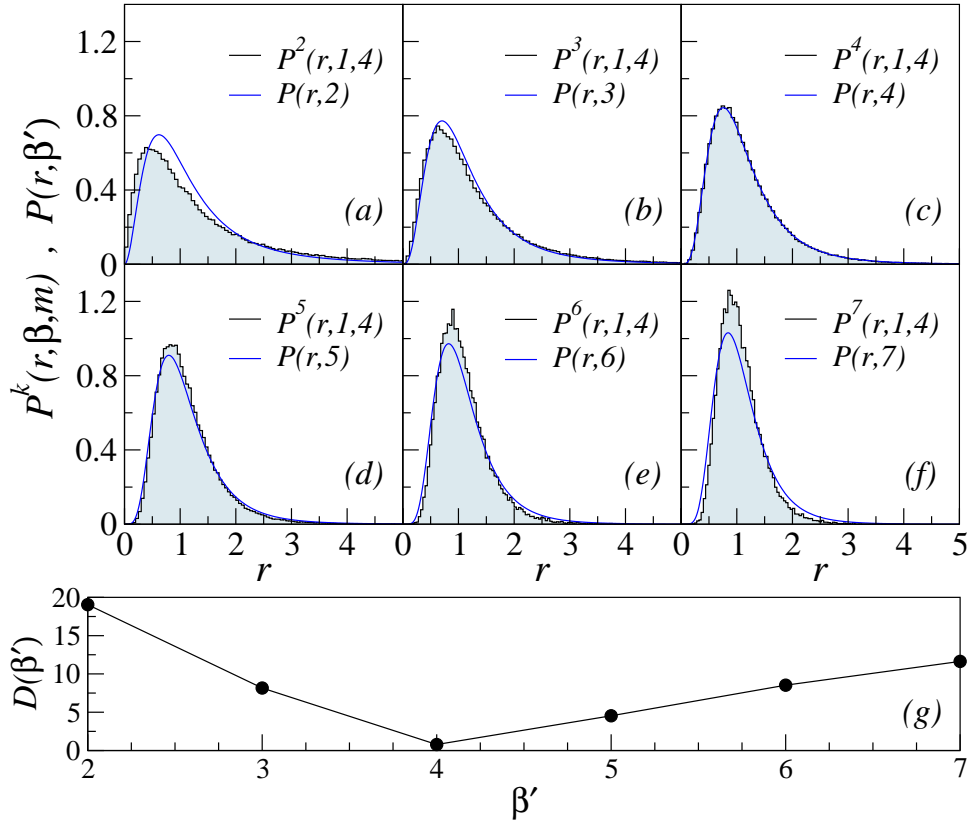
Figure 4.4: (a-f) Computed k-th order spacing ratio distribution for superposed spectra from four GOE matrices of order $N = 40000$. Note that the best agreement is obtained only for $\beta' = k = 4$. (g) A plot of $D(\beta')$ vs. β' displays a clear minima for $\beta' = 4$ supporting the claim in Eq. 4.7.

An intuitive understanding for the reason that higher order ratios pick up correlations that are masked by superposition is as follows: As discussed earlier, for a given sequence of levels consisting of superposition of several independent spectra, there is a very small probability that two neighboring eigenvalues would come from the same spectrum. However, on calculating higher order spacings or ratios, the probability of sampling spacings where both eigenvalues come from the same sequence is greater, and there is a true level repulsion, leading to the result given by Eq. 4.7.

Thus, for the superposed spectra, Eqs. 4.3 and 4.7 can be used to infer the correct nature of spectral fluctuations (level repulsion or clustering) and also to determine

the number of superposed independent blocks for a random matrix or the number of diagonal blocks (irreducible representations) in the Hamiltonian matrix of complex quantum system.

The validity of this result is verified using chaotic systems, notably billiards, and spin chains, possessing different symmetries and, most importantly, the experimentally observed data of nuclear resonances.

4.3 Symmetry deduction in chaotic spectra using higher order ratios

4.3.1 Quantum billiards

First, a family of quantum billiards is considered, whose boundary is parametrized by the equation

$$r(\phi) = r_0(1 + \epsilon_0 \cos(\epsilon_1 \phi)) \tag{4.8}$$

Fixing $\epsilon_1 = 1$, as ϵ_0 varies from 0 to 1, the system transitions from integrable to chaotic dynamics. For $\epsilon = 0$, a circular billiard shown in Fig. 4.1(a) is obtained. This is an integrable system and its higher order spacings are in agreement with Eq. 4.3, as shown in Fig. 4.2. For $\epsilon = 1$, the so-called cardioid billiard is obtained [147], with reflection symmetry about the x-axis. Therefore, it has two irreps, and its eigenlevels obtained disregarding symmetry would correspond to a superposition of two GOE spectra. As anticipated by Eq. 4.7, its second order spacing ratio distribution $P^2(r, 1, 2)$ is consistent with $P(r, 2)$ (Fig. 4.5(a)). A billiard with three irreps, similar in shape to one that has been experimentally realized previously [142], is obtained by considering $\epsilon_0 = 0.3$ and $\epsilon_1 = 3$, that is, $r(\phi) = r_0(1 + 0.3 \cos(3\phi))$. This billiard has C_{3v} symmetry with three irreps, one of them being two-dimensional, which gives rise to degeneracies. On ignoring the symmetries and after removing degeneracies arising from the two-dimensional irreps, the eigenlevels of this model correspond to a superposition of three chaotic spectra and the best fit for $P^3(r, 1, 3)$

is provided by $P(r, 3)$ (Fig. 4.5(b)). A chaotic billiard with four irreps is the well-studied Bunimovich stadium billiard [148] (shown in Fig. 4.5(c)). This has reflection symmetry about both x and y axes and, in accordance with Eq. 4.7, displays the best correspondence for $P^k(r, 1, 4)$ with $P(r, \beta')$ for $k = \beta' = 4$ (Fig. 4.5(c)). For all of these cases, insets in Fig. 4.5 show that the minima of $D(\beta')$ corresponds to $\beta' = k$, where k is the number of irreps. Thus, information about the fluctuation property and irreps can be obtained from higher order fluctuation statistics.
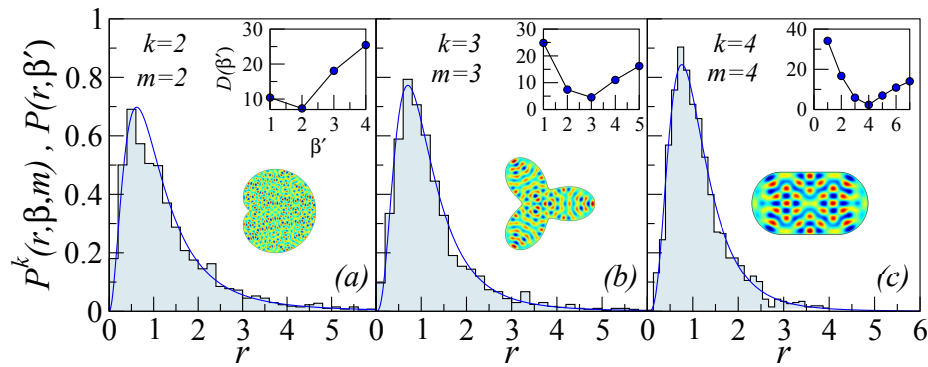
Figure 4.5: Higher order spacing ratio distribution (histogram) for the billiards family computed by ignoring their symmetries. This corresponds to superposition of spectra from (a) $k = 2$, (b) $k = 3$ and (c) $k = 4$ irreps. The higher order distributions are best described by $P(r, \beta')$ with $\beta' = k$ as dictated by Eq. 4.7. The insets display $D(\beta')$ and its minima corresponds to the correct number of irreps in the system. Also shown as inset is the shape of billiards with an arbitrarily chosen chaotic eigenstate to highlight its symmetry.

4.3.2 Chaotic spin chains

Next, a spin-$1/2$ chain with the Hamiltonian [41]

$$H = \sum_{i=1}^{L-1} [J_{xy}(S_i^x S_{i+1}^x + S_i^y S_{i+1}^y) + J_z S_i^z S_{i+1}^z]$$
$$+ \eta \sum_{i=1}^{L-2} [J'_{xy}(S_i^x S_{i+2}^x + S_i^y S_{i+2}^y) + J'_z S_i^z S_{i+2}^z] \tag{4.9}$$

is considered, where L is the number of sites, J_{xy} and J_z are the nearest neighbor coupling strengths in three directions (coupling along x and y being the same), and J'_{xy} and J'_z are the coupling strengths between an i-th spin and its next nearest neighbor. This system is integrable for $\eta = 0$ (as shown in Fig. 4.2), and chaotic for $\eta \gtrsim 0.2$. The total spin in the z-direction, S_z, is a conserved and in the S_z basis, the Hamiltonian is block diagonal, each block corresponds to a given value of S_z. However, there still exist other symmetries, which would lead to nearest neighbor $P(r)$ appearing to be integrable in this subspace (not shown here). For odd number of sites (L_{odd}), on computing the higher order spacing ratios and comparing with corresponding $P(r, \beta')$, $k = \beta' = 2$ has the best fit (Fig. 4.6(a)). For even number of sites(L_{even}), however, the best correspondence is for $k = \beta' = 4$ (Fig. 4.6(b)). This is because for L_{odd} or L_{even}, the parity operator (with eigenvalues ± 1) commutes with H, leading to two invariant subspaces in a given S_z block. For L_{even}, an additional rotational symmetry exists (with eigenvalues ± 1) for the corresponding operator giving rise to four irreps. The parameters used to obtain Figs. 4.6(a)-(b) are $J_{xy} = J'_{xy} = 1.0$, $J_z = J'_z = 0.5$, with $L_{even} = 14$ and $L_{odd} = 15$.
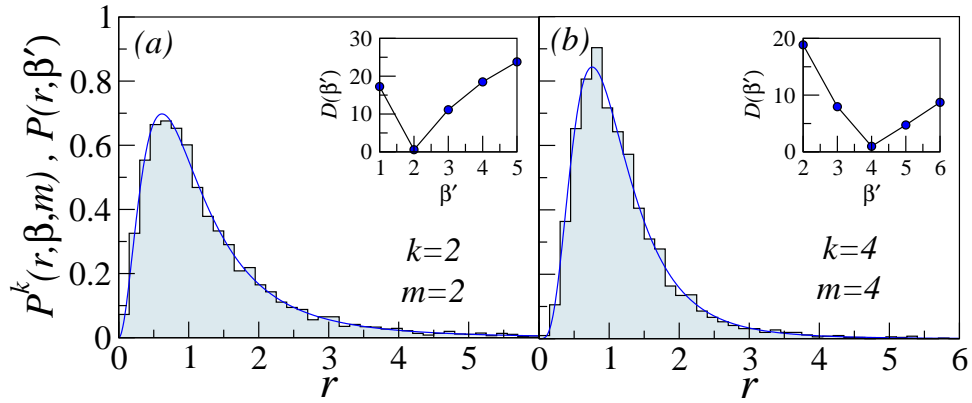
Figure 4.6: Higher order spacing ratio distribution computed for the spin-1/2 chain Hamiltonian in Eq. 4.9, with (a) odd number of sites with two irreps and (b) even number of sites with four irreps. The insets show $D(r, \beta')$ and its minima identifies the number of irreps.

4.3.3   Experimentally measured nuclear resonances for Ta^{181}

Even for systems whose Hamiltonian is not well-defined or not known as in the case of complex nuclei, experimentally observed nuclear resonance data can be analyzed to characterize its fluctuation statistics and find its number of irreps. A sequence of experimentally observed neutron resonances for Ta^{181} (Tantalum) nucleus [149] is considered, whose nearest neighbor spacing distribution is discussed in Ref. [150], and it does not match the Wigner surmise. On calculating higher order ratio distributions, remarkably, Eq. 4.7 holds good for $k = 2$, and this is further confirmed by the minima of $D(\beta')$ for $\beta' = 2$ in Fig. 4.7. This indicates that two independent symmetry sectors might be present, and the resonances drawn from each symmetry sector displays level repulsion. This is indeed the case, as confirmed in Refs. [149, 150], that this measured sequence consists of a superposition of levels having angular momentum $J = 3$ and 4 and, when symmetry decomposed, they are in broad agreement with Wigner surmise. Clearly, for an arbitrary sequence of measured levels, higher order spacing ratios based on Eq. 4.7 can unambiguously identify the true fluctuation character and the number of symmetry sectors.
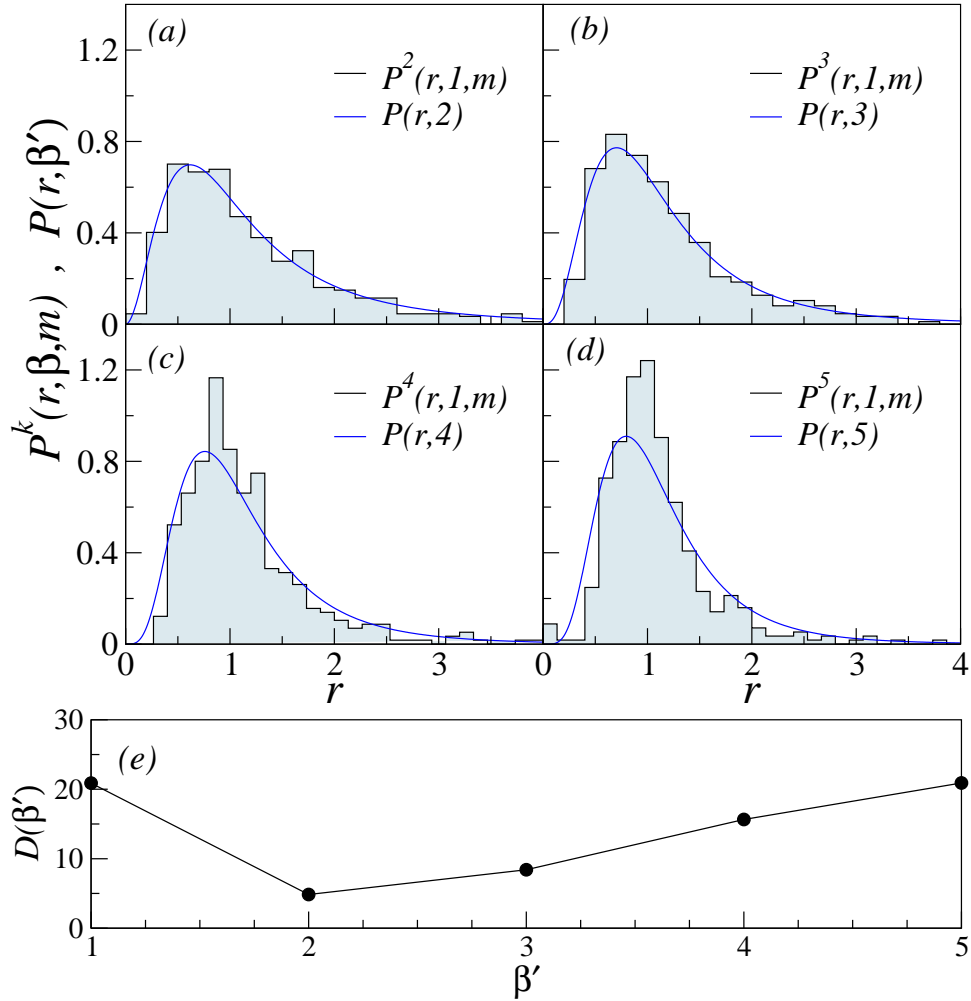
Figure 4.7: (a-d) The k-th order spacing ratio distribution (histogram) for the experimentally observed nuclear resonances for Tantalum (Ta[181]) atom. The solid line is $P(r, \beta' = k)$. Note that the best fit is observed for $k = 2$. (e) $D(\beta')$ shows minima at $\beta' = 2$, reinforcing the validity of Eq. 4.7.

4.4   Conclusion

To summarize, quantum systems must be symmetry decomposed in order to reveal its spectral fluctuation characteristics, level clustering or repulsion, without ambiguity. This implies that the fluctuations carry symmetry information though it was not possible to extract it from nearest neighbor fluctuation statistics.

In this chapter, we have demonstrated that the higher order spacing ratio dis-

tributions can reveal, apart from the fluctuation characteristics, quantitative information about symmetry structure of the quantum system being analyzed. For a superposition of k independent spectra, the central result is given by Eq. 4.7 relating k-th order spacing ratio distribution with Dyson index $\beta = 1$ to the corresponding nearest neighbor statistics with $\beta' = k$. This relation can be used to determine the number of irreducible representations (or the diagonal blocks) present in a Hamiltonian matrix. This powerful relation can be exploited to analyze any arbitrary sequence of experimentally measured or computed level spectra, even if the system's Hamiltonian and symmetry structure are unknown. Further, we have derived the higher order ratio distribution for uncorrelated eigenvalues, which might be used as a test of integrability. These results have been demonstrated using physical systems like billiards and spin chains in their integrable and chaotic limits, and also for the experimentally measured nuclear resonances.

Outlook

This thesis deals with eigenvalue statistics of random matrices and quantum chaotic systems, particularly the statistics of ratios of spacings, applied to various scenarios. Interestingly, the two subjects (random matrices and complex quantum systems) are so deeply connected, that problems motivated from one of these topics lead to interesting results in the other.

- For instance, in Chapter 2, the knowledge that the presence of localized states in a chaotic spectrum causes deviations from random matrix predictions, led to the development of a 3×3 model that took into account the fact that localized states interact differently with their nearest neighbors than generic states. An analytical form for spacing ratios coming from the localized-generic interactions could then be derived for the time reversal invariant and non invariant scenarios, which was then tested on physical systems. Thus, a problem motivated completely by the physical effects seen in chaotic systems, led to the development of a numerical and then analytical model that could bring the said effect (localization) into the purview of RMT itself.

  However, it still deals with a particular kind of localization, and the broader

question of how effects like dynamical localization and localization in momentum space could be modeled using a minimal model like the one described in Chapter 2 is a problem worth investigating. Also, this model does not differentiate between different kinds of localized states like bouncing ball modes, whispering gallery modes etc., and could be further refined to not only identify localized states but also distinguish between them. It would also be interesting to study the variation of the coupling strength k with the chaos parameter in a given system and determine the relation (if any) between the two. This could provide greater insight into the nature of quantum localization and also possibly, the quantum-classical correspondence.

• Further, an attempt to understand whether the correspondence between RMT and quantum chaotic systems extends beyond the nearest neighbor statistics, led to the discovery of a scaling relation involving the Dyson index β, that, in a certain sense generalized the concept of the level repulsion parameter beyond the idea of each β corresponding to a matrix representation.

The scaling in β with higher order ratios also possesses a universality, in that it applies to Gaussian, Circular and Wishart matrices (and physical systems corresponding to each of these classes) as demonstrated in Chapter 3, though it is not yet completely clear why this should be true. The result proved by Dyson in Ref. [145] relates the orthogonal and symplectic ensembles at the level of the joint probability distribution function. Whether a similar result can be proved for any general β is an open question. In fact, a rigorous explanation or derivation for the form taken by the higher order ratio distributions is necessary not only to understand the universality that it seems to show, but it could also provide insight into the finite size effects seen in higher order spacing ratio distributions. Obtaining specific limits for this effect would be useful, as it would then be possible to systematically compare higher order ratios coming from physical systems and random matrices and discern system-specific features based on conformity or deviations in the respective

distributions of higher order ratios.

- Finally, a direct application for the higher order spacing ratios was presented in Chapter 4, as a method of deducing the number of symmetries, or the number of independent spectra superposed in a given sequence of eigenvalues. The starting point was a conjecture of Dyson, later proved by Gunson, relating the orthogonal and unitary ensembles this time. Computing the higher order spacing ratios for a superposition of spectra led to another scaling result for the orthogonal ensembles in random matrices, relating the higher order spacing ratios and the number of superposed spectra with the modified Dyson index. This result turned out to be a straightforward method of symmetry deduction in a given system, making the process of Hamiltonian diagonalization easier. The derivation of the distribution of higher order spacing ratios for a sequence of uncorrelated levels could immediately be related with the eigenvalues of integrable systems as well, and, put together, is an important result in the context of complex quantum systems.

From the RMT perspective, the question remains about whether a similar scaling result exists superpositions of unitary and symplectic ensembles, and whether such a result may be analytically derived. This would certainly answer pertinent questions existing from the time of inception of RMT, regarding the special nature of the orthogonal ensembles in the hierarchy of random matrices. Further, the existing analytical results regarding superpositions of random matrices, implicitly assume that the dimensions of the matrices involved are the same. Would there be a similar scaling relation for matrices of unequal dimensions? There are no results of this kind for $\beta > 4$. This would be useful in dealing with cases where different kinds of symmetries divide the subspace into different dimensions (this is seen, for example, in spin chains where conservation of S_z implies that the dimensionality of each of the subspaces depend on the number of upspins or downspins in a given configuration). Also, there are indications of a new scaling relationship on

considering higher order spacing ratios for superpositions of random matrices in general, that has not been discussed in this thesis, and may be probed further to provide a larger, unifying picture of the interrelationships between random matrix ensembles corresponding to different values of β.

In summary, this thesis contains a body of work that straddles the fields of random matrix theory and quantum chaos, with results from both subjects aiding, supporting as well as influencing one another. In particular, eigenvalue statistics, in the form of distribution of spacing ratios, is the main object of interest here. In RMT, eigenvalue statistics are one of the easiest quantities to compute (especially after the introduction of spacing ratios). However, other quantities like the eigenvector statistics or N-point correlation functions are perceived more favorably, as they are purported to carry more information, or provide answers to more specific questions. This thesis shows (hopefully convincingly) that if adapted and applied suitably, spectral fluctuations like spacing ratios provide systematic and conclusive information about the object of study, be it different classes of random matrices, or quantum systems of varying degrees of complexity.

Appendix

A.1 Generalized Gaussian ensemble and ratio of consecutive level spacings

In order to derive the distribution of ratio of consecutive eigenvalue spacings, we need the joint probability density of the eigenvalues of the matrix model defined by Eq. (2.3). The cases of $\beta = 1$ and $\beta = 2$ are dealt with separately below.

A.1.1 $\quad \beta = 1$ (2×2 **GOE** $\oplus$ **Localized** $\rightarrow 3 \times 3$ **GOE**)

The joint probability density of eigenvalues in this case follows as

$$P(k; \lambda_1, \lambda_2, \lambda_3) \propto |\Delta(\{\lambda\})| \int_{\mathcal{O}_3} dO \exp\left(-\frac{1}{2}\Sigma^{-2} O \Lambda^2 O^T\right), \qquad \text{(A.1)}$$

where the integral is over the group of 3×3 orthogonal matrices with dO representing the corresponding Haar measure. Also, $\Delta(\{z\}) = \prod_{j>k}(z_j - z_k) = \det\left[z_k^{j-1}\right]_{j,k=1,\dots,N}$ is the Vandermonde determinant. For the unitary group, the celebrated Harischandra-Itzykson-Zuber formula [113, 114] gives the result for this

integral. Here we do not have such a result because Σ^{-2} and Λ^2 do not lie in the Cartan subalgebra corresponding to the orthogonal group. Nevertheless, for the 3-dimensional case, it is possible to make progress using the recursive approach suggested by Guhr and Kohler [151]. Then, we have

$$
\int_{\mathcal{O}_3} dO \exp\left(-s\operatorname{tr} XOYO^T\right) = \frac{1}{2\pi} \exp(-s(x_1 + x_2 + x_3)y_3)
$$
$$
\times \int_{x_1}^{x_2} dx_1' \int_{x_2}^{x_3} dx_2' \frac{(x_2' - x_1')}{\left(-\prod_{\substack{j=1,2,3 \\ k=1,2}} (x_j - x_k')\right)^{1/2}}
$$
$$
\times \exp\left(-s(x_1' + x_2')\left(\frac{y_1 + y_2}{2} - y_3\right)\right)
$$
$$
\times I_0\left(\frac{s(x_1' - x_2')(y_1 - y_2)}{2}\right), \tag{A.2}
$$

where $I_0(z)$ is the modified Bessel function of the first kind and zeroth order [152]. This result cannot be used directly for Eq. (A.1) since Σ^{-2} has two identical entries. We need to consider the limit $x_1, x_2 \to 1$. For this let us set $x_1 = 1 - \epsilon$ and $x_2 = 1$ and take the limit $\epsilon \to 0$. The crucial part in the above expression is

$$
\lim_{\epsilon \to 0} \int_{1-\epsilon}^1 dx_1' \frac{1}{\left[-(1-\epsilon-x_1')(1-x_1')\right]^{1/2}}
$$
$$
= \lim_{\epsilon \to 0} \int_{1-\epsilon}^1 dx_1' \frac{1}{\left[-(1-\epsilon-x_1')(1-x_1')\right]^{1/2}}
$$
$$
= 2\lim_{\epsilon \to 0} \int_0^{\pi/2} d\theta, \qquad \text{where } \epsilon \sin^2\theta = 1 - x_1'
$$
$$
= \pi.
$$

The other occurrences of x_1' can be taken as 1. Now, using Eq. (A.1), substituting $s = 1/2, x_3 = (2 - k^2)/k^2, y_1 = \lambda_1^2, y_2 = \lambda_2^2, y_3 = \lambda_3^2$, calling $x_2' = u$, and fixing

the normalization the joint probability density of eigenvalues is obtained as:

$$P(k; \lambda_1, \lambda_2, \lambda_3) = \frac{\sqrt{2 - k^2}}{24\pi k^2 \sqrt{1 - k^2}} |(\lambda_2 - \lambda_1)(\lambda_3 - \lambda_1)(\lambda_3 - \lambda_1)| e^{-\left(\frac{2+k^2}{2k^2}\right)\lambda_3^2}$$
$$\times \int_1^{2/k^2 - 1} du \frac{1}{\sqrt{2/k^2 - 1 - u}} e^{-\frac{(u+1)}{4}(\lambda_1^2 + \lambda_2^2 - 2\lambda_3^2)} I_0\left(\frac{(u-1)}{4}(\lambda_1^2 - \lambda_2^2)\right).$$

(A.3)

For calculating the ratio, the eigenvalues are restricted to the region defined by $-\infty < \lambda_1 \leq \lambda_3$, $-\infty < \lambda_3 < \infty$, $\lambda_3 \leq \lambda_2 < \infty$. The joint probability density of these ordered eigenvalues is then given by

$$\widetilde{P}(k; \lambda_1, \lambda_2, \lambda_3) = 3! P(k; \lambda_1, \lambda_2, \lambda_3).$$

(A.4)

The probability density function of the ratio of consecutive spacings $r = (\lambda_2 - \lambda_3)/(\lambda_3 - \lambda_1)$ can then be found as

$$p(k; r) = \int_{-\infty}^{\infty} d\lambda_3 \int_{-\infty}^{\lambda_3} d\lambda_1 \int_{\lambda_3}^{\infty} d\lambda_2 \, \delta\left(r - \frac{\lambda_2 - \lambda_3}{\lambda_3 - \lambda_1}\right)$$
$$\times \widetilde{P}(k; \lambda_1, \lambda_2, \lambda_3).$$

(A.5)

Let us call $\lambda_3 = \lambda$ and define $x = \lambda - \lambda_1$ and $y = \lambda_2 - \lambda$, then the above integral, in terms of these new variables, becomes

$$p(k; r) = \int_{-\infty}^{\infty} d\lambda \int_0^{\infty} dx \int_0^{\infty} dy \, \delta\left(r - \frac{y}{x}\right)$$
$$\times \widetilde{P}(k; \lambda - x, \lambda + y, \lambda).$$

(A.6)

The delta function integral over y can be trivially done to yield

$$p(k; r) = \int_{-\infty}^{\infty} d\lambda \int_0^{\infty} dx \, x \widetilde{P}(k; \lambda - x, \lambda + rx, \lambda).$$

(A.7)

Using Eq. (A.3) in this, we obtain

$$
\begin{aligned}
p(k; r) = &\frac{\sqrt{2-k^2}\, r(r+1)}{4\pi k^2 \sqrt{1-k^2}} \int_{-\infty}^{\infty} d\lambda \int_0^{\infty} dx \int_1^{2/k^2-1} du\, e^{-\frac{(2+k^2)\lambda^2}{2k^2}+\frac{(u+1)}{4}[2\lambda^2-(\lambda-x)^2-(\lambda+rx)^2]} \\
&\times x^4 \Big(\frac{2-k^2}{k^2}-u\Big)^{-1/2} I_0\Big(\frac{1}{4}x(u-1)(r+1)[2\lambda+(r-1)x]\Big). \qquad \text{(A.8)}
\end{aligned}
$$

It is found that the substitution $u = 1+2(1/k^2-1)\cos 2\phi$ leads to an expression which is comparatively more stable for numerical computation purposes :

$$
\begin{aligned}
p(k; r) = &\frac{\sqrt{2-k^2}}{\pi k^3} r(r+1) \int_{-\infty}^{\infty} d\lambda \int_0^{\infty} dx \int_0^{\pi/4} d\phi\, x^4 \cos\phi\, e^{-\frac{(2+k^2)}{2k^2}\lambda^2} \\
&\times e^{\frac{1}{2}\left[(\frac{1}{k^2}-1)\cos 2\phi+1\right]\left[2\lambda^2-(\lambda-x)^2-(\lambda+rx)^2\right]} I_0\Big(\frac{x}{2}\Big(\frac{1}{k^2}-1\Big)(r+1)[2\lambda+(r-1)x]\cos 2\phi\Big).
\end{aligned}
$$

$$\text{(A.9)}$$

A.1.2 $\;\beta = 2$ (2×2 **GUE** $\oplus$ **Localized** $\to 3 \times 3$ **GUE**)

The joint probability density of (unordered) eigenvalue in this case follows as

$$
P(k; \lambda_1, \lambda_2, \lambda_3) \propto \Delta^2(\{\lambda\}) \int_{\mathcal{U}_3} dU \exp\left(-\Sigma^{-2} U \Lambda^2 U^\dagger\right). \qquad \text{(A.10)}
$$

In this case, the unitary group integral can be performed using the Harish-Chandra-Itzykson-Zuber formula [113, 114],

$$
\begin{aligned}
\int_{\mathcal{U}_N} dU \exp\left(-s\operatorname{tr} XUYU^\dagger\right) = &\prod_{m=1}^{N-1} m! \cdot \left(-s\right)^{-N(N-1)/2} \\
&\times \frac{\det\left[\exp(-s\,x_j y_k)\right]_{j,k=1,\dots,N}}{\Delta(\{x\})\Delta(\{y\})}. \qquad \text{(A.11)}
\end{aligned}
$$

Here, dU is the Haar measure on unitary group $\mathcal{U}_N$, and $X = \operatorname{diag}(x_1, \dots, x_N)$, $Y = \operatorname{diag}(y_1, \dots, y_N)$. If there is some multiplicity in the entries of X or Y, then we must use the above formula using proper limits. This is the case here, as Σ^{-2} has two identical entries, viz. 1. We find

$$P(k; \lambda_1, \lambda_2, \lambda_3) \propto (\lambda_2 - \lambda_1)^2 (\lambda_3 - \lambda_1)^2 (\lambda_3 - \lambda_2)^2$$

$$\times \frac{\det \begin{bmatrix} e^{-\lambda_1^2} & -\lambda_1^2 e^{-\lambda_1^2} & e^{-(\frac{2-k^2}{k^2})\lambda_1^2} \\ e^{-\lambda_2^2} & -\lambda_2^2 e^{-\lambda_2^2} & e^{-(\frac{2-k^2}{k^2})\lambda_2^2} \\ e^{-\lambda_3^2} & -\lambda_3^2 e^{-\lambda_3^2} & e^{-(\frac{2-k^2}{k^2})\lambda_3^2} \end{bmatrix}}{(\lambda_2^2 - \lambda_1^2)(\lambda_3^2 - \lambda_1^2)(\lambda_3^2 - \lambda_2^2) \det \begin{bmatrix} 1 & 0 & 1 \\ 1 & 1 & (\frac{2-k^2}{k^2}) \\ 1 & 2 & (\frac{2-k^2}{k^2})^2 \end{bmatrix}} \tag{A.12}$$

$$\propto \frac{(\lambda_1 - \lambda_2)(\lambda_2 - \lambda_3)(\lambda_3 - \lambda_1)}{(\lambda_1 + \lambda_2)(\lambda_2 + \lambda_3)(\lambda_3 + \lambda_1)} \det \begin{bmatrix} e^{-\lambda_1^2} & \lambda_1^2 e^{-\lambda_1^2} & e^{-(\frac{2-k^2}{k^2})\lambda_1^2} \\ e^{-\lambda_2^2} & \lambda_2^2 e^{-\lambda_2^2} & e^{-(\frac{2-k^2}{k^2})\lambda_2^2} \\ e^{-\lambda_3^2} & \lambda_3^2 e^{-\lambda_3^2} & e^{-(\frac{2-k^2}{k^2})\lambda_3^2} \end{bmatrix}.$$

$$\tag{A.13}$$

On expanding the determinant and fixing the normalization factor, we get

$$P(k; \lambda_1, \lambda_2, \lambda_3) = -\frac{\sqrt{2 - k^2}}{3\pi^{3/2} k (1 - k^2)^2} \frac{(\lambda_1 - \lambda_2)(\lambda_2 - \lambda_3)(\lambda_3 - \lambda_1)}{(\lambda_1 + \lambda_2)(\lambda_2 + \lambda_3)(\lambda_3 + \lambda_1)} e^{-\lambda_1^2 - \lambda_2^2 - \lambda_3^2}$$

$$\times \left[e^{-2\left(\frac{1}{k^2} - 1\right)\lambda_1^2}(\lambda_2^2 - \lambda_3^2) + e^{-2\left(\frac{1}{k^2} - 1\right)\lambda_2^2}(\lambda_3^2 - \lambda_1^2) + e^{-2\left(\frac{1}{k^2} - 1\right)\lambda_3^2}(\lambda_1^2 - \lambda_2^2) \right].$$

$$\tag{A.14}$$

Proceeding similar to $\beta = 1$ case, we have Eq. (A.7), but with $\widetilde{P}(k; \lambda_1, \lambda_2, \lambda_3)$ obtained from Eq. (A.14). We find that

$$p(k; r) = \frac{2\sqrt{2 - k^2}}{\pi^{3/2} k (1 - k^2)^2} r(r + 1) \int_{-\infty}^{\infty} d\lambda_3$$

$$\times \int_0^{\infty} dx \, [t_1(\lambda, x) + t_2(\lambda, x) + t_3(\lambda, x)], \tag{A.15}$$

where

$$t_1(\lambda, x) = \frac{x^5 e^{-(1 - r^2 + \frac{2r^2}{k^2})x^2 + 2(1 + r - \frac{2r}{k^2})x\lambda - (1 + \frac{2}{k^2})\lambda^2}}{[(r - 1)x + 2\lambda](rx + 2\lambda)},$$

$$t_2(\lambda, x) = -\frac{(r+1)\,x^5 e^{-(1+r^2)x^2+2(1-r)x\lambda-(1+\frac{2}{k^2})\lambda^2}}{(-x+2\lambda)(rx+2\lambda)},$$

$$t_3(\lambda, x) = \frac{r\,x^5 e^{-(r^2+\frac{2}{k^2}-1)x^2+2(\frac{2}{k^2}-r-1)x\lambda-(1+\frac{2}{k^2})\lambda^2}}{(-x+2\lambda)[(r-1)x+2\lambda]}.$$

We notice that integrals involving t_1, t_2, t_3 are of a similar form, as given below:

$$\int_{-\infty}^{\infty} d\lambda \int_0^{\infty} dx \, \frac{x^5 e^{-\alpha^2 x^2+2\eta x\lambda-\gamma^2\lambda^2}}{(ux+2\lambda)(vx+2\lambda)} =$$
$$\frac{\sqrt{\pi}}{8(v-u)} \left[\frac{b\,(5a^2+2b^2)}{a^4\,(a^2+b^2)^2} + \frac{3\sinh^{-1}\left(\frac{b}{a}\right)}{(a^2+b^2)^{5/2}} - \frac{c\,(5a^2+2c^2)}{a^4\,(a^2+c^2)^2} - \frac{3\sinh^{-1}\left(\frac{c}{a}\right)}{(a^2+c^2)^{5/2}} \right].$$

$$(A.16)$$

Here $a^2 = \alpha^2 - \frac{\eta^2}{\gamma^2}$, $b = \frac{\gamma}{2}\left(u + \frac{2\eta}{\gamma^2}\right)$, $c = \frac{\gamma}{2}\left(v + \frac{2\eta}{\gamma^2}\right)$. The integral converges for $\alpha^2 > 0, \gamma^2 > 0, \alpha^2\gamma^2 - \eta^2 > 0$. Hence, we can write down a closed form result for $p(k; r)$ based on this integral. Define

$$a_1 = \frac{\sqrt{2[1+r(r+1)(2-k^2)]}}{\sqrt{2+k^2}}, \quad a_2 = \frac{\sqrt{2[1+r(r+k^2)]}}{\sqrt{2+k^2}},$$

$$b_1 = \frac{k^2(3r+1)-2(r+1)}{2k\sqrt{2+k^2}}, \quad b_2 = \frac{2+k^2(2r-1)}{2k\sqrt{2+k^2}}, \quad b_3 = \frac{2-k^2(2r+3)}{2k\sqrt{2+k^2}},$$

$$c_1 = \frac{k^2(3r+2)-2r}{2k\sqrt{2+k^2}}, \quad c_2 = \frac{k^2(r-2)-2r}{2k\sqrt{2+k^2}}, \quad c_3 = \frac{2(r+1)-k^2(r+3)}{2k\sqrt{2+k^2}}.$$

$$(A.17)$$

Then the PDF for ratio of spacings is given by

$$p(k; r) = \frac{\sqrt{2-k^2}}{4\pi k(1-k^2)^2} r(r+1) \sum_{j=1}^{3} \left[\frac{b_j(5a_j^2+2b_j^2)}{a_j^4(a_j^2+b_j^2)^2} + \frac{3}{(a_j^2+b_j^2)^{5/2}} \sinh^{-1}\left(\frac{b_j}{a_j}\right) \right.$$
$$\left. - \frac{c_j(5a_j^2+2c_j^2)}{a_j^4(a_j^2+c_j^2)^2} - \frac{3}{(a_j^2+c_j^2)^{5/2}} \sinh^{-1}\left(\frac{c_j}{a_j}\right) \right].$$

$$(A.18)$$

It should be noted that the factor $(v-u)$ in the denominator of Eq. (A.16) is 1,

$r + 1$, and r, respectively, for the integrals involving t_1, t_2, and t_3. The third one cancels the r factor in the numerator of Eq. (A.1.2), while the second one, when combined with $r + 1$ in the numerator of Eq. (A.1.2), leaves an overall negative sign. This sign has been absorbed in the definitions for b_2 and c_2 in Eq. (A.17), noting that $\sinh^{-1} z$ in an odd function of z.

Bibliography

[1] Kathleen T Alligood, Tim D Sauer, and James A Yorke. *Chaos*. Springer, 1996.

[2] Jeffrey A Cramer and Karl S Booksh. Chaos theory in chemistry and chemometrics: a review. *Journal of Chemometrics: A Journal of the Chemometrics Society*, 20(11-12):447–454, 2006.

[3] Larry S Liebovitch. *Fractals and chaos simplified for the life sciences*. Oxford University Press New York, 1998.

[4] Edgar E Peters and Donada Peters. *Fractal market analysis: applying chaos theory to investment and economics*, volume 24. John Wiley & Sons, 1994.

[5] L Douglas Kiel and Euel W Elliott. *Chaos theory in the social sciences: Foundations and applications*. University of Michigan Press, 1997.

[6] Steven H Strogatz. *Nonlinear dynamics and chaos: with applications to physics, biology, chemistry, and engineering*. CRC Press, 2018.

[7] Robert C Hilborn et al. *Chaos and nonlinear dynamics: an introduction for scientists and engineers*. Oxford University Press on Demand, 2000.

[8] Martin C Gutzwiller. Periodic orbits and classical quantization conditions. *Journal of Mathematical Physics*, 12(3):343–358, 1971.

[9] Michael Victor Berry. Semiclassical theory of spectral rigidity. *Proc. R. Soc. Lond. A*, 400(1819):229–251, 1985.

[10] Linda Reichl. *The transition to chaos: conservative classical systems and quantum manifestations*. Springer Science & Business Media, 2013.

[11] Hans-Jürgen Stöckmann. Quantum chaos: an introduction, 2000.

[12] Alfredo M Ozorio De Almeida. *Hamiltonian systems: chaos and quantization*. Cambridge University Press, 1990.

[13] Michael Berry. Quantum chaology, not quantum chaos. *Physica Scripta*, 40(3):335, 1989.

[14] Fritz Haake. *Quantum signatures of chaos*, volume 54. Springer Science & Business Media, 2013.

[15] John Wishart. The generalised product moment distribution in samples from a normal multivariate population. *Biometrika*, pages 32–52, 1928.

[16] D Delande and JC Gay. Quantum chaos and statistical properties of energy levels: Numerical study of the hydrogen atom in a magnetic field. *Physical review letters*, 57(16):2006, 1986.

[17] Hui Cao and Jan Wiersig. Dielectric microcavities: Model systems for wave chaos and non-hermitian physics. *Reviews of Modern Physics*, 87(1):61, 2015.

[18] RA Jalabert, J-L Pichard, and CWJ Beenakker. Universal quantum signatures of chaos in ballistic transport. *EPL (Europhysics Letters)*, 27(4):255, 1994.

[19] Oriol Bohigas, D Ullmo, and S Tomsovic. Manifestations of classical phase space structures in quantum mechanics. Technical report, Paris-11 Univ., 1992.

[20] VB Sheorey and MS Santhanam. Calculation of highly excited eigenstates of chaotic quantum systems. *Pramana*, 50(6):535–545, 1998.

[21] MS Santhanam, VB Sheorey, and Arul Lakshminarayan. Effect of classical bifurcations on the quantum entanglement of two coupled quartic oscillators. *Physical Review E*, 77(2):026213, 2008.

[22] KM Atkins and GS Ezra. Semiclassical density of states at symmetric pitchfork bifurcations in coupled quartic oscillators. *Physical Review A*, 50(1):93, 1994.

[23] KM Atkins and GS Ezra. Quantum-classical correspondence and the transition to chaos in coupled quartic oscillators. *Physical Review E*, 51(3):1822, 1995.

[24] MS Santhanam, VB Sheorey, and A Lakshminarayan. Chaos and localization in coupled quartic oscillators. *Pramana*, 48(2):439–457, 1997.

[25] Marko Robnik. Quantising a generic family of billiards with analytic boundaries. *Journal of Physics A: Mathematical and General*, 17(5):1049, 1984.

[26] Michael V Berry. Regularity and chaos in classical mechanics, illustrated by three deformations of a circular 'billiard'. *European Journal of Physics*, 2(2):91, 1981.

[27] Michael V Berry. Quantizing a classically ergodic system: Sinai's billiard and the kkr method. *Annals of Physics*, 131(1):163–216, 1981.

[28] Sudhir Ranjan Jain and Rhine Samajdar. Nodal portraits of quantum billiards: Domains, lines, and statistics. *Rev. Mod. Phys.*, 89:045005, Dec 2017.

[29] J Stein and H-J Stöckmann. Experimental determination of billiard wave functions. *Physical Review letters*, 68(19):2867, 1992.

[30] A Kudrolli, V Kidambi, and S Sridhar. Experimental studies of chaos and localization in quantum wave functions. *Physical Review letters*, 75(5):822, 1995.

[31] Steven W McDonald and Allan N Kaufman. Spectrum and eigenfunctions for a hamiltonian with stochastic trajectories. *Physical Review Letters*, 42(18):1189, 1979.

[32] H Schanze, H-J Stöckmann, M Martínez-Mares, and CH Lewenkopf. Universal transport properties of open microwave cavities with and without time-reversal symmetry. *Physical Review E*, 71(1):016223, 2005.

[33] Nir Friedman, Ariel Kaplan, Dina Carasso, and Nir Davidson. Observation of chaotic and regular dynamics in atom-optics billiards. *Phys. Rev. Lett.*, 86:1518–1521, Feb 2001.

[34] Benjamin Batistić. Fermi acceleration in chaotic shape-preserving billiards. *Phys. Rev. E*, 89:022912, Feb 2014.

[35] S. Bittner, B. Dietz, M. Miski-Oglu, P. Oria Iriarte, A. Richter, and F. Schäfer. Double-slit experiments with microwave billiards. *Phys. Rev. E*, 84:016221, Jul 2011.

[36] József Cserti, Imre Hagymási, and Andor Kormányos. Graphene andreev billiards. *Phys. Rev. B*, 80:073404, Aug 2009.

[37] V. Milner, J. L. Hanssen, W. C. Campbell, and M. G. Raizen. Optical billiards for atoms. *Phys. Rev. Lett.*, 86:1514–1517, Feb 2001.

[38] Stefan Gehler, Steffen Löck, Susumu Shinohara, Arnd Bäcker, Roland Ketzmerick, Ulrich Kuhl, and Hans-Jürgen Stöckmann. Experimental observation of resonance-assisted tunneling. *Physical review letters*, 115(10):104101, 2015.

[39] www.comsol.com. *COMSOL Multiphysics Reference Manual, version 5.1*. COMSOL Inc.

[40] Paul So, Steven M Anlage, Edward Ott, and Robert N Oerter. Wave chaos experiments with and without time reversal symmetry: Gue and goe statistics. *Physical Review Letters*, 74(14):2662, 1995.

[41] Aviva Gubin and Lea F. Santos. Quantum chaos: An introduction via chains of interacting spins 1/2. *American Journal of Physics*, 80(3):246–251, 2012.

[42] Kira Joel, Davida Kollmar, and Lea F Santos. An introduction to the spectrum, symmetries, and dynamics of spin-1/2 heisenberg chains. *American Journal of Physics*, 81(6):450–457, 2013.

[43] J. Sirker. Thermodynamics of multiferroic spin chains. *Phys. Rev. B*, 81:014419, Jan 2010.

[44] Federico Finkel, Artemio González-López, Iván León, and MA Rodríguez. Thermodynamics and criticality of supersymmetric spin chains with long-range interactions. *Journal of Statistical Mechanics: Theory and Experiment*, 2018(4):043101, 2018.

[45] TS Tavares and GAP Ribeiro. Thermodynamics of quantum spin chains with competing interactions. *Journal of Statistical Mechanics: Theory and Experiment*, 2013(09):P09007, 2013.

[46] Steven R. White. Density matrix formulation for quantum renormalization groups. *Phys. Rev. Lett.*, 69:2863–2866, Nov 1992.

[47] Ian Affleck, Doron Gepner, HJ Schulz, and Timothy Ziman. Critical behaviour of spin-s heisenberg antiferromagnetic chains: analytic and numerical results. *Journal of Physics A: Mathematical and General*, 22(5):511, 1989.

[48] Anatol N Kirillov and N Yu Reshetikhin. Exact solution of the integrable xxz heisenberg model with arbitrary spin. i. the ground state and the excitation spectrum. *Journal of Physics A: Mathematical and General*, 20(6):1565, 1987.

[49] FDM Haldane, ZNC Ha, JC Talstra, D Bernard, and V Pasquier. Yangian symmetry of integrable quantum chains with long-range interactions and a new description of states in conformal field theory. *Physical review letters*, 69(14):2021, 1992.

[50] Martin Kruczenski. Spin chains and string theory. *Phys. Rev. Lett.*, 93:161602, Oct 2004.

[51] Sougato Bose. Quantum communication through an unmodulated spin chain. *Physical review letters*, 91(20):207901, 2003.

[52] Florian Meier, Jeremy Levy, and Daniel Loss. Quantum computing with spin cluster qubits. *Physical review letters*, 90(4):047901, 2003.

[53] Hans Bethe. Zur theorie der metalle. *Zeitschrift für Physik*, 71(3-4):205–226, 1931.

[54] Shoudan Liang. Monte carlo calculations of the correlation functions for heisenberg spin chains at t=0. *Phys. Rev. Lett.*, 64:1597–1600, Mar 1990.

[55] Takahiro Fukui and Norio Kawakami. Spin chains with a periodic array of impurities. *Phys. Rev. B*, 55:R14709–R14712, Jun 1997.

[56] Masaki Oshikawa, Masanori Yamanaka, and Ian Affleck. Magnetization plateaus in spin chains: "haldane gap" for half-integer spins. *Physical review letters*, 78(10):1984, 1997.

[57] Yuri B Kudasov. Steplike magnetization in a spin-chain system: $ca_3co_2o_6$. *Physical review letters*, 96(2):027212, 2006.

[58] Guifre Vidal, José Ignacio Latorre, Enrique Rico, and Alexei Kitaev. Entanglement in quantum critical phenomena. *Physical review letters*, 90(22):227902, 2003.

[59] Aldo Isidori, Annika Ruppel, Andreas Kreisel, Peter Kopietz, Alexander Mai, and Reinhard M. Noack. Quantum criticality of dipolar spin chains. *Phys. Rev. B*, 84:184417, Nov 2011.

[60] H. T. Quan, Z. Song, X. F. Liu, P. Zanardi, and C. P. Sun. Decay of loschmidt echo enhanced by quantum criticality. *Phys. Rev. Lett.*, 96:140604, Apr 2006.

[61] L. F. Santos, G. Rigolin, and C. O. Escobar. Entanglement versus chaos in disordered spin chains. *Phys. Rev. A*, 69:042304, Apr 2004.

[62] Adriana Moreo. Ground-state properties of heisenberg spin chains. *Phys. Rev. B*, 35:8562–8565, Jun 1987.

[63] Niels Bohr. Neutron capture and nuclear constitution, 1936.

[64] Aage Bohr and Ben R Mottelson. *Nuclear structure*, volume 1. World Scientific, 1998.

[65] Madan Lal Mehta. *Random matrices*, volume 142. Elsevier, 2004.

[66] H. A. Weidenmüller and G. E. Mitchell. Random matrices and chaos in nuclear physics: Nuclear structure. *Rev. Mod. Phys.*, 81:539–589, May 2009.

[67] G. E. Mitchell, A. Richter, and H. A. Weidenmüller. Random matrices and chaos in nuclear physics: Nuclear reactions. *Rev. Mod. Phys.*, 82:2845–2901, Oct 2010.

[68] Peter J Forrester. *Log-gases and random matrices (LMS-34)*. Princeton University Press, 2010.

[69] Carlo WJ Beenakker. Random-matrix theory of quantum transport. *Reviews of modern physics*, 69(3):731, 1997.

[70] Jacobus Verbaarschot. Spectrum of the qcd dirac operator and chiral random matrix theory. *Physical Review Letters*, 72(16):2531, 1994.

[71] A. V. Andreev, O. Agam, B. D. Simons, and B. L. Altshuler. Quantum chaos, irreversible classical dynamics, and random matrix theory. *Phys. Rev. Lett.*, 76:3947–3950, May 1996.

[72] Gernot Akemann, Jinho Baik, and Philippe Di Francesco. *The Oxford handbook of random matrix theory*. Oxford University Press, 2011.

[73] Alan Edelman and Yuyang Wang. Random matrix theory and its innovative applications. In *Advances in Applied Mathematics, Modeling, and Computational Science*, pages 91–116. Springer, 2013.

[74] Thomas Guhr, Axel Müller-Groeling, and Hans A Weidenmüller. Random-matrix theories in quantum physics: common concepts. *Physics Reports*, 299(4-6):189–425, 1998.

[75] PJ Forrester, NC Snaith, and JJM Verbaarschot. Developments in random matrix theory. *Journal of Physics A: Mathematical and General*, 36(12):R1, 2003.

[76] Charles E Porter. Statistical theories of spectra: fluctuations. Technical report, 1965.

[77] Oriol Bohigas, Marie-Joya Giannoni, and Charles Schmit. Characterization of chaotic quantum spectra and universality of level fluctuation laws. *Physical Review Letters*, 52(1):1, 1984.

[78] Eugene P Wigner. On the statistical distribution of the widths and spacings of nuclear resonance levels. In *Mathematical Proceedings of the Cambridge Philosophical Society*, volume 47, pages 790–798. Cambridge University Press, 1951.

[79] Michael Victor Berry and Michael Tabor. Level clustering in the regular spectrum. *Proc. R. Soc. Lond. A*, 356(1686):375–394, 1977.

[80] YY Atas, E Bogomolny, O Giraud, and G Roux. Distribution of the ratio of consecutive level spacings in random matrix ensembles. *Physical Review Letters*, 110(8):084101, 2013.

[81] YY Atas, E Bogomolny, O Giraud, P Vivo, and E Vivo. Joint probability densities of level spacing ratios in random matrices. *Journal of Physics A: Mathematical and Theoretical*, 46(35):355204, 2013.

[82] S Harshini Tekur, Santosh Kumar, and MS Santhanam. Exact distribution of spacing ratios for random and localized states in quantum chaotic systems. *Physical Review E*, 97(6):062212, 2018.

[83] S. Harshini Tekur, Udaysinh T. Bhosale, and M. S. Santhanam. Higher-order spacing ratios in random matrix theory and complex quantum systems. *Phys. Rev. B*, 98:104305, Sep 2018.

[84] Udaysinh T. Bhosale, S. Harshini Tekur, and M. S. Santhanam. Scaling in the eigenvalue fluctuations of correlation matrices. *Physical Review E*, 98(5):052133, 2018.

[85] S. Harshini Tekur and M. S. Santhanam. Symmetry deduction from spectral fluctuations in complex quantum systems. *arXiv preprint arXiv:1808.08541*, 2018.

[86] Mark G Raizen. Quantum chaos with cold atoms. *Advances in Atomic, Molecular, and Optical Physics*, 41(43):199, 1999.

[87] MG Raizen. Experimental study of quantum chaos with cold atoms. *Philosophical Magazine B*, 80(12):2109–2117, 2000.

[88] Eric J Heller. Bound-state eigenfunctions of classically chaotic hamiltonian systems: scars of periodic orbits. *Physical Review Letters*, 53(16):1515, 1984.

[89] Benjamin Batistić and Marko Robnik. Quantum localization of chaotic eigenstates and the level spacing distribution. *Physical Review E*, 88(5):052913, 2013.

[90] Benjamin Batistić and Marko Robnik. Semiempirical theory of level spacing distribution beyond the berry–robnik regime: modeling the localization and the tunneling effects. *Journal of Physics A: Mathematical and Theoretical*, 43(21):215101, 2010.

[91] Jan Wiersig. Formation of long-lived, scarlike modes near avoided resonance crossings in optical microcavities. *Physical Review Letters*, 97(25):253901, 2006.

[92] Sang-Bum Lee, Jai-Hyung Lee, Joon-Sung Chang, Hee-Jong Moon, Sang Wook Kim, and Kyungwon An. Observation of scarred modes in asymmetrically deformed microcylinder lasers. *Physical Review Letters*, 88(3):033903, 2002.

[93] Chang-Hwan Yi, Sang Hun Lee, Myung-Woon Kim, Jinhang Cho, Jinhyung Lee, Soo-Young Lee, Jan Wiersig, and Chil-Min Kim. Light emission of a scarlike mode with assistance of quasiperiodicity. *Physical Review A*, 84(4):041803, 2011.

[94] PB Wilkinson, TM Fromhold, L Eaves, FW Sheard, N Miura, and T Takamasu. Observation of 'scarred' wavefunctions in a quantum well with chaotic electron dynamics. *Nature*, 380(6575):608, 1996.

[95] RV Jensen, MM Sanders, M Saraceno, and B Sundaram. Inhibition of quantum transport due to "scars" of unstable periodic orbits. *Physical Review Letters*, 63(26):2771, 1989.

[96] D Wintgen and A Hönig. Irregular wave functions of a hydrogen atom in a uniform magnetic field. *Physical Review Letters*, 63(14):1467, 1989.

[97] Peter M Koch. Experimental evidence for the influence of "scars" in hydrogen atoms driven by strong microwave fields. *Chaos: An Interdisciplinary Journal of Nonlinear Science*, 2(1):131–144, 1992.

[98] Harald Friedrich and Hieter Wintgen. The hydrogen atom in a uniform magnetic field - an example of chaos. *Physics Reports*, 183(2):37–79, 1989.

[99] Hongya Xu, Liang Huang, Ying-Cheng Lai, and Celso Grebogi. Chiral scars in chaotic dirac fermion systems. *Physical Review Letters*, 110(6):064102, 2013.

[100] Perttu JJ Luukko, Byron Drury, Anna Klales, Lev Kaplan, Eric J Heller, and Esa Räsänen. Strong quantum scarring by local impurities. *Scientific reports*, 6:37656, 2016.

[101] Jonas Larson, Brandon M Anderson, and Alexander Altland. Chaos-driven dynamics in spin-orbit-coupled atomic gases. *Physical Review A*, 87(1):013624, 2013.

[102] Diego Wisniacki and Gabriel G Carlo. Scarring in open quantum systems. *Physical Review E*, 77(4):045201, 2008.

[103] F Revuelta, E Vergini, RM Benito, and F Borondo. Scar functions, barriers for chemical reactivity, and vibrational basis sets. *The Journal of Physical Chemistry A*, 120(27):4928–4938, 2016.

[104] F Revuelta, E Vergini, RM Benito, and F Borondo. Semiclassical basis sets for the computation of molecular vibrational states. *The Journal of chemical physics*, 146(1):014107, 2017.

[105] F Revuelta, RM Benito, F Borondo, and E Vergini. Using basis sets of scar functions. *Physical Review E*, 87(4):042921, 2013.

[106] Alexander V Goltsev, Sergey N Dorogovtsev, Joao G Oliveira, and Jose FF Mendes. Localization and spreading of diseases in complex networks. *Physical Review Letters*, 109(12):128702, 2012.

[107] Travis Martin, Xiao Zhang, and MEJ Newman. Localization and centrality in networks. *Physical Review E*, 90(5):052808, 2014.

[108] TA Brody. A statistical measure for the repulsion of energy levels. *Lettere al Nuovo Cimento (1971-1985)*, 7(12):482–484, 1973.

[109] FM Izrailev. Quantum localization and statistics of quasienergy spectrum in a classically chaotic system. *Physics Letters A*, 134(1):13–18, 1988.

[110] Michael V Berry and Marko Robnik. Semiclassical level spacings when regular and chaotic orbits coexist. *Journal of Physics A: Mathematical and General*, 17(12):2413, 1984.

[111] Steven Tomsovic and Denis Ullmo. Chaos-assisted tunneling. *Physical Review E*, 50(1):145, 1994.

[112] Vadim Oganesyan and David A Huse. Localization of interacting fermions at high temperature. *Physical Review B*, 75(15):155111, 2007.

[113] Harish-Chandra. Differential operators on a semisimple lie algebra. *American Journal of Mathematics*, pages 87–120, 1957.

[114] Claude Itzykson and J-B Zuber. The planar approximation. ii. *Journal of Mathematical Physics*, 21(3):411–421, 1980.

[115] Bruno Mirbach and Hans Jürgen Korsch. A generalized entropy measuring quantum localization. 1999.

[116] Sven Gnutzmann and Karol Zyczkowski. Rényi-wehrl entropies as measures of localization in phase space. *Journal of Physics A: Mathematical and General*, 34(47):10123, 2001.

[117] GE Powell and IC Percival. A spectral entropy method for distinguishing regular and irregular motion of hamiltonian systems. *Journal of Physics A: Mathematical and General*, 12(11):2053, 1979.

[118] Benjamin Batistić and Marko Robnik.   Quantum localization of chaotic eigenstates and the level spacing distribution.   *Physical Review E*, 88(5):052913, 2013.

[119] MS Santhanam, VB Sheorey, and A Lakshminarayan. Chaos and exponentially localized eigenstates in smooth hamiltonian systems. *Physical Review E*, 57(1):345, 1998.

[120] Bruno Eckhardt, Gabriel Hose, and Eli Pollak. Quantum mechanics of a classically chaotic system: Observations on scars, periodic orbits, and vibrational adiabaticity. *Physical Review A*, 39(8):3776, 1989.

[121] A Bäcker, R Schubert, and P Stifter. On the number of bouncing ball modes in billiards. *Journal of Physics A: Mathematical and General*, 30(19):6783, 1997.

[122] Dilip Angom and VKB Kota. Chaos and localization in the wave functions of complex atoms nd i, pm i, and sm i. *Physical Review A*, 71(4):042504, 2005.

[123] MS Santhanam, Jayendra N Bandyopadhyay, and Dilip Angom. Quantum spectrum as a time series: Fluctuation measures. *Physical Review E*, 73(1):015201, 2006.

[124] KG Dyall, IP Grant, CT Johnson, FA Parpia, and EP Plummer. Grasp: A general-purpose relativistic atomic structure program. *computer physics communications*, 55(3):425–456, 1989.

[125] M Brack and RK Bhaduri. Semiclassical physics (boulder, 2003.

[126] Kartiek Agarwal, Ehud Altman, Eugene Demler, Sarang Gopalakrishnan, David A Huse, and Michael Knap. Rare-region effects and dynamics near the many-body localization transition. *Annalen der Physik*, 529(7):1600326, 2017.

[127] PB Kahn. Pb kahn and ce porter, nucl. phys. 48, 385 (1963). *Nucl. Phys.*, 48:385, 1963.

[128] AY Abul-Magd and MH Simbel. Wigner surmise for high-order level spacing distributions of chaotic systems. *Physical Review E*, 60(5):5371, 1999.

[129] Madan Lal Mehta and Freeman J Dyson. Statistical theory of the energy levels of complex systems. v. *Journal of Mathematical Physics*, 4(5):713–719, 1963.

[130] HI Liou, HS Camarda, S Wynchank, M Slagowitz, G Hacken, F Rahn, and J Rainwater. Neutron-resonance spectroscopy. viii. the separated isotopes of erbium: Evidence for dyson's theory concerning level spacings. *Physical Review C*, 5(3):974, 1972.

[131] Y Avishai, J Richert, and R Berkovits. Level statistics in a heisenberg chain with random magnetic field. *Physical Review B*, 66(5):052416, 2002.

[132] Fritz Haake, M Kuś, and Rainer Scharf. Classical and quantum chaos for a kicked top. *Zeitschrift für Physik B Condensed Matter*, 65(3):381–395, 1987.

[133] Rémy Dubertrand, Ignacio Garcia-Mata, Bertrand Georgeot, Olivier Giraud, Gabriel Lemarié, and John Martin. Multifractality of quantum wave functions in the presence of perturbations. *Physical Review E*, 92(3):032914, 2015.

[134] Giacomo Livan, Simone Alfarano, and Enrico Scalas. Fine structure of spectral properties for random correlation matrices: An application to financial markets. *Physical Review E*, 84(1):016113, 2011.

[135] Vasiliki Plerou, Parameswaran Gopikrishnan, Bernd Rosenow, Luís A Nunes Amaral, and H Eugene Stanley. Universal and nonuniversal properties of cross correlations in financial time series. *Physical review letters*, 83(7):1471, 1999.

[136] Laurent Laloux, Pierre Cizeau, Jean-Philippe Bouchaud, and Marc Potters. Noise dressing of financial correlation matrices. *Physical review letters*, 83(7):1467, 1999.

[137] Vasiliki Plerou, Parameswaran Gopikrishnan, Bernd Rosenow, Luis A Nunes Amaral, Thomas Guhr, and H Eugene Stanley. Random matrix approach to cross correlations in financial data. *Physical Review E*, 65(6):066126, 2002.

[138] Raj Kumar Pan and Sitabhra Sinha. Collective behavior of stock price movements in an emerging market. *Physical Review E*, 76(4):046116, 2007.

[139] M. S. Santhanam and Prabir K Patra. Statistics of atmospheric correlations. *Physical Review E*, 64(1):016102, 2001.

[140] RW Robinett. Visualizing the solutions for the circular infinite well in quantum and classical mechanics. *American Journal of Physics*, 64(4):440–446, 1996.

[141] C Ellegaard, T Guhr, K Lindemann, J Nygård, and M Oxborrow. Symmetry breaking and spectral statistics of acoustic resonances in quartz blocks. *Physical review letters*, 77(24):4918, 1996.

[142] B Dietz, A Heine, V Heuveline, and A Richter. Test of a numerical approach to the quantization of billiards. *Physical Review E*, 71(2):026703, 2005.

[143] Jonathan P Keating and JM Robbins. Discrete symmetries and spectral statistics. *Journal of Physics A: Mathematical and General*, 30(7):L177, 1997.

[144] Christopher H Joyner, Sebastian Müller, and Martin Sieber. Semiclassical approach to discrete symmetries in quantum chaos. *Journal of Physics A: Mathematical and Theoretical*, 45(20):205102, 2012.

[145] Freeman J Dyson. Statistical theory of the energy levels of complex systems. i. *Journal of Mathematical Physics*, 3(1):140–156, 1962.

[146] J Gunson. Proof of a conjecture by dyson in the statistical theory of energy levels. *Journal of Mathematical Physics*, 3(4):752–753, 1962.

[147] Arnd Bäcker, Frank Steiner, and P Stifter. Spectral statistics in the quantized cardioid billiard. *Physical Review E*, 52(3):2463, 1995.

[148] H Alt, C Dembowski, H-D Gräf, R Hofferbert, H Rehfeld, A Richter, and C Schmit. Experimental versus numerical eigenvalues of a bunimovich stadium billiard: A comparison. *Physical Review E*, 60(3):2851, 1999.

[149] G. Hacken, R. Werbin, and J. Rainwater. Neutron resonance spectroscopy: Ta. *Phys. Rev. C*, 17:43–50, Jan 1978.

[150] Tómas A Brody, J Flores, J Bruce French, PA Mello, A Pandey, and Samuel SM Wong. Random-matrix physics: spectrum and strength fluctuations. *Reviews of Modern Physics*, 53(3):385, 1981.

[151] Thomas Guhr and Heiner Kohler. Recursive construction for a class of radial functions. i. ordinary space. *Journal of Mathematical Physics*, 43(5):2707–2740, 2002.

[152] Milton Abramowitz and Irene A Stegun. *Handbook of mathematical functions: with formulas, graphs, and mathematical tables*, volume 55. Courier Corporation, 1965.